# Regional characteristics of winter cyclone activity around Hokkaido and its multidecadal trend associated with surface pressure patterns over Northeast Asia

(北海道周辺における冬季低気圧活動の地域特性と北東アジアの気圧配置に関連した数十年規模の傾向)

**Kenta Tamura**

*Division of Environmental Science Development,*

*Graduate School of Environmental Science,*

*Hokkaido University*

June 2022

# Abstract

In East Asia, strong winter monsoon and high baroclinicity enhance cyclone activity. Winter cyclone activity modulates the daily weather over Japan by inducing low temperatures and snowfall. Strong wind and heavy precipitation induced by the winter cyclone can cause disasters. It is well known that mesoscale cyclones frequently occur in the Sea of Japan, causing locally but strong winds and heavy snowfall. Despite the high frequency of genesis of mesoscale cyclones around the Sea of Japan, most previous studies on the cyclone activity in the decadal timescale have focused only on synoptic-scale cyclones. Since mesoscale cyclones cause local snowfall, the understanding of the decadal trends in winter cyclone activity, including mesoscale cyclones, can provide new insight into regional response to climate change, especially in Hokkaido where the frequency of mesoscale cyclone is high. The purpose of this study is to clarify the decadal trends of winter cyclone activity that include mesocyclones over and around northern Japan. In addition, the regional features of mesoscale cyclogenesis in the northern part of the Sea of Japan were investigated by using numerical experiments.

This decadal trend of the passage of cyclones over and around Japan, including mesoscale cyclones, was investigated during 62 winter seasons (December–March) from 1958/1959 to 2019/2020 using the long-term reanalysis dataset JRA-55. During the study period, the passage of cyclones around northern Japan showed a decreasing trend. Most of the cyclones that pass around northern Japan are generated over the northern part of the Sea of Japan, where mesoscale cyclogenesis frequently occurs. It was also found that the duration of the cyclones generated in the northern part of the Sea of Japan is relatively short compared to the cyclones that originated in the

other regions.

Analyses based on the weather pattern classification revealed that the passage of upper-level troughs and lower-level cold air outbreaks over the northern part of the Sea of Japan are preferential conditions for the cyclogenesis in the northern part of the Sea of Japan. These conditions are consistent with the conditions for the development of mesoscale cyclones in this region. Statistical analysis indicated that magnitude of the cold air outbreak in this region was weakened. Hence, the changes in atmospheric conditions due to climate change may have reduced mesocyclone genesis over the northern Sea of Japan, resulting in the number of cyclones passing over and around Hokkaido over the past 60 years.

In this study, the role of the surrounding topography in the cyclogenesis over the northern part of the Sea of Japan was also investigated. Long-term numerical experiments using the regional climate model WRF (The Weather Research and Forecasting Model) were conducted to investigate the effects of mountains located on the eastern coast of the Eurasian continent (i.e., the Sikhote-Alin mountain range) on the mesoscale cyclones generated over the northern part of the Sea of Japan. Weather pattern classification clarified that the effects of the mountains on the mesoscale cyclone vary depending on synoptic-scale atmospheric conditions. The difference in sensitivity is due to the difference in the development mechanism of the mesoscale cyclones. Mesoscale cyclogenesis over the northern part of the Sea of Japan associated with the Siberian high and Aleutian low is caused by the lower-level horizontal wind shear formed over the offshore region west of Hokkaido. This horizontal wind shear is caused by the northwesterly winds that blow across the Sikhote-Alin mountain range. Sensitivity experiment revealed that the removal of the Sikhote-Alin mountain

range weakens the horizontal shear of the lower-level winds over the northern part of the Sea of Japan and decreases this type of mesoscale cyclogenesis. Therefore, the mesoscale cyclogenesis caused by lower-level horizontal wind shear is very sensitive to the local topography. In contrast, the number of occurrences of mesoscale cyclogenesis induced by baroclinic instability did not vary even after the removal of mountains. It is suggested that formation of the mesoscale cyclones, is not affected by the surrounding topography if their development is driven by upper-level atmospheric conditions.

The analysis using reanalysis dataset and high-resolution datasets derived from the regional climate model clarified the regional characteristics of winter cyclone activities around northern Japan. The results are summarized as follows; 1) the passages frequency of winter cyclones around Hokkaido originated from the northern part of the Sea of Japan has decreased since the 1960s, 2) the weakening of the cold air outbreak over the northern part of the Sea of Japan suppressed the mesoscale cyclogenesis in this region, and 3) the mesoscale cyclogenesis over the northern part of the Sea of Japan associated with the Siberian high and Aleutian low is caused by the lower-level wind shear formed by the mountains along the eastern coast of the Eurasian continent. Decadal trend of cyclone activity over recent years and the factors behind that revealed in this study can provide new insight into the response of regional climate in Hokkaido under ongoing climate change.

## Contents

# 1. Introduction

## 1.1 Winter climate and surface pressure pattern around Japan

In winter, a surface high pressure over the eastern Eurasian Continent and low pressure over the Northwest Pacific Ocean causes cold air advection over Japan (e.g., Murakami and Sumi 1981; Lau and Lau 1984; Boyle and Chen 1987; Kashiwabara 1988). The surface high pressure, which is formed by the radiative cooling over the continent, is called the Siberian high (e.g., Ding and Krishnamurti 1987; Takaya and Nakamura 2005). The cold air mass on the Siberian high is the source of the East Asia winter monsoon, and that outflows cause the cold surge over East Asia (Chang et al. 1979; Ding and Krishnamurti 1987; Gong et al. 2001; Jhun and Lee 2004; Iwasaki et al. 2014). Figure 1.1 shows the topography and winter averaged (December to March) sea level pressure (SLP) in East Asia. A high pressure corresponding to the Siberian high exists on the Eurasian continent, and a quasi-stationary low pressure called the Aleutian low is identified around the Kamchatka Peninsula. This west-east high and low surface pressure pattern around northern Japan, formed by the Siberian high and Aleutian low, is generally known as the typical pressure pattern that induces cold winter in Japan.

Numerous studies have shown that the pressure pattern determines the synoptic-scale atmospheric circulation and affects the regional weather systems (e.g., Lund 1963). In recent years, long-term observations and the development of reanalysis datasets have made it possible to highlight the statistical relationship between pressure patterns and extreme weather events. For example, Esteban et al. (2005) showed that heavy snowfall in the Pyrenees between France and Spain was caused by the warm air advection from the sea and the cold air advection from the continent induced by a specific synoptic-scale surface pressure pattern. Farukh and Yamada (2018)

showed that the extreme low temperatures in winter in Sapporo, the largest city in Hokkaido located in northern Japan, were caused by the cold air advection induced by the west-east high and low surface pressure pattern. Conversely, extreme high temperatures were caused by warm air advection due to an opposite pressure pattern (west-east low and high surface pressure). Recently, Kawazoe et al. (2020) revealed that heavy snowfall in Sapporo tends to occur under three typical pressure patterns: high pressure on the eastern end of the Eurasian Continent, low pressure to the east of Hokkaido, or low pressure over central Japan. Thus, the analysis based on pressure patterns helps to provide a statistical understanding of regional weather events.

## 1.2 Winter cyclone activity around Japan

Winter synoptic-scale cyclones passing over and around Japan develop over the Eurasian continent and surrounding oceans (e.g., Chen et al. 1991; Adachi and Kimura 2007). Meanwhile, mesoscale cyclones develop in the Sea of Japan due to cold air advection caused by the strong winter monsoon (e.g., Asai 1988; Yanase et al. 2016). Activity of these synoptic-scale and mesoscale cyclones characterize the winter climate in Japan. This section describes the climatological features of the cyclones around Japan. Section 1.2.1 deals with synoptic-scale cyclones, and Section 1.2.2 deals with mesoscale cyclones.

### 1.2.1 Synoptic-scale cyclone

Storm track refers to the region with frequent cyclone passage (e.g., Blackmon et al. 1977; Chang 1993). Japan is located on the part of the storm track and strong winter monsoon and high baroclinicity enhance cyclone activity (e.g., Chung et al. 1976; Chen et al. 1991; Adachi and

Kimura 2007). Analysis of cyclone tracking revealed that major genesis locations of the extratropical cyclones passing over and around Japan are the northwestern Pacific Ocean, Sea of Japan, East China Sea, Yangtze River basin, and over the eastern Eurasian Continent (e.g., Chen et al. 1991; Adachi and Kimura 2007; Lee et al. 2020). Many cyclones generated over the continent is originated from the lee of the mountains, such as the Mongolia Plateau (Chung et al. 1976; Chen et al. 1991). Development of the maritime extratropical cyclone is related to the distribution of sea surface temperature (e.g., Chen et al. 1992; Iizuka et al. 2013). Especially around Japan, warm ocean current (Kuroshio current) enhances lower tropospheric baroclinicity, and the extratropical cyclones develop rapidly (Sanders and Gyakum 1980; Hanson and Long 1985). These cyclones are called explosive (or bomb) cyclones and cause strong wind and precipitation events in Japan (e.g., Yoshida and Asuma 2004; Tsukijihara et al. 2019; Hirata 2021).

Many studies have investigated the relationship between cyclone activity and snowfall. For example, heavy snowfall years in the Sea of Japan side of central Japan, the passage of explosive cyclones tend to concentrate over the Sea of Japan and the Pacific coast of Japan (Yamashita et al. 2012). On the other hand, snowfall in the Kanto region located on the Pacific coast of central Japan is induced by the extratropical cyclone that passes through the southeastern coast of Japan (e.g., Takano 2002; Yamazaki et al. 2015; Kawase et al. 2018). Inatsu et al. (2021) has shown that slight differences in the location of extratropical cyclones significantly alter the amount of regional snowfall in Hokkaido, pointing out the importance of the synoptic-scale atmospheric condition such as cyclone activity for snowfall. Furthermore, along the Sea of Japan coast, mesoscale cyclones (described in a later section) cause localized but intense snowstorms (e.g., Ninomiya 1991;

Ninomiya et al. 1993). Therefore, winter cyclonic activities that can trigger severe weather events are an essential component of the winter climate in Japan.

Global climate models have projected the reduction of the total number of winter cyclones in the Northern Hemisphere in response to human-induced climate change, but the tendency of this decrease varies with region and cyclone intensity (Mizuta et al. 2011). Regional variations of this decline tendency have also been captured in reanalysis datasets. For example, the frequency of occurrence of extratropical cyclones has decreased in parts of East Asia, although the change is not statistically significant (Lee et al. 2020). In contrast, an increase in the frequency of explosive cyclones over ocean areas to the east of Hokkaido (Tsukijihara et al. 2019) is indicative of recent change in cyclone intensity. These changes revealed in reanalysis datasets suggest that regional cyclone activity may have already altered owing to ongoing climate change.

### 1.2.2 Mesoscale cyclone

Over the high latitude oceans, small cyclone features, called polar mesocyclones (PMCs), often occur. PMCs have a horizontal scale of meso-α (200–2000 km) to meso-β (20–200 km) scale (definition of scale: Orlanski 1975). Intense (surface wind speed exceeds 15 m $s^{-1}$) meso-α scale PMCs are called polar lows (Rasmussen and Turner 2003). Polar lows are observed over various oceans, such as the Northern Atlantic Ocean (e.g., Harold et al. 1999), the Barents Sea (e.g., Rasmussen 1985), the Labrador Sea (e.g., Mailhot et al. 1996), the Southern Ocean (e.g., Carleton and Carpenter 1990), and the Sea of Japan (e.g., Ninomiya 1989). They often cause locally heavy precipitation and strong wind around coastal seas and land areas in the circumpolar region. Therefore, the genesis and development processes of such mesoscale cyclones have attracted

considerable scientific attention.

Case studies suggested that multiple mechanisms contribute to polar low development. For example, baroclinic instability is necessary during the initial stage of polar low development (Reed and Duncan 1987), whereas conditional instability of the second kind and wind-induced surface heat exchange processes can help their rapid development (Rasmussen 1979; Emanuel and Rotunno 1989). An idealized numerical simulation revealed that the primary energy source for polar low development varies according to synoptic-scale baroclinicity (Yanase and Niino 2007). These studies highlighted that PMCs, including polar lows, have a variety of formation and development processes, and thus, the role of environmental conditions differ from case to case.

Besides meteorological and oceanic effects, topographic effects can have a crucial role on PMCs. Over the Barents Sea, cold air outbreaks originating from the Arctic Sea can be split by the Svalbard islands, forming lower-tropospheric vorticity filaments that later grow into polar lows (Sergeev et al. 2018). The mountains located in the north of the Korean Peninsula can intensify a convergence zone over the southern Sea of Japan, along which frequent PMC genesis is observed (Watanabe et al. 2018). Despite the substantial impact of topographic effects on such mesoscale cyclogenesis, previous discussions have tended to focus on case studies or idealized numerical experiments (Kristjánsson et al. 2011). Therefore, because the role of topographic effects on the genesis of various forms of PMC is not fully understood, the impact of topographic effect on the climatological features of PMCs also remains unexplored.

Despite the relatively lower latitude region, the frequency of PMCs is high over the northern Sea of Japan (Asai 1988), especially offshore region west of Hokkaido (Fujiyoshi et al. 1988). In

this region, the PMC tends to be generated under cold air advection induced by the northerly wind (e.g., Watanabe et al. 2017), and/or strong horizontal wind shear caused by warm easterly wind and cold westerly wind associated with a synoptic-scale cyclone located to the east of the PMC (Ninomiya 1991; Ninomiya et al. 1993). Topography of the Eurasian continent and Hokkaido are one of the factors of PMC genesis in this region. The mountain range on the eastern edge of the Eurasian continent (i.e., the Sikhote-Alin mountain range) weakens the westerly wind over the Sea of Japan, establishing conditions suitable for PMC growth that allow PMCs to remain longer over the sea (Watanabe et al. 2017). Additionally, the mountain range creates local (Tamura and Sato 2020) and synoptic-scale (Ninomiya 1991) horizontal temperature gradients in the lower troposphere which are likely to affect PMC genesis.

### 1.3 Objective of the present study

Related studies for the interannual variation of cyclone activities have focused mainly on the extratropical cyclones (e.g., Lee et al. 2020), whose horizontal scale is typically >1000 km. Conversely, mesocyclones have not been the target of intensive research despite their substantial impact on regional climate. Research has shown that the lifecycle of a mesocyclone is sensitive to regional geographical factors such as topography and local atmospheric conditions (e.g., Tamura and Sato 2020). Therefore, the response of a mesocyclone to regional climate change can differ from that of an extratropical cyclone. For example, Stoll et al. (2018) found that the frequency of mesocyclones over the offshore region south of Svalbard in recent years (2001–2016) was higher than that of past years (1979–1994).

The objective of this study is to clarify the interannual variation of winter cyclone activity over

northern Japan using an original cyclone tracking product that includes mesocyclones. Additionally, the mechanism behind the interannual variation is investigated by considering synoptic-scale weather pattern classifications. The present study also examines the characteristics of mesocyclones in the offshore region west of Hokkaido by using the regional climate model and the weather pattern classifications.

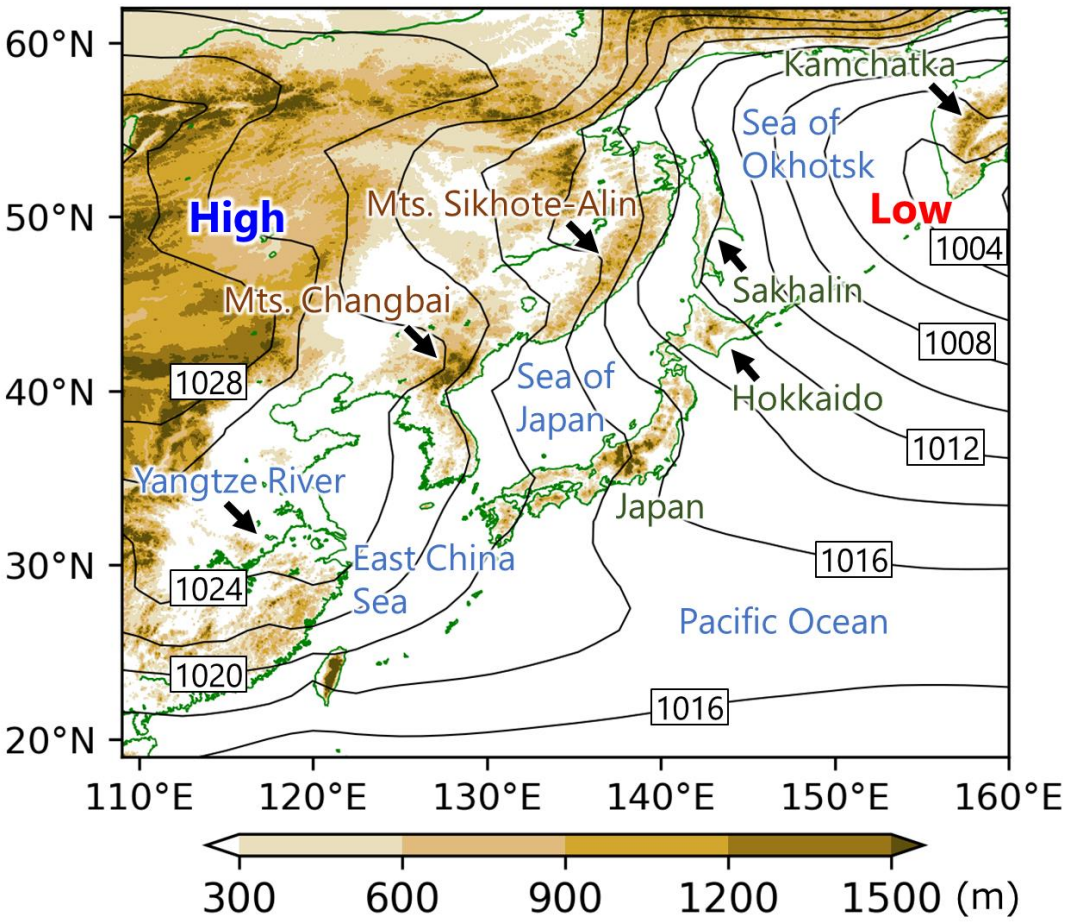


Figure 1.1. Geography around East Asia and average sea level pressure for December–March during 1958/1959–2019/2020 (contour interval is 2 hPa). Topography above 300 meters is shown by color shading.

# 2. Data and methodology

## 2.1 Dataset

In this study, the Japanese 55-year Reanalysis dataset (JRA-55), obtained from the Japan Meteorological Agency (Kobayashi et al. 2015), was used for the detection and tracking of cyclones (Chapter 3), classification of pressure patterns (Chapter 4), and the analysis of the atmospheric conditions (Chapter 3 and 4). This dataset has 1.25° horizontal resolution and a 6-hourly time interval. To validate the impact of data assimilation on the cyclone tracking shown in Chapters 3 and 4, the JRA-55 Conventional reanalysis (JRA-55C) and the JRA-55 Atmospheric Model Intercomparison Project type simulation (JRA-55AMIP) were used. JRA-55C is produced by the same model, data assimilation system, and boundary conditions as JRA-55, but satellite observations are not assimilated (only the observations over land, sea, and upper-level air are used) (Kobayashi et al. 2014). JRA-55AMIP is produced by the same model and boundary conditions as JRA-55 without data assimilation. Numerical experiments described in Chapter 5 used JRA-55, the NOAA 0.25° daily Optimum Interpolation Sea Surface Temperature v2.0 (OISST v2.0), and the distribution of sea ice dataset (Reynolds et al. 2007) as the initial and boundary conditions.

## 2.2 Algorithm for tracking cyclones

Cyclone tracks were determined using the methodology described in Adachi and Kimura (2007) and Hayasaki and Kawamura (2012) with slight modifications to ensure detection of mesoscale cyclones. The algorithm first detects a grid point with a local minimum sea level pressure (SLP) that is lower than that at any of the neighboring eight grids. The second step eliminates topographically anchored SLP minima. A cyclone center is designated only when an anomalous

SLP minimum remains at least 0.5 hPa lower than that at the neighboring eight grids after removal of the 31-day running mean SLP field. A cyclone track is created by connecting the positions of the nearest cyclone center at each 6-hour interval. If there are no cyclone centers within the search area (i.e., four grids to the north, six grids to the east, four grids to the south, and three grids to the west relative to the current cyclone center) in the subsequent time step, cyclone tracking is terminated. The algorithm was applied to the region 0°–80°N and 90°–180°E, and cyclones that persisted for more than 24 h were analyzed. This algorithm is capable of detecting intense but relatively small cyclones that were previously removed through spatial filtering in the study of the decadal trend of cyclone activity (Lee et al. 2020). From the reanalysis dataset JRA-55 used in this study, it is possible to detect the cyclone with a diameter of approximately 300 km, corresponding to a horizontal scale of three grids. However, cyclones with a diameter of less than 300 km occur, such as meso-β scale cyclones (Tsuboki and Asai 2004; Watanabe and Niino 2014; Watanabe et al. 2018), in the Sea of Japan, the area covered by the present study. Such small cyclones cannot be detected by this algorithm. Hence, the cyclone tracking algorithm is suitable for studying the synoptic-scale cyclones and meso-α scale cyclones (greater than 300 km) like polar low, but not suitable for mesocyclone smaller than 300km. Note that this algorithm does not use wind speed as a threshold. Therefore, the small cyclones detected by this algorithm include polar lows and polar mesoscale cyclones.

### 2.3 Validation of the tracking algorithm

This section validates the accuracy of the tracking algorithm used in the present study by checking whether some cyclones cases are detected appropriately. In the following subsections, as

two examples, the cyclone that was detected by the algorithm (Case 1) and the cyclone that was not detected (Case 2) are shown.

### 2.3.1 Case 1: 9 December 1985

This subsection compares the cyclone introduced in Ninomiya (1991). Ninomiya (1991) investigated the development of mesoscale cyclone over the offshore region west of Hokkaido generated on 9 December 1985. In this case, mesocyclone developed over the offshore region west of Hokkaido where lower-level temperature gradient was strong. The temperature gradient was formed between the warm air advection from the Pacific Ocean and cold air advection from the continent induced by the synoptic-scale cyclone located on the east of Hokkaido.

Figure 2.1 shows the surface whether chart and the location of cyclones on 9 December 1985 (Ninomiya 1991). Synoptic-scale cyclone formed over the Sea of Japan at 00 UTC 8 December 1985 moved northeastward and reached the Okhotsk Sea. The mesocyclone was generated over the offshore region west of Hokkaido at 00 UTC 9 December 1985 and moved southeastward. Satellite infrared images at (a) 00 UTC and (b) 12 UTC on 9 December is shown in Figure 2.2 (Ninomiya 1991). Large and upper-level (cloud top temperature is low) cloud system corresponding to the synoptic-scale cyclone (Figure 2.1) is seen over the Pacific Ocean, and there is a small and lower-level (cloud top temperature is high) cloud over the northwest of Hokkaido (red circle) (Figure 2.2a). This small and lower-level cloud developed into a large comma-shaped cloud with a diameter of about 500 km after 12 hours (Figure 2.2b). This comma-shaped cloud corresponds to the mesocyclone located on the offshore region west of Hokkaido shown in Figure 2.1. SLP fields and the location of the cyclones detected by the cyclone tracking algorithm in the present study are

shown in Figure 2.3. The algorithm in the present study well captured the pathway of the synoptic-scale cyclone which reached the Sea of Okhotsk. Although the mesocyclone at the initial developmental stage (Figure 2.2a) was not detected (Figure 2.3a), the mesocyclone was detected 12 hours later in the offshore region west of Hokkaido as a cyclogenesis (cross mark in Figure 2.3b). Therefore, this cyclone tracking algorithm can detect the synoptic-scale cyclone and the mesoscale cyclone that has a clear local pressure minimum.

### 2.3.2 Case 2: 10 January 1987

This subsection compares the cyclone introduced in Ninomiya et al. (1996). Figure 2.4 shows the surface weather chart (Figure 2.4a), satellite infrared image (Figure 2.4b), and SLP and cyclone tracks (Figure 2.4c) detected by the present study at 12 UTC 10 January 1987. In this case, the synoptic-scale cyclone which had passed through over Hokkaido was accompanied by mesoscale cyclogenesis over the offshore region west of Hokkaido. A mesocyclone was located over southwest of Hokkaido (Figure 2.4a), and a small cloud cover ranging about 200 to 300 km can be seen (Figure 2.4b; red circle). The cyclone tracking algorithm in the present study, however, was not able to detect the cyclone (Figure 2.4c). SLP field shows the west-east high and low surface pressure gradient over the offshore region west of Hokkaido, but there is no local pressure minimum (Figure 2.4c). Since the tracking algorithm in this study aims to detect the local pressure minimum, the cyclone with a relatively small horizontal size or those without local pressure minimum is not detected. Hence, the tracking algorithm in the present study can detect two types of cyclones, i.e., (1) synoptic-scale cyclones (extratropical cyclones) and (2) mesoscale cyclones with a distinct pressure minimum, such as intense mesoscale cyclones (i.e., polar lows).

## 2.4 Determination of horizontal size of cyclones

In Chapter 3, the horizontal scale of cyclones was defined by using low-level relative vorticity. Figure 2.5 shows a flow chart of the determination of the horizontal scale of the cyclones. This algorithm is adapted from Watanabe et al. (2016). In this algorithm, the vortex area that includes only one cyclone center detected by the cyclone tracking algorithm (Section 2.3) was determined. This enables the identification of small-scale cyclone which appear near synoptic-scale cyclone, and hence, it allows statistical analysis of cyclone size.

## 2.5 Classification of pressure patterns

The synoptic-scale atmospheric conditions over northern Japan in winter seasons were examined using the classification method based on self-organizing maps (SOMs) (Kohonen 1982). The SOMs approach offers visualization of high-dimensional datasets via reduction to a two-dimensional map through neural network techniques. In meteorological studies, this technique has been used widely in the classification of temporally varying atmospheric conditions such as SLP patterns (e.g., Lennard and Hegerl 2015; Ohba et al. 2015; Kawazoe et al. 2020). In this study, the SOMs was used to classify the SLP patterns leading to cyclogenesis. The SOM was trained using 6-hourly standardized SLP fields over northern Japan (35°−55°N, 127°−157°E). The training was performed using 30,072 input vectors (4 times daily × 121/122 winter days × 62 years).

To consider the optimum number of nodes for the SOM, the below examinations were conducted. In this study, Quantization Error (QE) and Topographic Error (TE) (Kohonen 2001;

Sakai et al. 2010) were measured. QE is the difference between the input vector and the best-matching reference vector (node in trained SOM) and is computed by the following equation:

$$QE_i = \frac{1}{N}\sum_{j=1}^{N}\sqrt{\frac{1}{k}\left\|z_{i,j} - m_i\right\|}$$

where $i$ is node number, $j$ indicates the number of the input vector, $z_{i,j}$ is $j$th input vector in node $i$, $m_i$ is the reference vector in node $i$, $k$ is the dimension of the input vector, and N is a total number of input vectors assigned in node $i$. As the number of nodes increases, trained SOM can represent finer patterns, and average $QE_i$ (QE) decreases. TE measures the preservation of topology in a reference vector and is defined as the following equation:

$$TE = \frac{1}{N}\sum_{p=1}^{N} S_p$$

where $N$ is the total number of input vectors. $S_p$ is decided as 0 if the second-best-matching node is located on the neighboring node of the best-matching node, and otherwise, $S_p$ is 1. Low TE means similar reference vectors tend to be located on the nearby nodes. Table 2.1 shows QE and TE for each size of SOM. Rate of change in QE becomes smaller from 4 × 4 to 5 × 5 nodes and the values of QE are also relatively low at 4 × 4, 4 × 5, 5 × 4, and 5 × 5. Thus, these four sizes of SOMs are adopted in this study. In addition, interpretation of classification based on the SOMs is ensured by K-means clustering. The analysis using these classification methods is shown in Chapters 4 and 5.

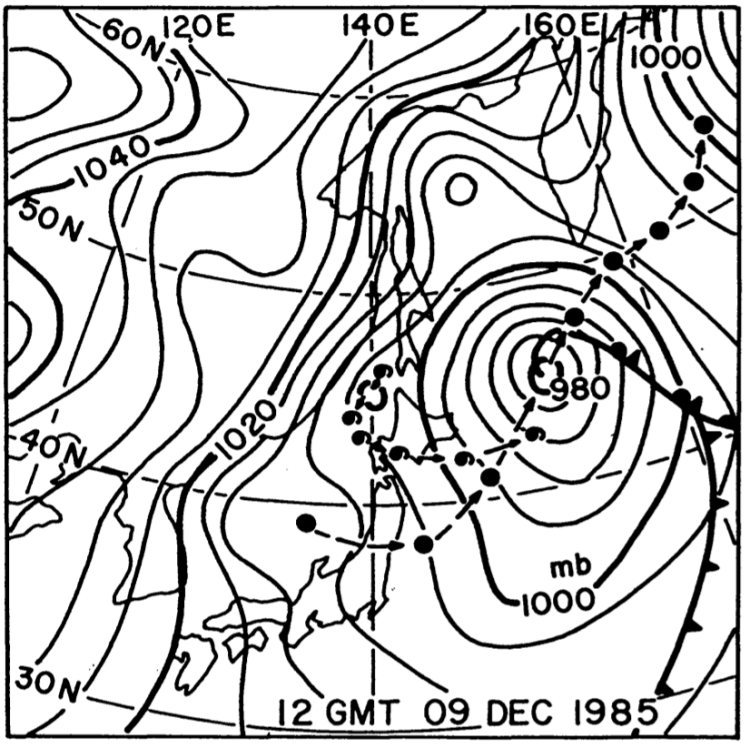


Figure 2.1. Surface weather chat at 12 UTC 9 December 1985 (Ninomiya 1991). The center of the synoptic-scale low (indicated by the blacked circle) and the mesocyclone (indicated by the comma) are shown at 12-hour intervals.

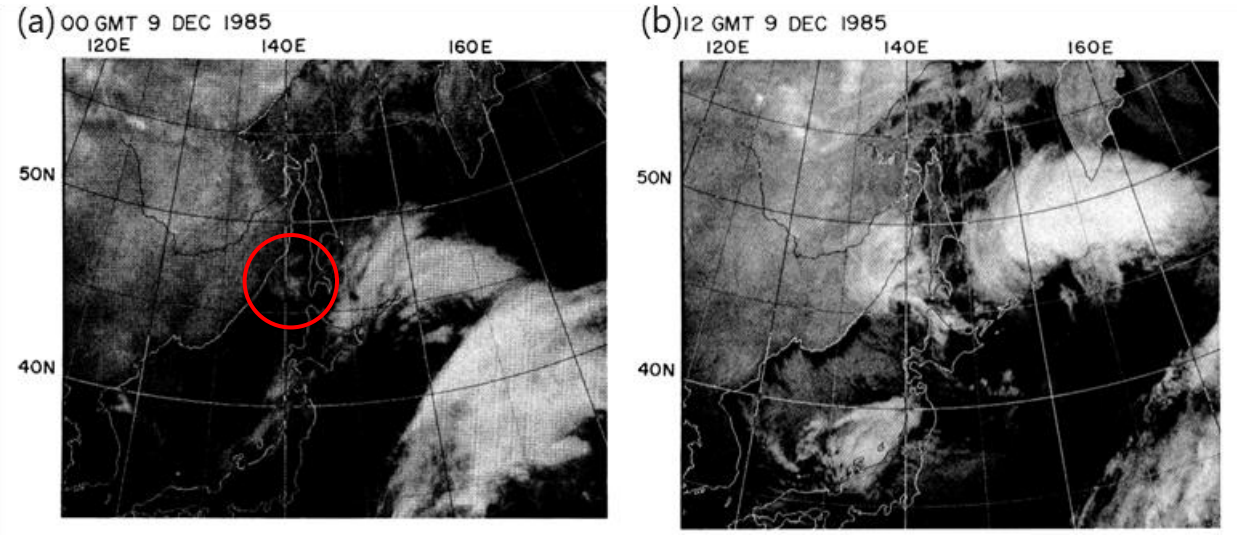


Figure 2.2. Infrared images obtained by the geostationary meteorological satellite of the Japan Meteorological Agency (Ninomiya 1991). (a) 00 UTC 9 December 1985, (b) 12 UTC 9 December 1985.

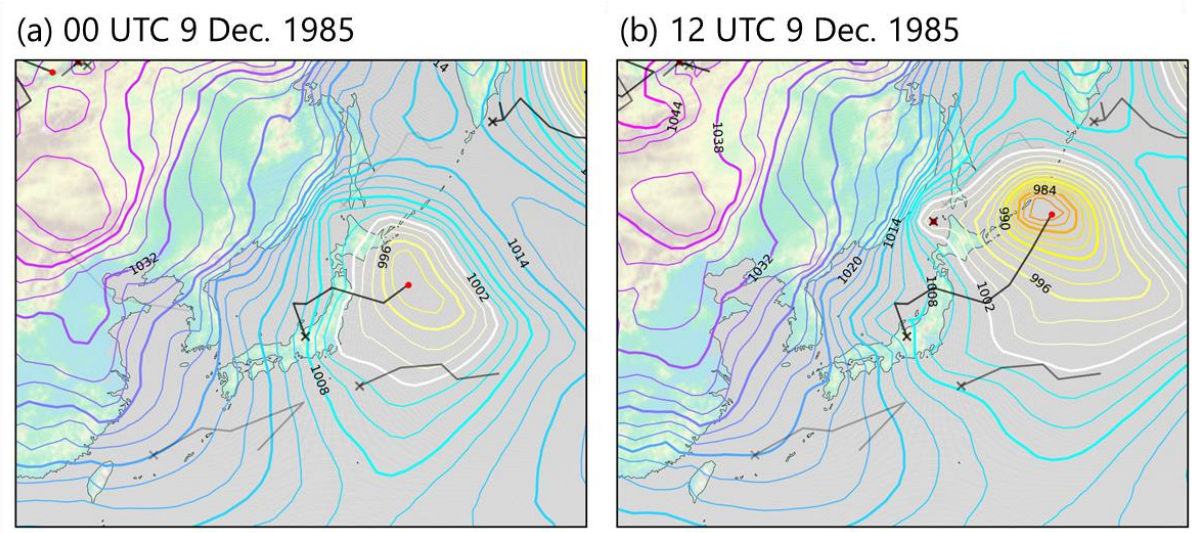


Figure 2.3. Sea level pressure (contour) and cyclone tracks (brack line) detected in this study. Red dot indicates the cyclone center. Black cross indicates the location of occurrence of cyclogenesis. (a) 00 UTC 9 December 1985, (b) 12 UTC 9 December 1985.

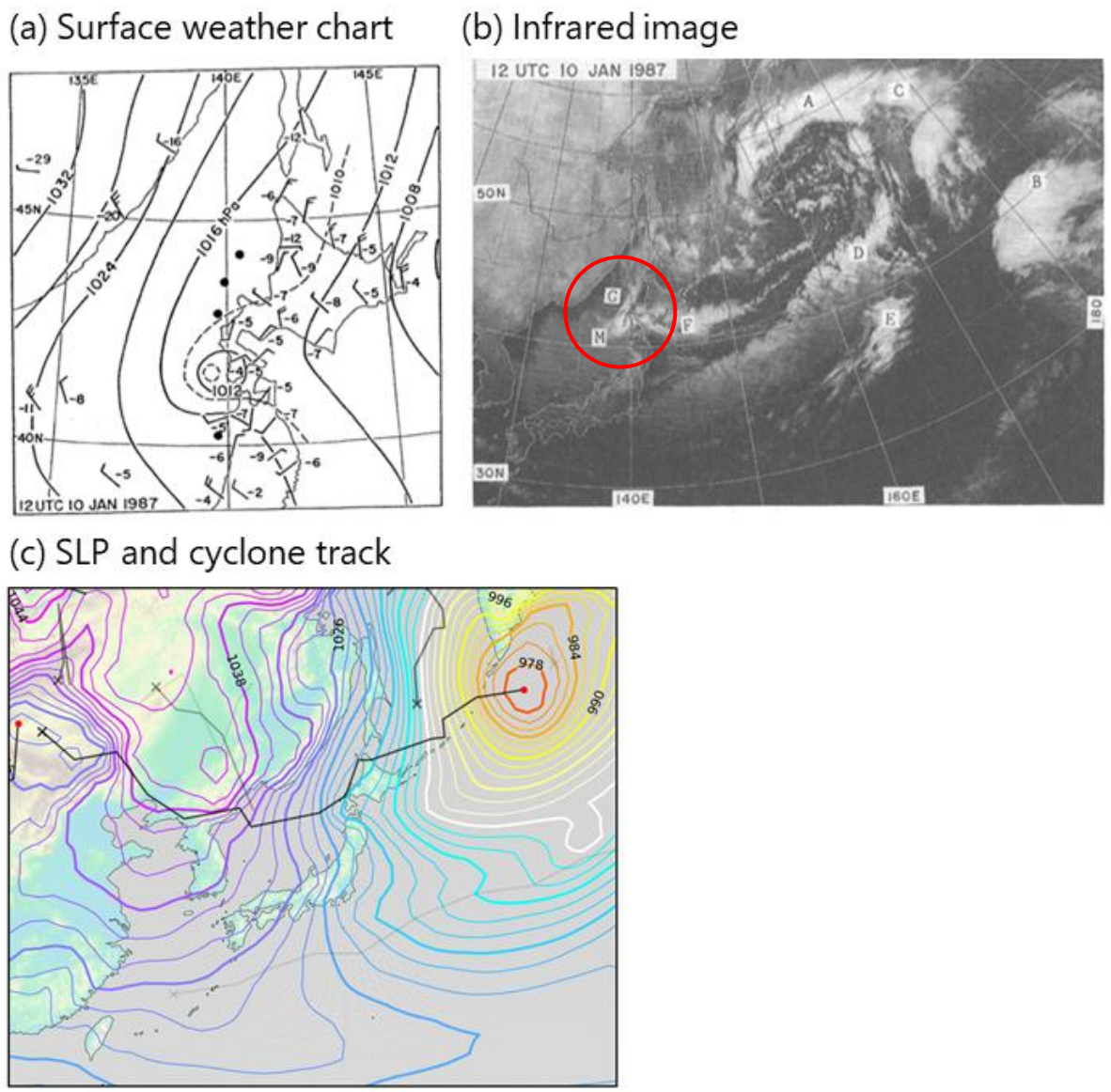


Figure 2.4. (a) Surface weather chart and (b) infrared images at 12 UTC 10 January 1987 (Ninomiya et al., 1996). (c) Same as Figure 2.3 for 12 UTC 10 January 1987.

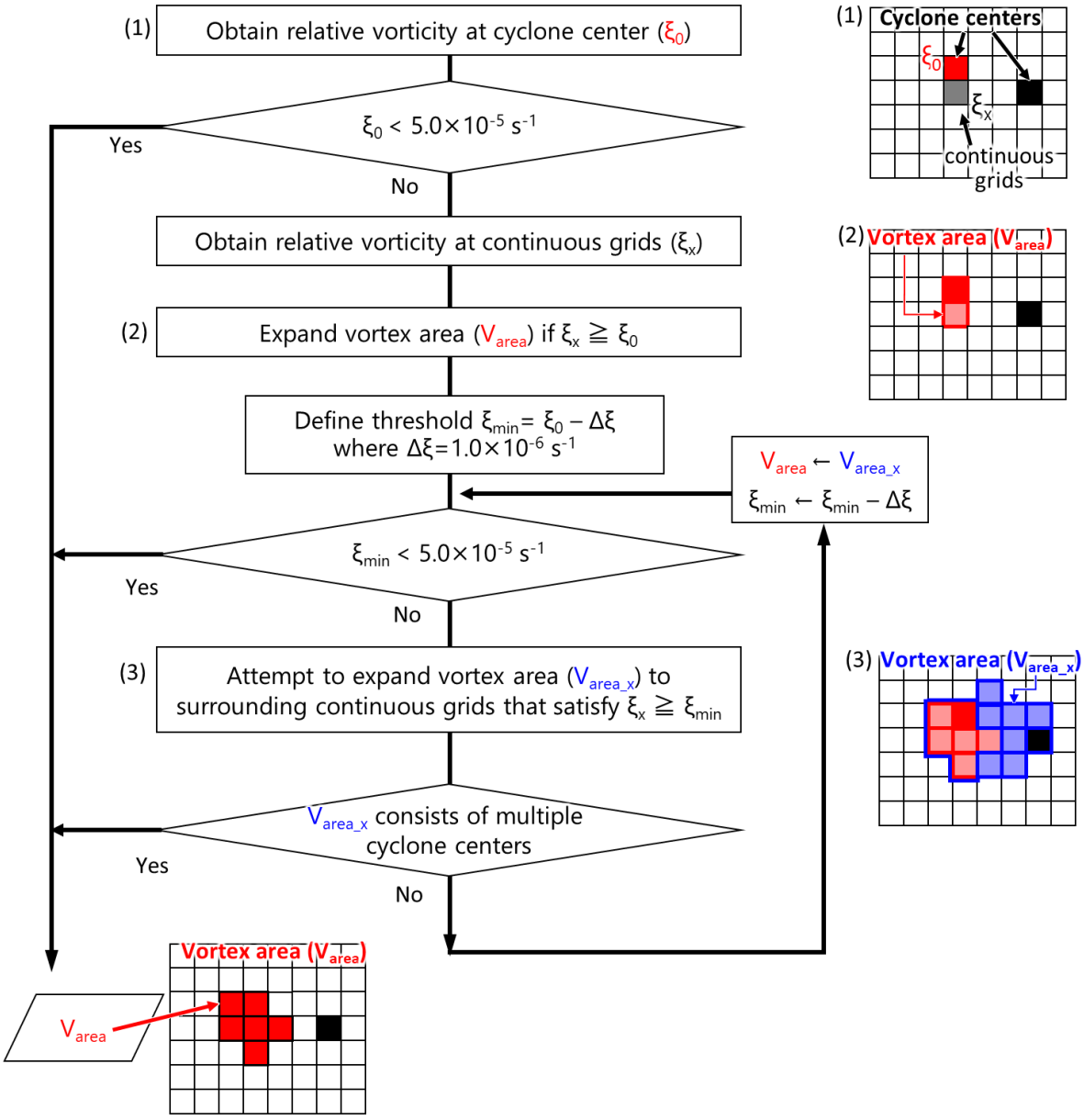


Figure 2.5. Flow chart and schematic of the definition of vortex area of the cyclone. (1) Relative vorticity (900 hPa level) at the cyclone center is defined as $\zeta_0$. If $\zeta_0$ is smaller than $5.0 \times 10^{-5}$ $s^{-1}$, terminate the analysis. (2) Expand the vortex area ($V_{area}$) to the surrounding continuous grids if relative vorticity is equal or greater than $\zeta_0$. (3) Using the vorticity threshold ($\zeta_{min}$), attempt to expand the vortex area ($V_{area\_x}$). Repeat the steps until $\zeta_{min}$ becomes below $5.0 \times 10^{-5}$ $s^{-1}$ or the expanded vortex area contains multiple cyclone centers.

Table 2.1. QE and TE for SOM maps.

| Size of SOM | 2×2 | 3×3 | 4×4 | 5×5 | 6×6 |
|---|---|---|---|---|---|
| QE | 0.46 | 0.41 | 0.38 | 0.36 | 0.34 |
| TE | 0.0 | 0.007 | 0.05 | 0.06 | 0.10 |
| Size of SOM | 3×2 | 4×3 | 5×4 | 6×5 | 7×6 |
| QE | 0.44 | 0.40 | 0.37 | 0.35 | 0.34 |
| TE | 0.01 | 0.12 | 0.06 | 0.10 | 0.12 |
| Size of SOM | 10×2 | 4×5 | 2×10 | | |
| QE | 0.37 | 0.37 | 0.37 | | |
| TE | 0.13 | 0.06 | 0.13 | | |

# 3. Winter-cyclone activity around Japan

## 3.1 Introduction

In the winter season, frequent passage of cyclones brings strong winds and heavy snowfall in Japan. Changes in cyclone activity associated with climate change can influence the frequency of strong winds and snowfall (Kawazoe et al. 2020; Kawase et al. 2021; Inatsu et al. 2021). Therefore, it is important to identify interannual variations in cyclone activity from adaptation to climate change.

Despite the high genesis frequency of mesoscale cyclones recently pointed out in the Sea of Japan (Yanase et al. 2016), related studies aimed to elucidate the long-term trends of the synoptic-scale disturbances (e.g., Lee et al. 2020). The method of extracting cyclones by using thresholds confines the number of cyclones to be analyzed. Therefore, new insight is expected by the consideration of cyclones at various horizontal scales. The cyclone tracking method described in Chapter 2 detects cyclones of varying sizes. This method has the potential to detect the regional climate changes in cyclone activity over oceans where the frequency of the mesoscale cyclogenesis is high such as the Sea of Japan.

In this chapter, the number of cyclone passages was examined using an original cyclone tracking product that includes mesocyclones described in Chapter 2 to quantify the winter cyclone activity around Japan. The interannual variation of the number of cyclones passage and the possible reasons for the interannual variation are discussed.

## 3.2 Result

### 3.2.1 Climatology of cyclone genesis and passage

Figure 3.1a shows the number of cyclone passages in winter (December–March) over Japan from 1958–2019. The number of cyclone passages means the number of individual cyclones, i.e., a cyclone that remained longer or passed over the same grid multiple times was counted as one. The number of cyclone passages was high over the Sea of Japan and the northwestern Pacific, consistent with the findings of Lee et al. (2020). Figure 3.1a shows that the number of cyclone passages around Hokkaido was also relatively high. This result is a feature not seen in Lee et al. (2020) that investigated only synoptic-scale cyclones. Therefore, this high passage frequency implies that the cyclones ignored in the related study make a contribution to the climatology of cyclonic activity in the studied area.

The distribution of the number of occurrences of cyclogenesis is shown in Figure 3.1b. The large number of occurrences of cyclogenesis evident over the western Sea of Japan might reflect the topographic effects of the Changbai Mountains, which are located in the region of the border between China and North Korea (Chung et al. 1976; Shimizu et al. 2017; Watanabe et al. 2018; Shinoda et al. 2021). Over the offshore region east of Japan, cyclogenesis occurred predominantly along the track of the Kuroshio Current (Hanson and Long 1985; Gyakum et al. 1989; Chen et al. 1991; Yoshida and Asuma 2004; Tsukijihara et al. 2019). The concentration of cyclogenesis over the offshore region west of Hokkaido corresponds to the high frequency of the mesoscale cyclogenesis investigated in the previous studies (Asai 1988; Yanase et al. 2016; Tamura and Sato 2020). Figure 3.1c shows the linear trends of the number of cyclone passages. The number of cyclone passages increased along the eastern and southern coasts of Japan but decreased around Hokkaido. This tendency of increase along the eastern and southern coasts of Japan appears consistent with the

increase in explosive cyclone activity reported in Tsukijihara et al. (2019).

The factors controlling the tendency of decrease of cyclone passages around Hokkaido were investigated. The area in which the number of cyclone passages decreased substantially (41.25°–46.25°N, 138.75°–146.25°E; red rectangle in Figure 3.1c) was defined as the target area of the analysis. Figure 3.1d illustrates the pathways of cyclones reaching the target area. Majority of the cyclones that passed over the target area developed over nearby upwind seas, i.e., the offshore region west of Hokkaido and the western Sea of Japan near the Korean Peninsula (Figure 3.1d). Overall, 52% of the cyclones that passed over the target area developed in these two genesis regions. The remaining 48% of cyclones that passed over the target area developed over the East China Sea, northwestern Pacific, and the Far East of the Eurasian Continent. The following sections focus on those cyclones that developed over the offshore region west of Hokkaido and the western Sea of Japan and investigate their contribution to the trend of decline in the number of cyclone passages across northern Japan.

### 3.2.2 Interannual variation of cyclone activity

Cyclones that pass over and around Hokkaido are generated mainly over the offshore region west of Hokkaido and the western Sea of Japan (Figure 3.1d). Cyclones are classified into four types and are designated based on their genesis location as followings (see also Figure 3.2): Local-cyclones for those generated over and around Hokkaido, including the offshore area west of Hokkaido, Remote-cyclones for those generated over the Sea of Japan region except for the Local-cyclone, Continental-cyclones generated over the land except for Japanese Islands, and Oceanic-cyclones generated over other oceans.

Figure 3.3 shows the interannual variation of the number of cyclones passing over and around Hokkaido, and the number of occurrences of cyclogenesis. The total number of all cyclones passing over and around Hokkaido decreased significantly at a rate of −1.0 decade$^{-1}$ (black line in Figure 3.3a). The highest number of cyclone passages occurred in 1985/1986 when a strong winter monsoon brought a cold winter to East Asia (Jhun and Lee 2004). Interannual variation of the number of occurrences of Local-cyclone genesis (red line in Figure 3.3b) was almost identical to the number of cyclone passages over Hokkaido (red line in Figure 3.3a), and both showed significant trends of decrease (genesis: −0.65 decade$^{-1}$, passage: −0.62 decade$^{-1}$). In contrast, interannual variation of the number of occurrences of Remote-cyclone genesis (blue line in Figure 3.3b) and passage (blue line in Figure 3.3a) did not show significant trends (genesis: −0.06 decade$^{-1}$, passage: −0.17 decade$^{-1}$). Other cyclone passages also showed no significant trends (Continental-cyclones: −0.13 decade$^{-1}$, Oceanic-cyclones: −0.09 decade$^{-1}$) (Figure 3.3a). The observed rate of decrease in Local-cyclones genesis (−0.62 decade$^{-1}$) corresponds to 60% of that for all cyclones passing over and around Hokkaido (−1.0 decade$^{-1}$). Furthermore, the interannual variation of all cyclone passages over Hokkaido and the genesis of Local-cyclones are highly correlated with a correlation coefficient of 0.62. The number of passages of Continental-cyclones is also highly correlated with All passages (correlation coefficient of 0.59), but the decadal trend of the number of cyclone passages is not significant (−0.13 decade$^{-1}$). These results suggest that reduction in Local-cyclone genesis was the main reason for the observed decrease in the number of cyclone passages over and around Hokkaido.

Synoptic-scale conditions at the cyclogenesis and the time of passage over Hokkaido for each

type of cyclone are shown in Figures 3.4, 3.5, and 3.6. Here, the time of passage refers to the time when the cyclone first reached around Hokkaido (red rectangle in Figure 3.1c). There is little difference in the synoptic-scale condition of the Local-cyclone between the cyclogenesis (Figures 3.4a and 3.4c) and the passage (Figures 3.4b and 3.4d) because its region of cyclogenesis (Figure 3.1b) overlaps with the region around Hokkaido (red rectangle in Figure 3.1c). Local-cyclones were generated on the west-east high and low surface pressure pattern consisting with the Siberian high and the Aleutian low (Figure 3.4a), and the upper-level trough on the eastern end of the Eurasian continent (Figure 3.4c). These synoptic-scale conditions are similar to the condition at the mesoscale cyclogenesis in this region (e.g., Yanase et al. 2016). However, because cyclones occur in this region at various synoptic-scale conditions (e.g., Yanase et al. 2016), the composite fields in Figure 3.4 might be an average of the different fields. At the Remote-cyclone genesis, synoptic-scale low pressure was located on the Changbai Mountains (Figure 3.5a). This synoptic-scale low pressure induces cyclogenesis on the east of the Changbai Mountains (Watanabe and Niino 2014; Shimizu et al. 2017; Watanabe et al. 2018; Shinoda et al. 2021). In addition, as the upper-level trough moved eastward, Remote-cyclones developed and reached over Hokkaido (Figures 3.5b and 3.5d). Therefore Remote-cyclone is considered to be extratropical cyclones that originated in the topographic effect of the Changbai Mountains. Since the synoptic-scale conditions of Continental- and Oceanic-cyclones when they pass over and around Hokkaido (Figure 3.6) were similar to that of the Remote-cyclone (Figure 3.5), these cyclones are also considered to be extratropical cyclones.

Here, this study describes the characteristics of each cyclone. Horizontal size of each cyclone type is shown in Figure 3.7. Here, the horizontal size of the cyclones is defined as the vortex area determined using relative vorticity at 900 hPa (Section 2.4). It can be seen that more than half (54%, 752 cases) of the total cyclones have small vortex areas of less than $35 \times 10^4$ km$^2$ (Figure 3.7). The area $35 \times 10^4$ km$^2$ is approximately equivalent to 4.5 times the land area of Hokkaido ($7.8 \times 10^4$ km$^2$). Proportions of cyclones that have such small vortex area are different for each cyclone type (Local-cyclone: 72% (345 cases); Remote-cyclone: 42% (116 cases); Continental-cyclone: 49% (215 cases); Oceanic-cyclone: 39% (76 cases)). This implies that most of the Local-cyclones did not develop as large as other cyclone types. Figure 3.8a shows the duration of the cyclones. All cyclone (white bars) and Local-cyclone (red bars) tend to have shorter lifespans. The short duration cyclones ($\leqq$ 2 days) occupy 39% (572 cases) for all cyclone and 63% (301 cases) of the Local-cyclones. In contrast, majority (70%, 190 cases) of the Remote-cyclones have duration longer than 2 days. Figure 3.8b shows the relation between the duration and horizontal size of the cyclones. Cyclones with a short duration were relatively small. These results clearly show that most of the Local-cyclones were relatively short-lived and small-scale cyclones like polar mesoscale cyclones.

### 3.3. Discussion and conclusion

Cyclone tracking, including mesocyclones, revealed that the number of cyclones passing over and around Hokkaido had decreased significantly since the 1960s. There were the two major genesis regions of the cyclones that reached Hokkaido: (1) the offshore region west of Hokkaido and (2) the western Sea of Japan. In this study, the former cyclone is referred to as Local-cyclone

and the latter as Remote-cyclone.

The genesis number of Local-cyclones showed significant tendency of decrease, while the Remote-cyclone did not vary (Figure 3.3). Most of the Local-cyclones are relatively small cyclones associated with west-east high and low surface pressure patterns (Figures 3.4a and 3.7), and most of them are short-lived (Figure 3.8a). These characteristics are consistent with the mesocyclones generated over the offshore region west of Hokkaido (e.g., Watanabe et al. 2017), suggesting that most of the Local-cyclones are the mesocyclone. Over the western Sea of Japan, the lee side of the Changbai Mountains has many cyclogeneses (Watanabe and Niino 2014; Shimizu et al. 2017; Watanabe et al. 2018; Shinoda et al. 2021). Among them, the mesocyclones generated by cold air advection from the continent are relatively small, short lifespan, and move southward over the Sea of Japan (Watanabe et al. 2018). Thus, the mesocyclones, which are formed in the western Sea of Japan, cannot reach Hokkaido. In addition, synoptic-scale cyclones located in the west of the Changbai Mountains can cause cyclogenesis over the western Sea of Japan (Shimizu et al. 2017). Analyses of the atmospheric conditions showed that the synoptic-scale cyclone is located on the Changbai Mountain at the time of cyclogenesis for the Remote-cyclone (Figure 3.5a). The Remote-cyclone developed and moved east toward Hokkaido (Figure 3.5b), accompanied by the upper-level trough (Figure 3.5d). Therefore, most of the Remote-cyclones are considered to be eastward-moving extratropical cyclones generated by the synoptic-scale cyclone and Changbai Mountains. Results in this section are summarized in Figure 3.9. The number of Local-cyclones (i.e., cyclones that originated around Hokkaido and reached over Hokkaido) was significantly decreased ($-0.62$ decade$^{-1}$). In contrast, other cyclones (i.e., cyclones that originate in distant areas and pass

over Hokkaido) did not show a significant decrease. Therefore, the decrease in the number of cyclone passages over and around Hokkaido is considered to be mainly due to the decrease in the number of cyclogeneses around Hokkaido.

This analysis suggests that the decrease in the number of cyclone passages around Hokkaido is due to a decrease in the mesoscale cyclogenesis over the offshore region west of Hokkaido. However, the mesocyclones are formed under the various types of synoptic-scale conditions (e.g., Yanase et al., 2016). Therefore, the composite fields in Figure 3.4 are also likely to be a composite of various types of synoptic-scale conditions, and it is not clear which types of synoptic-scale conditions are attributable to the decrease in the number of cyclogeneses. In order to clarify the factors behind the decrease in the number of cyclogeneses over the offshore region west of Hokkaido, it is necessary to investigate the interannual variations of the number of cyclogeneses on the various types of synoptic-scale conditions.

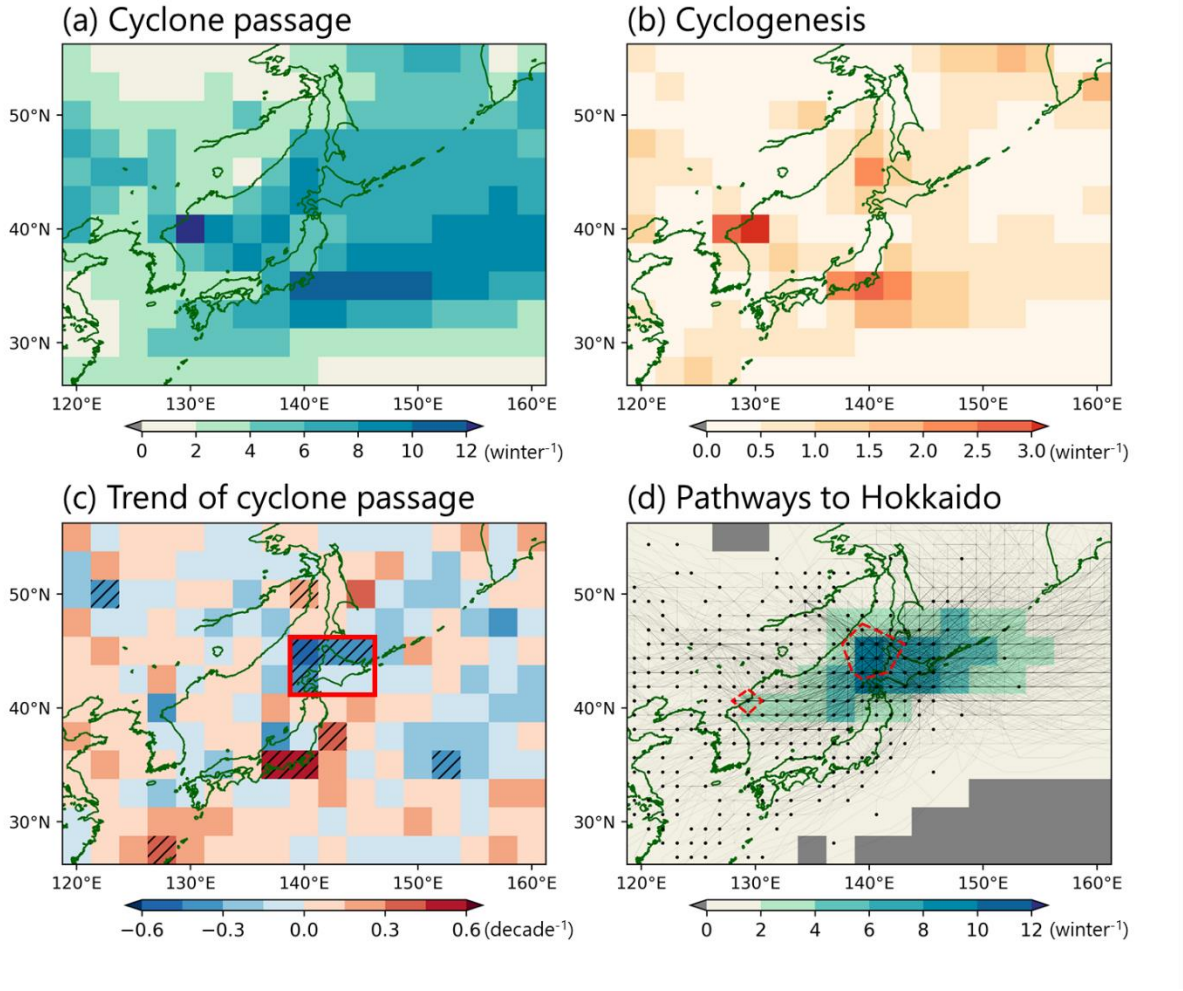


Figure 3.1. Climatology of winter cyclone activity around Japan per 2.5° grid from 1958–2019: (a) number of cyclone passages, (b) occurrence of cyclogenesis, (c) linear trend of the number of cyclone passages, and (d) number of cyclone passages that reached Hokkaido (red rectangle in (c)). Red broken lines in (d) indicate areas in which the number of occurrences of cyclogenesis exceeds 1.0 winter$^{-1}$, and thin black lines indicate the pathways of cyclones. Hatched grids in (c) indicate the trend exceeding the 95% confidence level in the t-test for ordinary least squares regression.

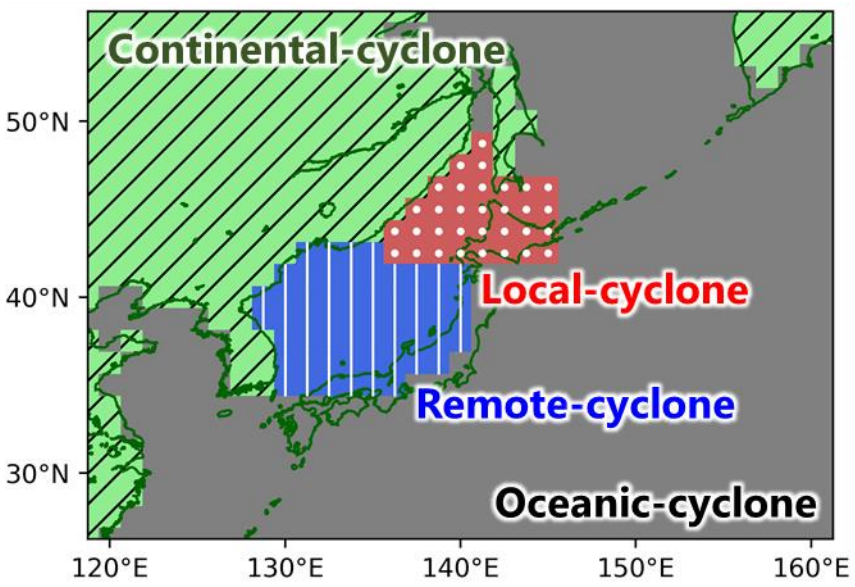


Figure 3.2. Map showing the definition of cyclone classification. Local-cyclone is defined as the cyclone generated over the offshore area west of Hokkaido and around Hokkaido (red shading and white dot). Remote-cyclone is defined as the cyclone generated over the Sea of Japan (blue shading and white line). Continental-cyclone is defined as the cyclone generated over the land except for Japanese Islands (light green). Cyclone generated over the other oceans is defined as the Oceanic-cyclone (gray).

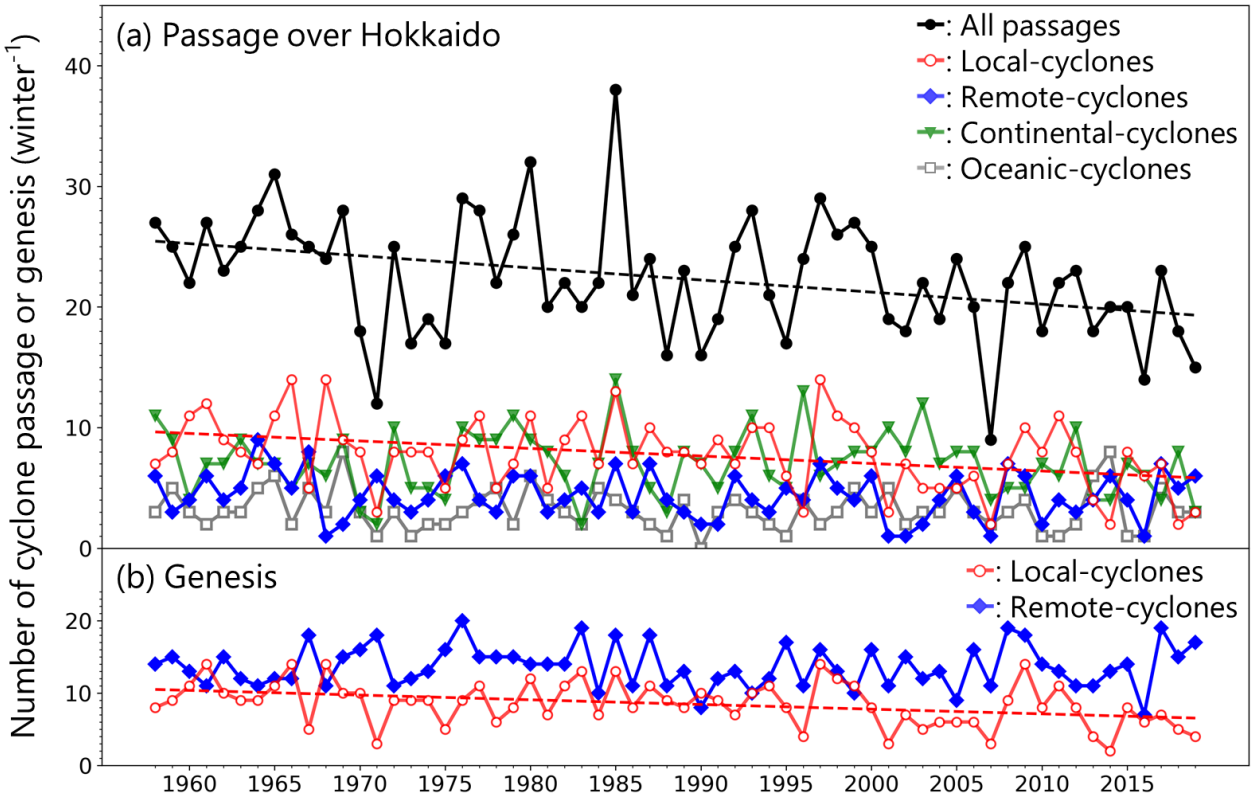


Figure 3.3. Interannual variations of cyclone passage and of genesis. (a) Number of cyclones passing over the Hokkaido area (black line) and its decomposition into four cyclone types. (b) Number of geneses for Local-cyclones (red line and circle) and Remote-cyclones (blue line and rhombus). Broken straight lines indicate significant trends exceeding the 95% confidence level in the t-test for ordinary least squares regression.

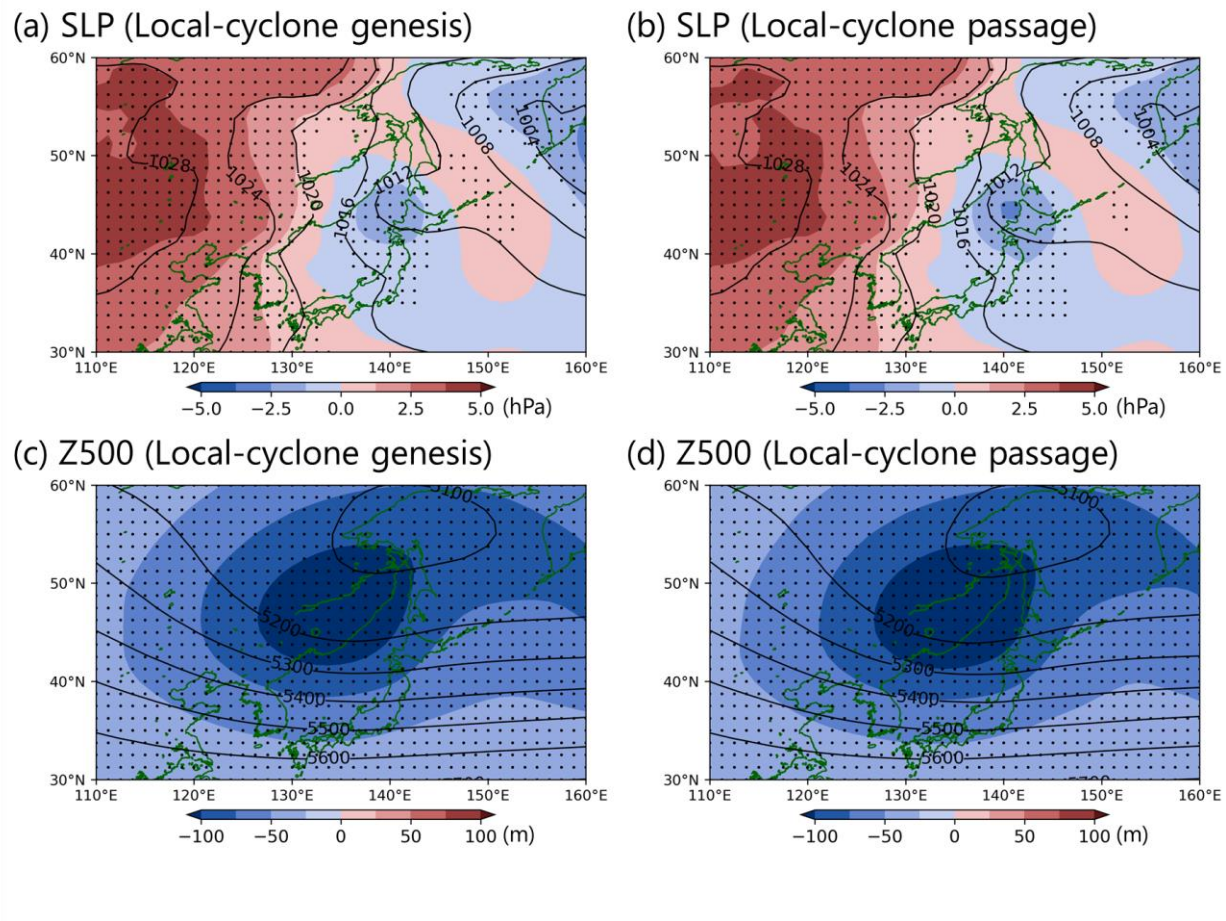


Figure 3.4. Composite of SLP (a and b) and geopotential height fields at 500-hPa level (c and d) for Local-cyclone genesis (a and c) and passage (b and d). Contours show SLP and geopotential height. Colors indicate deviations from the daily climatology. Hatching indicates the difference is significant at the 95% confidence level (Welch's t-test).

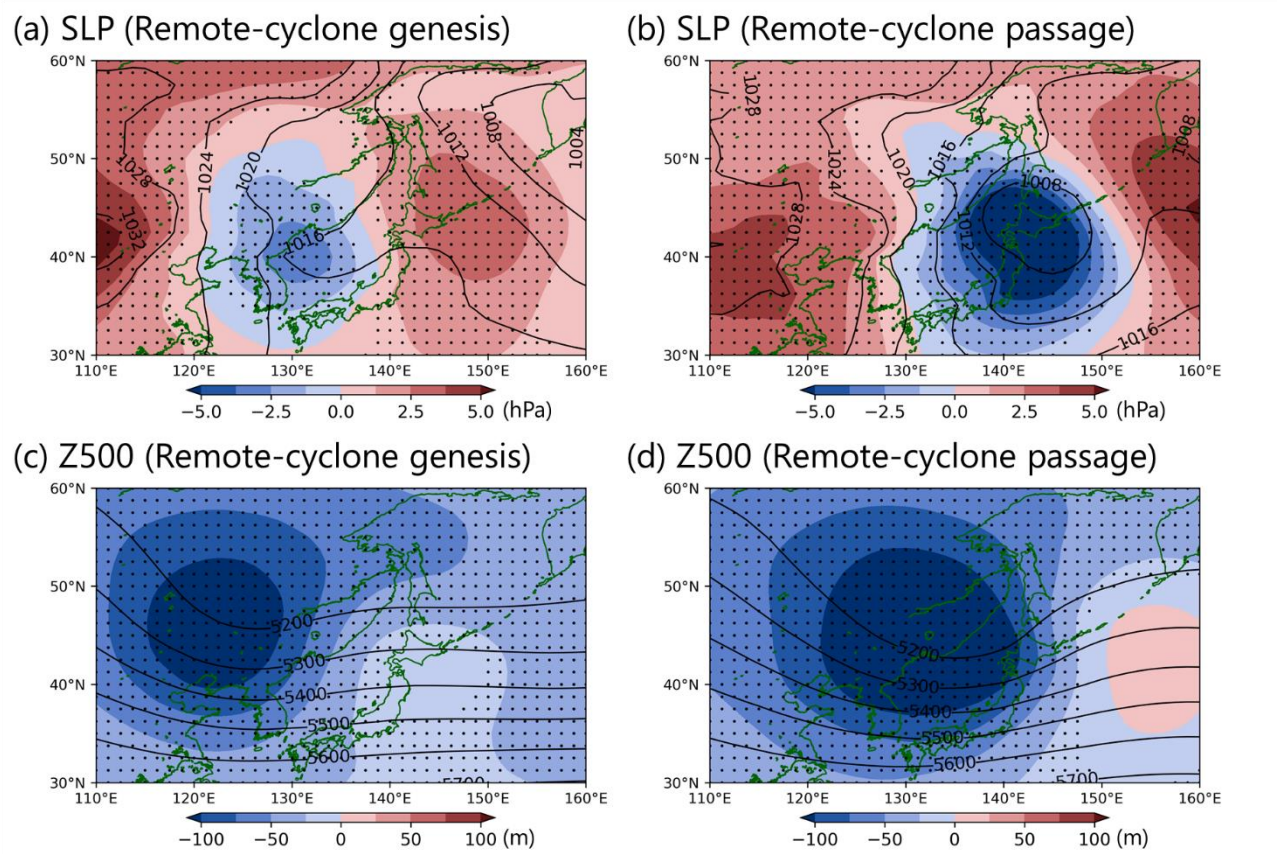


Figure 3.5. As in Figure 3.4 but for the Remote-cyclone.

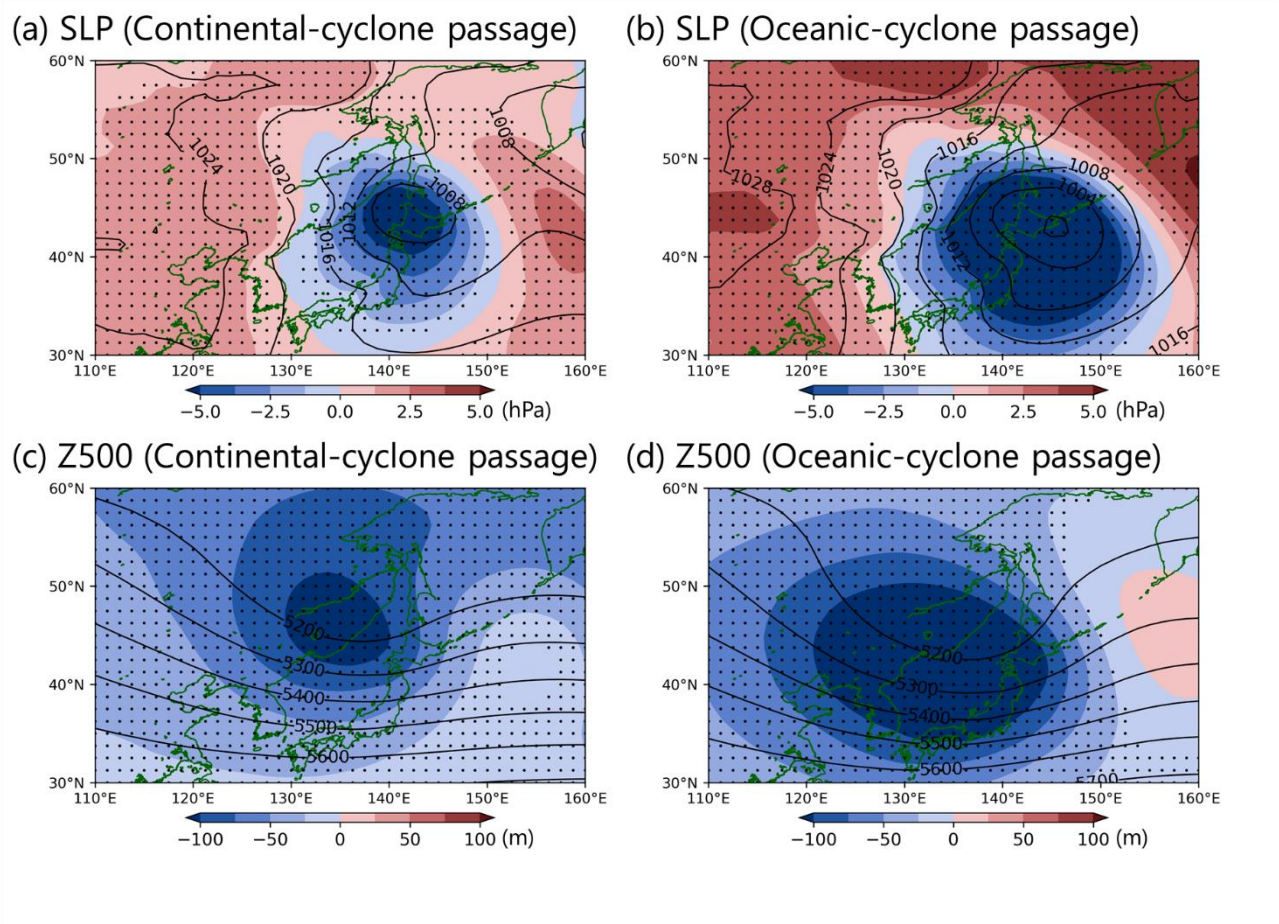


Figure 3.6. As in Figure 3.4 but for the Continental-cyclone and Oceanic-cyclone only for the passage.

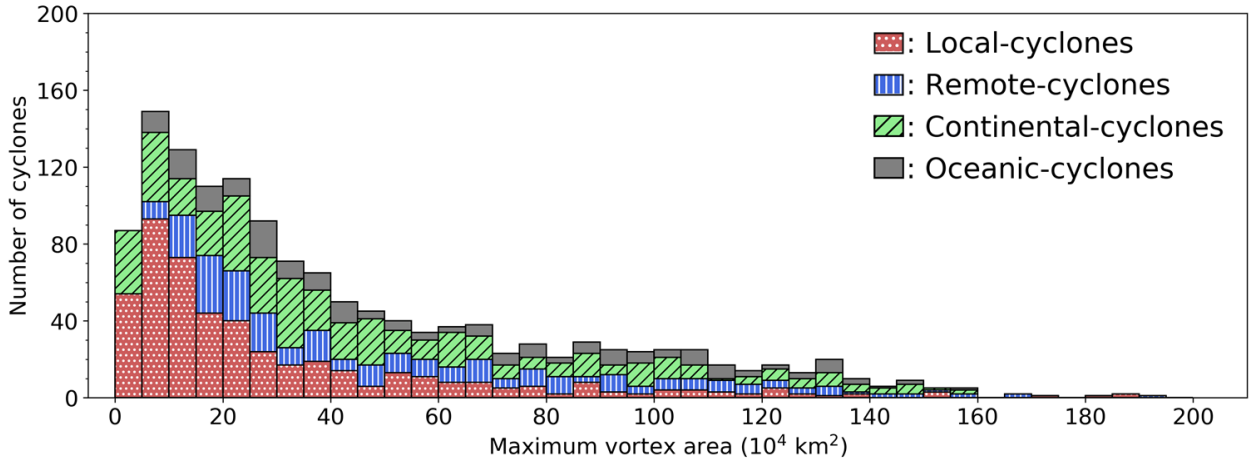


Figure 3.7. Histogram of the maximum vortex area for each cyclone. Maximum vortex area is defined based on the relative vorticity at 900 hPa level (Section 2.4).

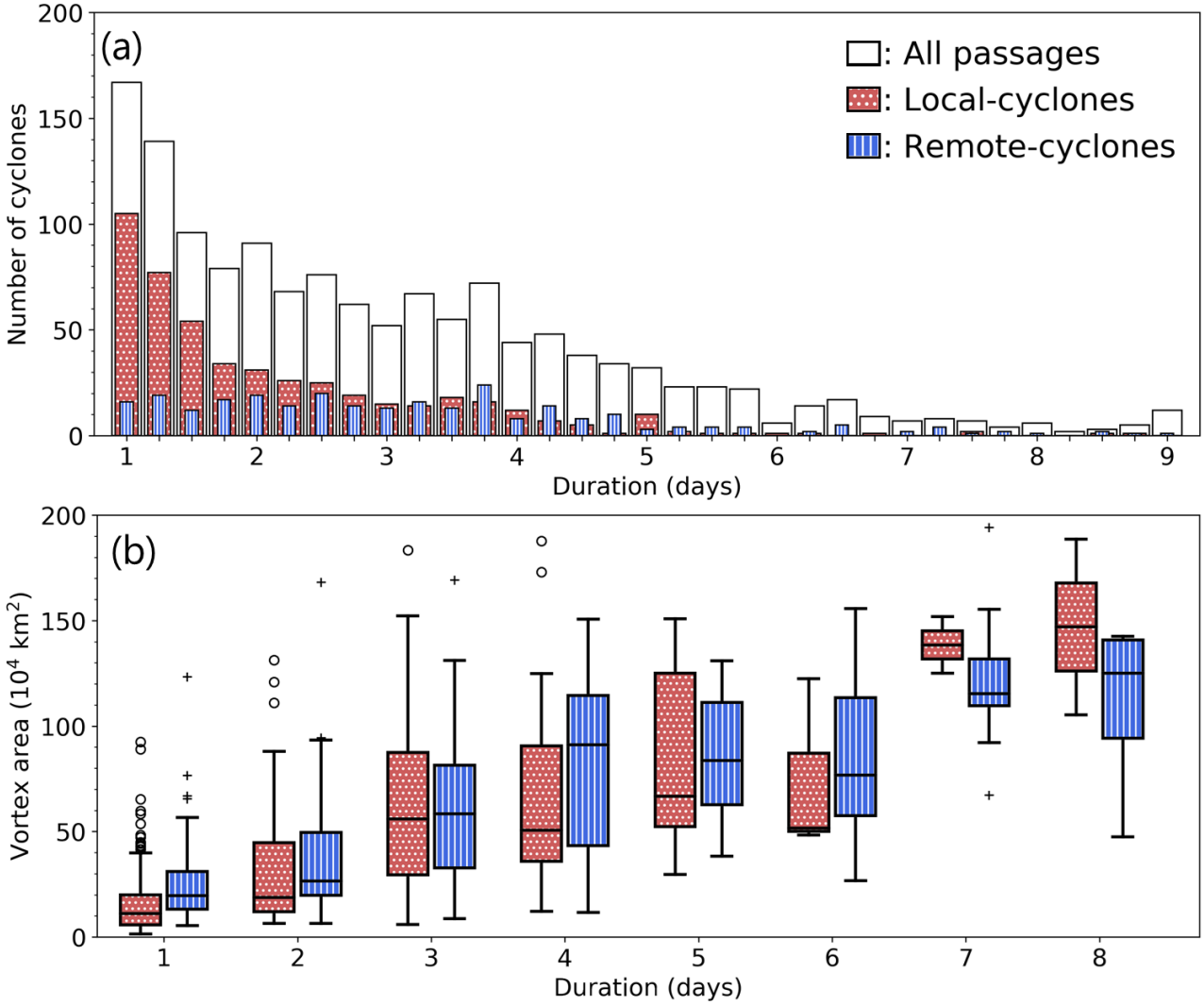


Figure 3.8. (a) Histogram for the duration of the cyclone passing over Hokkaido (white: all cyclone, red: Local-cyclone, blue: Remote-cyclone, see Figure 3 for definition). (b) Box plot for the maximum vortex area against the duration of the cyclone. Box represents interquartile range and the middle horizontal line in the box means median. Whisker indicates the range of ±1.5 times the interquartile range, and the values outside of this range are plotted as outliers (circle and plus mark).

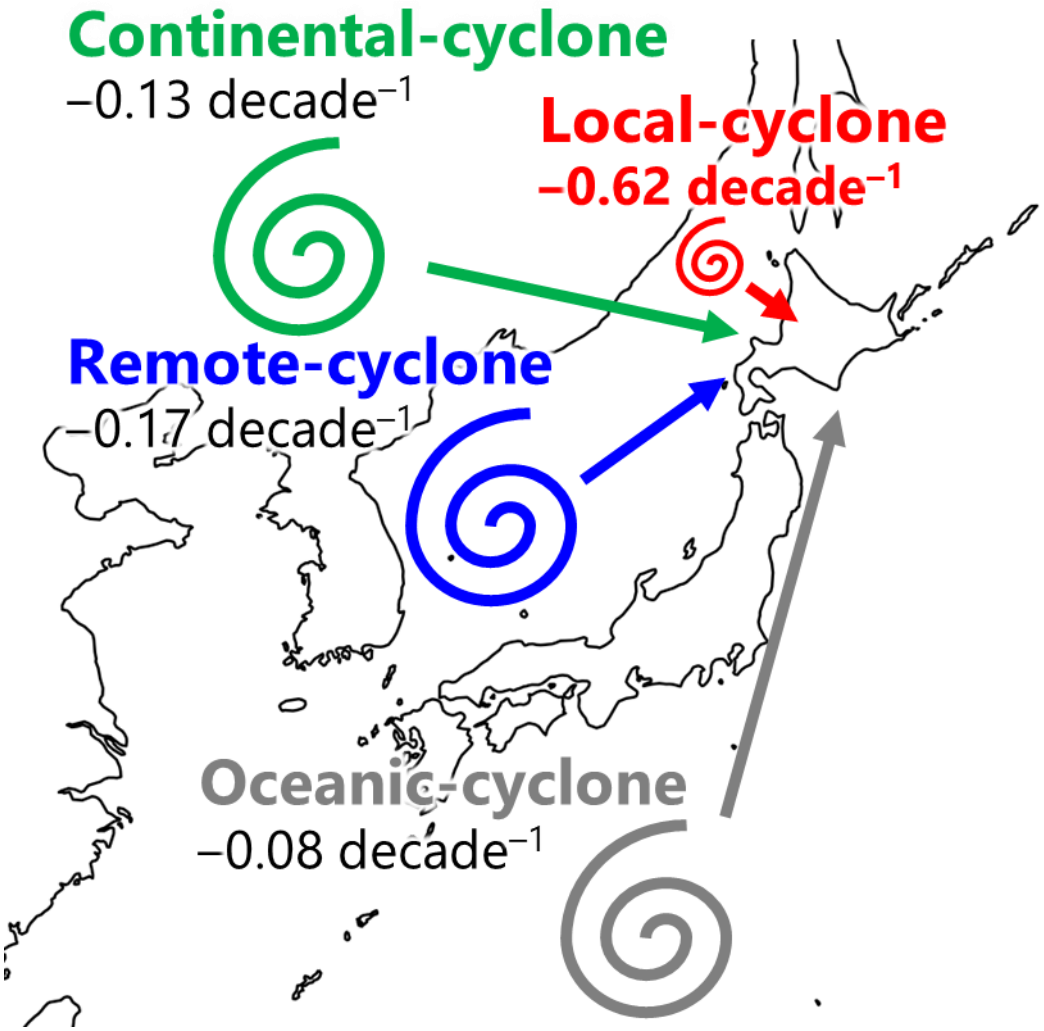


Figure 3.9. Schematic illustration of the decadal trend of the number of cyclone passages over Hokkaido for each cyclone. The numbers in the arrows show the trend of the number of cyclones passing over and around Hokkaido (decade$^{-1}$).

# 4. Surface weather pattern analysis in winter season around Hokkaido

## 4.1 Introduction

Chapter 3 revealed that the number of cyclone passages around Hokkaido is significantly decreased, and the tendency of decrease is mainly due to the decrease of cyclogenesis over and around Hokkaido (Local-cyclone) especially in the offshore region west of Hokkaido. Because of the high similarity of the synoptic-scale atmospheric conditions, most of the Local-cyclones are likely to the mesoscale cyclones.

West-east high and low surface pressure pattern, the averaged synoptic-scale atmospheric condition at the time of the occurrence of the Local-cyclone, was consistent with the typical pressure pattern in which the mesocyclones occur over the offshore region west of Hokkaido (Yanase et al. 2016). The synoptic-scale surface low pressure causes lower-level cyclonic horizontal wind shear over the offshore region west of Hokkaido and develops mesocyclone (Watanabe et al. 2017). However, mesocyclones also occur under the opposite surface pressure patterns (west-east low and high surface pressure) induced by the approaching upper-level trough. In this condition, upper-level baroclinicity is a main agent for mesoscale cyclone development (Yanase et al. 2016). Therefore, since mesoscale cyclones occur in various synoptic-scale conditions in this region, there remain questions for the relationship between the synoptic-scale conditions and decrease of the Local-cyclones.

In this chapter, characteristics of the synoptic-scale conditions related to the cyclogenesis over the offshore region west of Hokkaido (Local-cyclone) are investigated to clarify the factors of the decreasing tendency of the cyclogenesis. Weather pattern classification described in Section 2.4 was

conducted, and the analyses in this chapter are based on that classification.

## 4.2 Result

### 4.2.1 Weather pattern analysis

Figure 4.1 shows standardized SLP patterns produced by the SOM. To focus on the synoptic-scale pressure patterns around Hokkaido, the analysis targets the domain from Northeast Asia to the Sea of Okhotsk and part of the northwestern Pacific Ocean. The pressure pattern at each node is characterized by the contrast between low pressure (blue shading in Figure 4.1) and high pressure (red shading in Figure 4.1). Nodes in the three left-hand columns (columns 1–3 in Figure 4.1) include synoptic-scale low pressure located northeast/southeast of Hokkaido and high pressure over western/southwestern areas of the domain. Upper-right nodes (columns 4 and 5 and rows a and b in Figure 4.1) include relatively weak low pressure close to Hokkaido. Lower-right nodes (columns 4 and 5 and rows c and d in Figure 4.1) include weak low pressure located to the west/north of Hokkaido and high pressure to the southeast/south of Hokkaido. The frequency of the nodes in the three left-hand columns (6.9 days), which include the eastern low pressure and western high pressure, is higher than that in the two right-hand columns (4.9 days). This clear low–high pressure pattern with high frequency indicates that the nodes in the three left-hand columns represent the typical winter surface pressure pattern of northeast Asia, comprising the Aleutian Low and the Siberian High.

To ensure the above interpretation is reasonable, trained 5 × 4 SLP patterns were classified by K-means clustering and three clusters were obtained: left-hand 12 nodes in columns 1–3 (3 × 4 nodes), upper-right four nodes (2 × 2 nodes), and lower-right four nodes (2 × 2 nodes) (Figure 4.1).

These clusters are defined as Cluster 1, Cluster 2, and Cluster 3 as indicated by red, blue, and green rectangles in Figure 4.1, respectively. This classification consisting of left-hand columns, upper-right nodes, and bottom-right nodes, is robust regardless of SOM settings (4 × 4, 4 × 5, and 5 × 5 settings were tested; not shown). Figure 4.2 summarizes the counts of Local-cyclone genesis for every 6-hourly snapshot categorized into each SOM node (Figure 4.1). The average number of occurrences of Local-cyclone genesis under the typical winter pressure pattern (Cluster 1) is 28 cases, while that of the remainder of the pattern, upper-right nodes (Cluster 2) is 16 cases, and lower-right nodes (Cluster 3) is 19 cases, respectively. Hereafter, Local-cyclones generated under synoptic conditions corresponding to Cluster 1, Cluster 2, and Cluster 3 are defined as C1-cyclones, C2-cyclones, and C3-cyclones, respectively. The probability of cyclogenesis at each node can be obtained from the total number of occurrences of cyclogenesis (Figure 4.2) divided by the number of days (Figure 4.1). There is no significant difference in the probability of Local-cyclone genesis with respect to the background surface pressure pattern (C1-cyclones: 6.6%, C2-cyclones: 6.2%, C3-cyclones: 6.5%).

### 4.2.2 Synoptic-scale atmospheric conditions

Figures 4.3a–c shows the synoptic-scale conditions for Local-cyclone genesis for each node. In this section, the nodes in the three left-hand columns in which the SLP anomaly fields (Figure 4.3a) include the western high pressure anomaly (Siberian high) and the eastern low pressure anomaly (Aleutian low) are highlighted. The upper-level pressure patterns are characterized by the low pressure anomaly (upper-level trough) located over the offshore region west of Hokkaido (Figure

4.3b). The lower-level temperature fields show strong cold air advection over the Sea of Japan, which reflects the cold air outbreaks from the continent induced by the Siberian High and the Aleutian Low (Figure 4.3c). These atmospheric conditions coincide with the synoptic-scale conditions known to enhance mesocyclone genesis over the offshore region west of Hokkaido (e.g., Ninomiya et al. 1996; Watanabe et al. 2017). Therefore, Local-cyclones generated under the synoptic conditions assigned in the three left-hand columns of the SOMs are likely to represent mesocyclones produced by cold air outbreaks from the continent.

Considering the SOM nodes aligned in the two right-hand columns in Figure 4.3a, the surface low pressure anomaly is located close to Hokkaido or over the Eurasian Continent. The upper-level trough extends over eastern parts of the Eurasian Continent (Figure 4.3b). Lower-level temperature fields show warm advection from the Pacific Ocean or the Sea of Japan toward Hokkaido (Figure 4.3c). Especially in relation to the upper right four nodes (4,a), (5,a), (4,b), and (5,b), the synoptic-scale low pressure over Hokkaido (Figure 4.3a) encourages warm advection from the Pacific Ocean and cold advection from the Eurasian Continent over the offshore region west of Hokkaido (Figure 4.3c). These advective motions intensify the low-level horizontal temperature gradient embedded within the cyclonic circulation of the synoptic-scale low pressure, causing cyclogenesis over the offshore region west of Hokkaido (e.g., Ninomiya et al. 1993). The upper right four nodes show relatively large surface low pressure over the offshore region west of Hokkaido, and a corresponding mid-tropospheric trough is evident to the west of the surface low pressure (Figures 4.3a and 4.3b). Therefore, Local-cyclones at these nodes can be developed through baroclinic instability (Yanase et al. 2016).

Another cyclone-formation process that might be relevant in such a synoptic condition is lee-cyclogenesis, which is found to dominate the offshore region west of Hokkaido owing to the presence of mountains on the eastern coast of the Eurasian Continent (the Sikhote-Alin mountain range in Figure 1.1) (e.g., Chung et al. 1976). Surface low pressure over the Eurasian Continent shown in the bottom right four nodes can cause cyclogenesis over the offshore region west of Hokkaido through this process (Figure 4.3a).

The characteristics of the atmospheric conditions for the C1-, C2- and C3-cyclone genesis are summarized in Figures 4.4, 4.5, and 4.6. C1-cyclone is characterized as a small cyclone feature generated locally over the offshore region west of Hokkaido, as evidenced by northwestward extension of the low pressure area (contour) shown in Figure 4.4a. C1-cyclone tends to develop between the synoptic-scale low pressure anomaly located over the Kamchatka Peninsula and the Siberian High (Figure 4.4a). Upper-level trough (Figure 4.4b) and the cold air advection (Figure 4.4c) exist over the offshore region west of Hokkaido. These are the typical conditions of mesoscale cyclogenesis developed in the northerly wind caused by the synoptic-scale cyclone to the east of Hokkaido and northwesterly winter monsoon (Yanase et al. 2016; Watanabe et al. 2017). In contrast, C2-cyclone is characterized as a relatively large-scale cyclone with a high pressure anomaly located over the south of the Kamchatka Peninsula (Figure 4.5a) and an upper-level trough over the continent (Figure 4.5b). These conditions are similar to the mesocyclones developing through baroclinic interaction (Yanase et al. 2016). Since there is a surface low pressure anomaly located over the continent at the time of C3-cyclone genesis (Figure 4.6), it is possible that C3-cyclone is a cyclone associated with secondary cyclogenesis such as lee cyclogenesis (Chung et al. 1976).

Interannual variation of the cyclogenesis for each cluster (Figure 4.7a) reflects that the number of occurrences of C1-cyclone genesis (red) is significantly decreased (−0.54 decade$^{-1}$; p = 0.003), while the change in C2-cyclone genesis (blue) (−0.08 decade$^{-1}$; p = 0.26) and C3-cyclone genesis (green) (0.002 decade$^{-1}$; p = 0.98) are not significant. These trends are similar in the other SOM settings. Figure 4.7b shows the relation between the number of occurrences of C1-cyclone genesis and the frequency of Cluster 1. The frequency of occurrence of the weather pattern for the C1-cluster is decreased (−0.70 decade$^{-1}$; p = 0.17) but this trend depends on SOM settings, meaning that the decadal trend of the likelihood of a west-east high and low surface pressure pattern (Figure 4.4a) is weak. However, the ratio of C1-cyclone genesis to the number of days of Cluster 1, i.e., C1-cyclone number divided by the number of Cluster 1 snapshots, shows a significant tendency of decrease (−0.15 decade$^{-1}$; p = 0.003). This trend is robust regardless of SOM settings. These results suggest that the decrease in the number of occurrences of cyclogenesis over the offshore region west of Hokkaido (C1-cyclones) is not only attributable to the reduction in the frequency of occurrence of the favorable pressure pattern.

C1-cyclones occur in association with lower-level cold air outbreaks (Figure 4.4c). In considering the interannual variation in the frequency of the cold air outbreaks over the offshore region west of Hokkaido, CAO-index is utilized that defined as follows:

$$\text{CAO-index}_{850} \equiv \theta_{\text{skt}} - \theta_{850}$$

where $\theta_{850}$ the potential temperature at 850 hPa level, and $\theta_{\text{skt}}$ the surface skin potential temperature. This index is utilized in many studies to focus on the air–sea temperature difference induced by the cold air outbreaks (Kolstad et al. 2009; Kolstad 2017; Terpstra et al. 2021). The frequency of cold

air outbreaks was defined as the number of events with the averaged CAO-index$_{850}$ over the sea in the target area (Figure 3.2; red) of more than +1 standard deviation. Similarly, the frequency of upper-level trough events was defined as the number of events with the geopotential height at 500 hPa averaged over the target area of less than −1 standard deviation. Figure 4.7c indicates the frequency of occurrence of cold air outbreaks (light blue line) and upper-level trough (violet line) in Cluster 1. The frequency of the cold air outbreaks (light blue) showed a weak decrease (−2.2 decade$^{-1}$; p = 0.09). The frequency of the upper-level trough event also decreases (−0.5 decade$^{-1}$; p = 0.6), but both trends are not statistically significant. However, the averaged CAO-index$_{850}$ at the events of cold air outbreak (black line) decreased significantly at the 95% confidence level (0.05 decade$^{-1}$; p < 0.005). This decreasing trend is observed in other SOM settings. It suggests that the intensity of the cold air outbreak in this region has weakened in recent years. The correlation against the interannual variation of C1-cyclones genesis (red line in Figure 4.7a) for the frequency of cold air outbreaks (correlation coefficient of 0.19; p = 0.14), the trough events (correlation coefficient of 0.09; p = 0.5), and the average CAO-index$_{850}$ (correlation coefficient of 0.23; p = 0.07) are not statistically significant. Although the decisive factors are not found, the decrease and weakening in the cold air outbreak events on the west-east high and low surface pressure pattern might have suppressed cyclogenesis in this region, resulting in the reduction in the number of cyclones passing over and around Hokkaido.

### 4.2.3 Impact of data assimilation on the decadal trend of cyclone activity

According to the analysis in Chapters 3 and 4, the number of cyclone passages around Hokkaido has been decreasing since the 1960s. However, because of satellite data assimilation since

November 1972, quality of the JRA-55 data set is not uniform during the study period. Therefore, the observed decreasing tendency of the number of cyclones in this study may have included the effect of data assimilation. In this section, these effects on the cyclone activities are evaluated by comparing the cyclone activity in JRA-55 and JRA-55C. A comparison of the cyclone activity between the JRA-55 and JRA-55AMIP is also conducted to figure out the characteristics of the forecast model and the effect of external forcings such as SST, greenhouse gases, and aerosols used in these datasets.

Climatological features of winter cyclone activity around Japan in each dataset (JRA-55, JRA-55C, and JRA-55AMIP) are shown in Figure 4.8. For comparison, the same period (1958–2011 winters) is used. The distributions of cyclone passage and cyclogenesis in JRA-55 (Figures 4.8a and 4.8b) and JRA-55C (Figures 4.8d and 4.8e) are similar to the original results shown in Chapter 3 (Figures 3.1a and 3.1b). In JRA-55AMIP, the frequency of cyclone passage is relatively higher in the western Sea of Japan and lower in the northwestern Pacific and the offshore region west of Hokkaido (Figures 4.8g and 4.8h). Trends of cyclone passage in JRA-55 and JRA-55C are also similar, but the decreasing tendencies around Hokkaido are not significant (red rectangles in Figures 4.8c and 4.8f). In this area, a significant decline trend was observed in the original result (Figure 3.1c), indicating that the decreasing tendency in the number of cyclone passages around Hokkaido has been enhanced after 2012. In the JRA-55AMIP, the number of cyclone passages around Hokkaido is relatively small, but some grids show a significant decreasing tendency (Figure 4.8i). These results suggest that the decreasing tendency of cyclone passage around Hokkaido produced by the model (JRA-55AMIP) was mitigated by the data assimilation.

Figure 4.9 shows interannual variations of the cyclone passage. Comparison of the interannual variation is summarized in Table 4.1. The variation of all cyclone passages in JRA-55C is similar to that of JRA-55 (Figure 4.9a) and these are significantly correlated with a correlation coefficient of 0.82 (Table 4.1). The interannual variations of cyclone passages in JRA-55C are also significantly correlated with JRA-55 (Figure 4.9a–e, Table 4.1). The similarity of the interannual variation between JRA-55 and JRA-55C indicates that the effect of the assimilation of satellite observation data on the number of cyclone passages is small. This lends credibility to the cyclone activity before 1972, when only conventional observations were assimilated.

On the other hand, the interannual variations of cyclone passages in JRA-55AMIP are different from JRA-55. Focusing on the period from 1958 to 1971, the number of all passages around Hokkaido (Figure 4.9a) in JRA-55AMIP is smaller than the JRA-55 (JRA-55: 341, JRA-55AMIP: 300). Most of this difference is caused by Local-cyclone (JRA-55: 126, JRA-55AMIP: 94), with almost no differences in Remote-cyclone (JRA-55: 70, JRA-55AMIP: 65), Continental-cyclone (JRA-55: 93, JRA-55AMIP: 91), and Oceanic-cyclone (JRA-55: 52, JRA-55AMIP: 50). This result suggests that the model underestimates the number of Local-cyclones geneses.

Comparisons of the number of C1-cyclone geneses, CAO-index$_{850}$, and trough events are shown in Figure 4.10. Decadal trends (1958–2011) of the interannual variations of C1-cyclone genesis (Figure 4.10a) are similar, and all trends are not significant (JRA-55: −0.34 decade$^{-1}$, JRA-55C: −0.29 decade$^{-1}$, JRA-55AMIP: −0.36 decade$^{-1}$). Correlation with JRA-55 is significant only for JRA-55C (JRA-55C: 0.70, JRA-55AMIP: −0.007). Therefore, the effect of the assimilation of the satellite datasets on the decreasing trend in the number of cyclogeneses around Hokkaido

shown in this study is likely to be small. Average CAO-index$_{850}$ at the at the CAO events showed a significant decreasing trend for JRA-55 and JRA-55C but not for JRA-55AMIP (JRA-55: −0.04 decade$^{-1}$, JRA-55C: −0.04 decade$^{-1}$, JRA-55AMIP: 0.009 decade$^{-1}$). Decadal trends of the number of CAO events (JRA-55: −1.6 decade$^{-1}$, JRA-55C: −2.0 decade$^{-1}$, JRA-55AMIP: 1.4 decade$^{-1}$) and the number of trough events (JRA-55: 0.1 decade$^{-1}$, JRA-55C: 0.2 decade$^{-1}$, JRA-55AMIP: 3.0 decade$^{-1}$) are not significant (Figure 4.10b–c). Correlations of the interannual variations in the atmospheric conditions between JRA-55 and JRA-55C are high (average CAO-index$_{850}$: 0.85, CAO events: 0.89, trough events: 0.96). These high correlations suggest that assimilation of conventional observations is likely to determine the number of cyclone formations around Hokkaido. Comparing the number of cyclogeneses between 1958 and 1971, JRA-55 (88 geneses) has more cyclogenesis than JRA-55AMIP (68 geneses). In this study, the reason for the relatively small number of cyclones in JRA-55AMIP is not figured out. Kanno et al. (2016) showed that the JRA-55AMIP tends to underestimate the warming trend in the Arctic and overestimate the decrease in cold air mass around Japan. However, the CAO-index$_{850}$ in JRA-55AMIP (Figure 4.10b) did not show a decreasing trend. This difference may be due to the difference between the CAO-index$_{850}$ and the cold air mass. Additionally, the CAO-index$_{850}$ used in this study was calculated only for the specific pressure pattern (west-east high and low surface pressure pattern), whereas the cold air mass (Kanno et al. 2016) is a winter average (December to February). The factor is unclear, but that may also reflect differences in the pressure pattern.

## 4.3 Discussion and conclusion

Synoptic-scale weather pattern classification based on the SOM approach showed that

cyclogenesis over the offshore region west of Hokkaido is mainly caused by the cold air outbreaks from the Eurasian Continent induced by the west-east high and low surface pressure pattern. Mesocyclones tend to form preferentially in an area with a low-level horizontal temperature gradient induced by cold air outbreaks, and they develop in association with instabilities triggered by upper-level intrusion of cold air when the trough migrates (e.g., Ninomiya et al. 1996; Kolstad 2011; Watanabe et al. 2017). In this region, the intensity of the cold air outbreaks (CAO index) is significantly decreased (Figure 4.7c; black line), and the interannual variation in the frequency of cold air outbreaks showed a weak tendency of decrease (Figure 4.7c; light blue line). Hence, the decreasing chance of occurrence of such favorable conditions is probably the reason for the significant reduction in the number of cyclones passing over and around Hokkaido over the past 60 years. The trend of decrease and weakening of cold air outbreaks is likely related to global warming.

The interannual variations of the cyclogenesis associated with cold air advection over the offshore west of Hokkaido were similar between JRA-55 and JRA-55C (Figure 4.10a). This result suggests that the interannual variation in the genesis and development of the cyclones around Hokkaido is determined by the assimilation of conventional observations. This might be because the conventional observation can capture the atmospheric conditions over Eurasia, which is located on the upwind side of Hokkaido. In other words, the satellite data assimilation may not be necessary to reproduce the occurrence of cold air advection and passage of the upper-level trough over Hokkaido if conventional observations are available.

Enhanced heat and moisture fluxes associated with high sea surface temperature (SST)

promote the development of mesocyclones (Watanabe et al. 2017). Despite SST warming in recent years, the number of occurrences of cyclogenesis has decreased over the offshore area west of Hokkaido. Therefore, most mesocyclones generated in this region could be affected more by cold air outbreaks (intensified low-level horizontal temperature gradient) than by high SST (strong heat and moisture fluxes). However, high SST can cause stronger mesocyclones if other conditions remain the same. Hence, it is undeniable that the number of stronger mesocyclones will increase in the future as SST experiences further warming. To evaluate the various effects of SST on mesocyclones, sensitivity experiments using a numerical model should be conducted in future studies.

A mesocyclone is a crucial winter disturbance that can trigger extreme weather events such as local severe snowstorms. Ongoing climate change is projected to decrease the amount of snowfall in Hokkaido. The decrease in mesocyclone genesis revealed in this study is likely to contribute to the further reduction of snowfall in this region. This means that if mesoscale cyclogenesis in this region decreases in the future climate, the occurrence of local snowfall induced by the mesocyclone is decreased. The key environmental factors, including synoptic-scale atmospheric conditions and SST, are found to respond to climate change (Gan and Wu 2013), which could potentially lead to substantial modification of the behavior of mesocyclones. From the perspective of predicting future changes in regional climate, the results of this study highlight the climate change signal apparent in mesoscale weather systems. Further studies on historical and future changes in mesoscale phenomena should be conducted in other regions of the world.

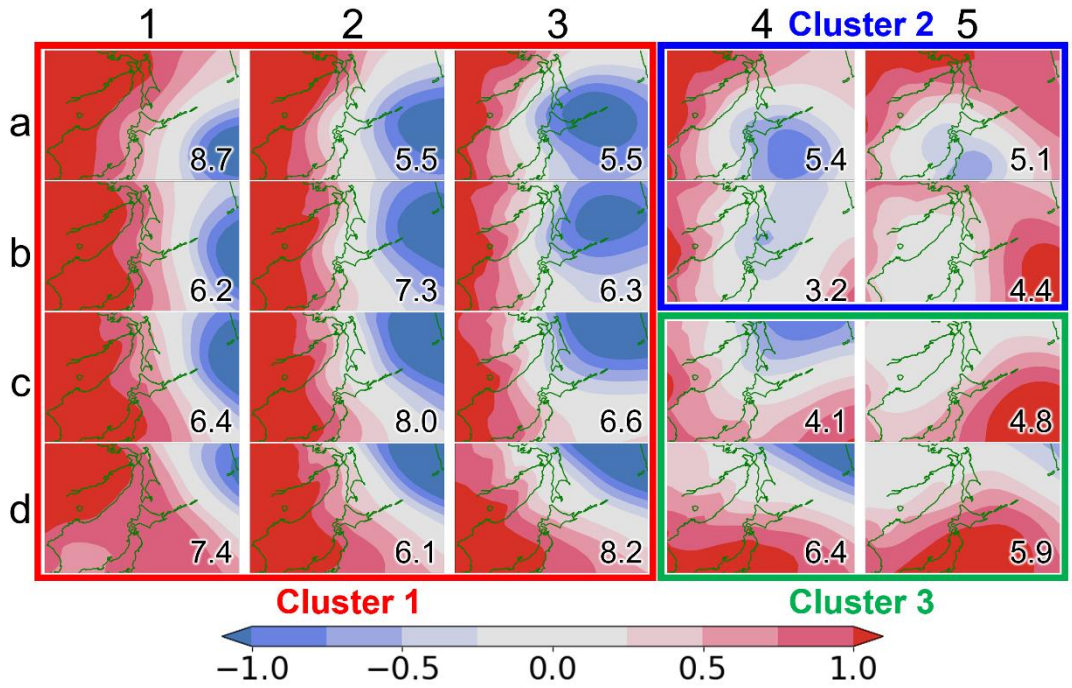


Figure 4.1. Composite map of standardized SLP patterns on 5 × 4 SOM. The classification is based on standardized 6-hourly SLP snapshots around Hokkaido (35°–55°N, 127°–157°E) for December–March during 1958/1959–2019/2020. Numbers shown in the lower-right corner of each node indicate the number of days classified into each node (winter$^{-1}$). The definitions of Cluster 1, Cluster 2, and Cluster 3 are documented in Section 4.2.

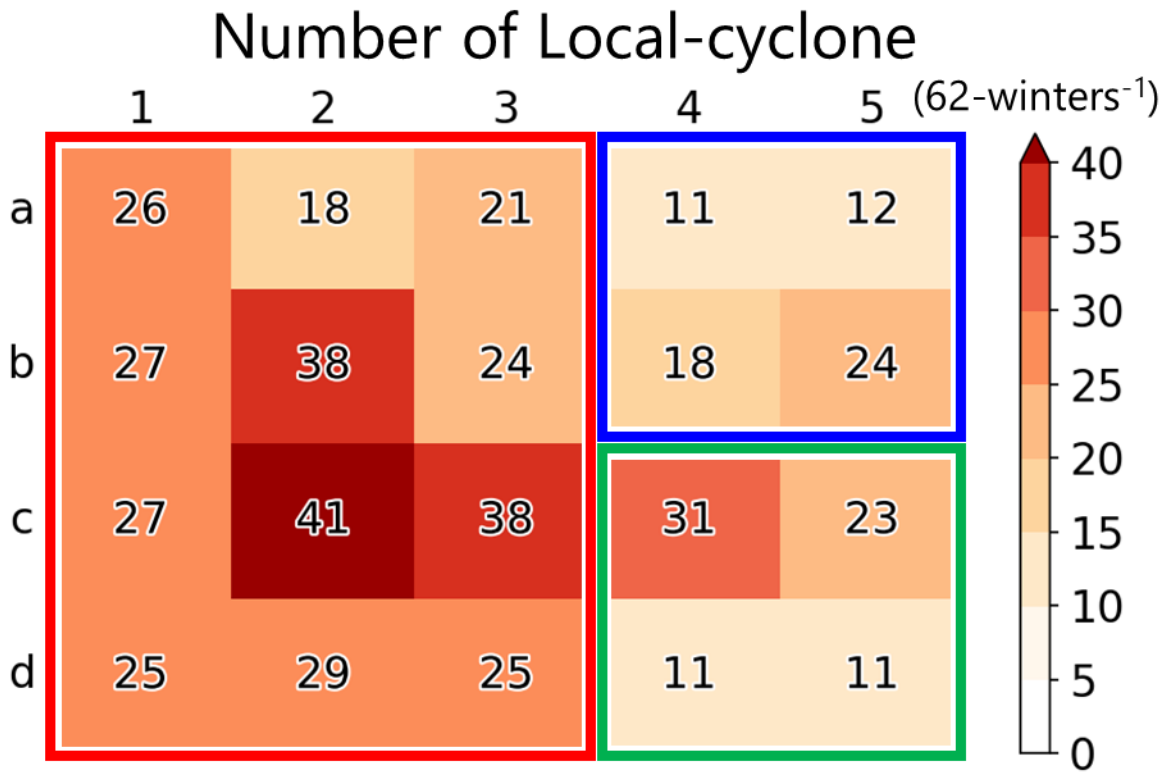


Figure 4.2. Number of occurrences of Local-cyclone genesis (color and numbers) in each SOM node illustrated in Figure 4.1. Color rectangles indicate the clustering (red: Cluster 1, blue: Cluster 2, green: Cluster 3) defined in Figure 4.1.

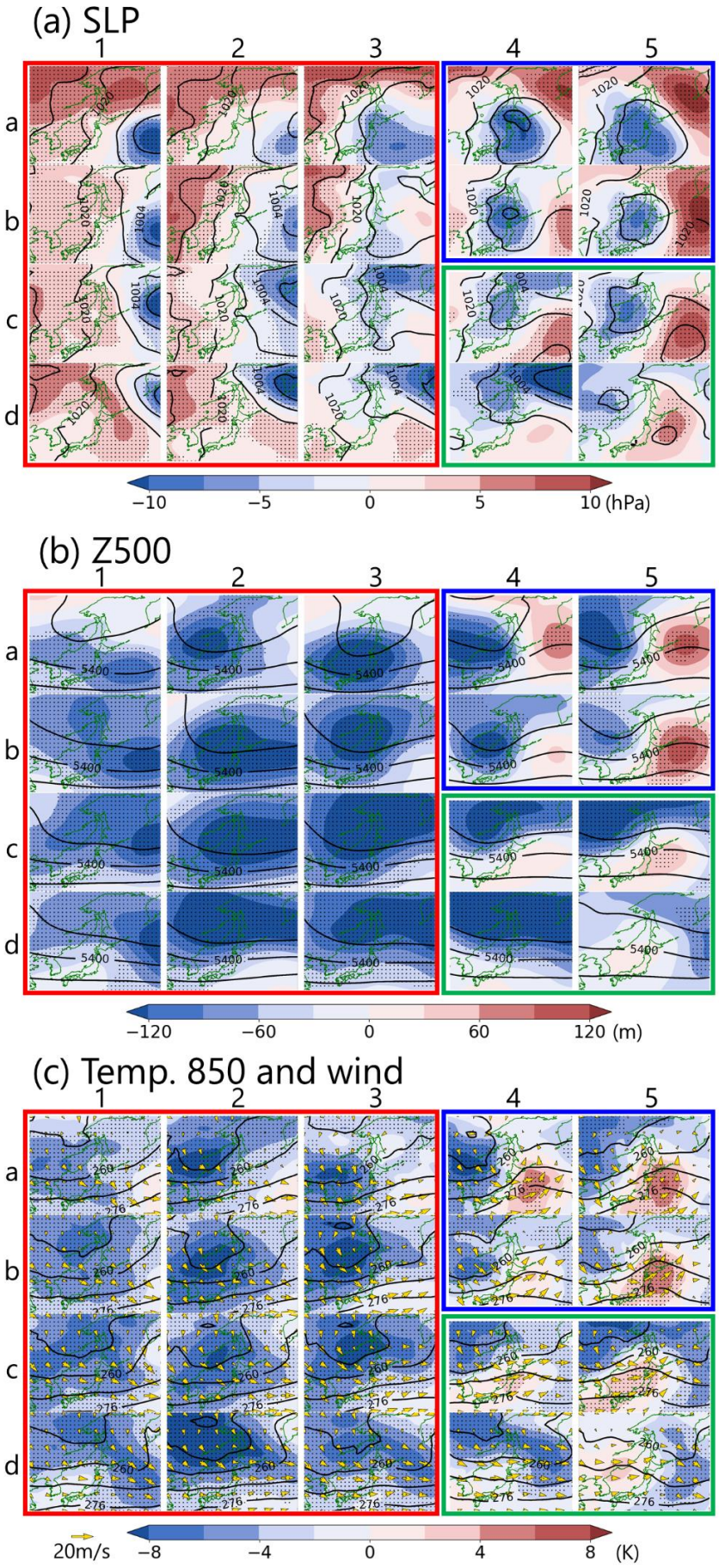
(a) SLP
1
2
3
4
5
a
b
c
d
−10
−5
0
5
10 (hPa)
(b) Z500
−120
−60
0
60
120 (m)
(c) Temp. 850 and wind
20m/s
−8
−4
0
4
8
(K)

Figure 4.3. Composite map of (a) SLP (hPa), (b) geopotential height at 500 hPa (m), and (c) 850-hPa temperature (K) fields averaged for cases having Local-cyclone genesis. Shading indicates the mean differences between the raw data (contours) in each case and the daily climatology of 1958–2019 winters. Hatching indicates the difference is significant at the 95% confidence level (Welch's t-test). Color rectangles indicate the clustering (red: Cluster 1, blue: Cluster 2, green: Cluster 3) defined in Figure 4.1.

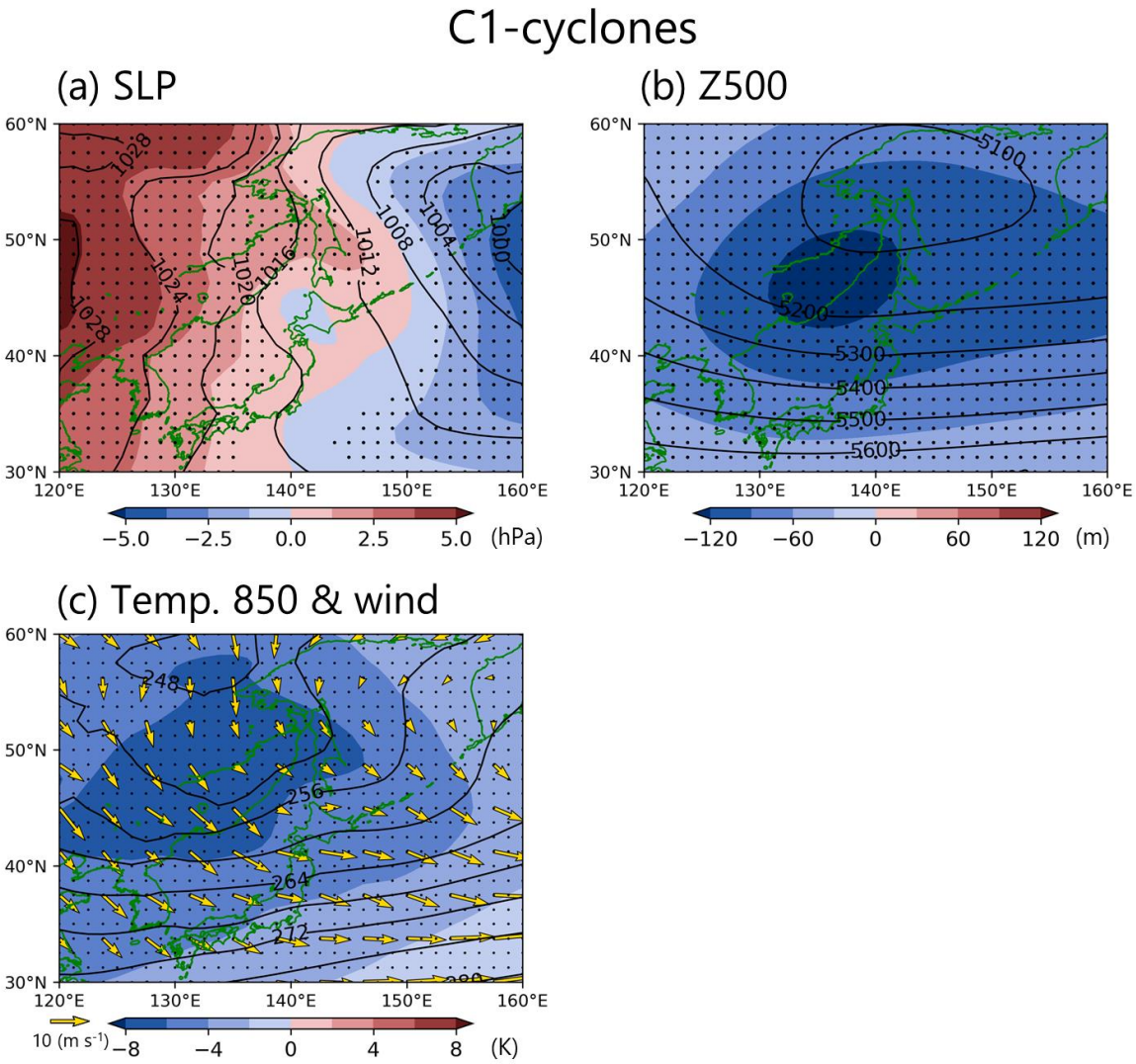


Figure 4.4. Composite map of (a) SLP, (b) geopotential height at 500 hPa, and (c) 850-hPa temperature and wind fields (vector) averaged for C1-cyclone cases. Shading indicates the mean differences between the raw data (contours) in each case and the daily climatology of 1958–2019 winters. Hatching indicates the difference is significant at the 95% confidence level (Welch's t-test).

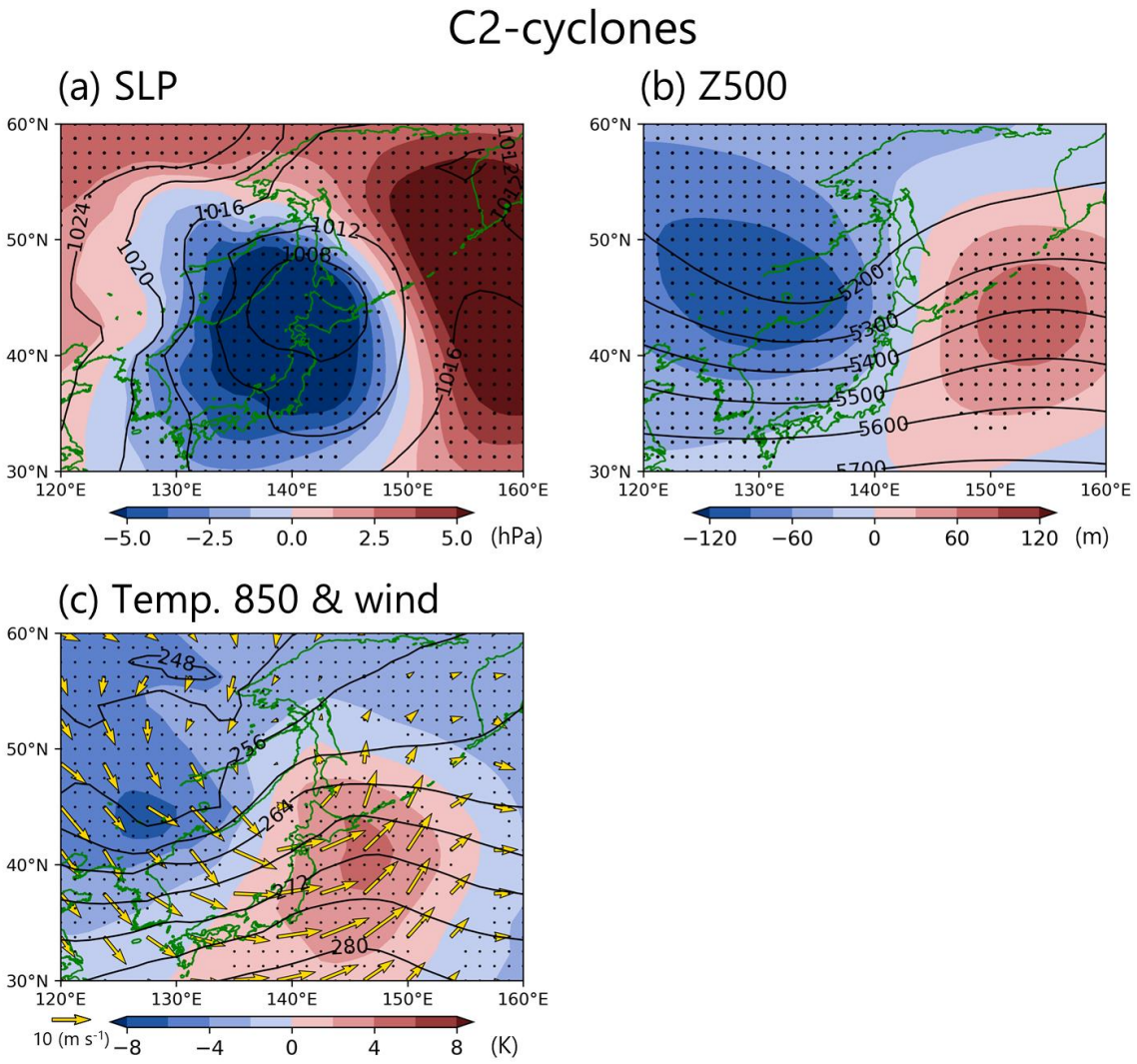


Figure 4.5. As in Figure 4.4 but for the C2-cyclones.

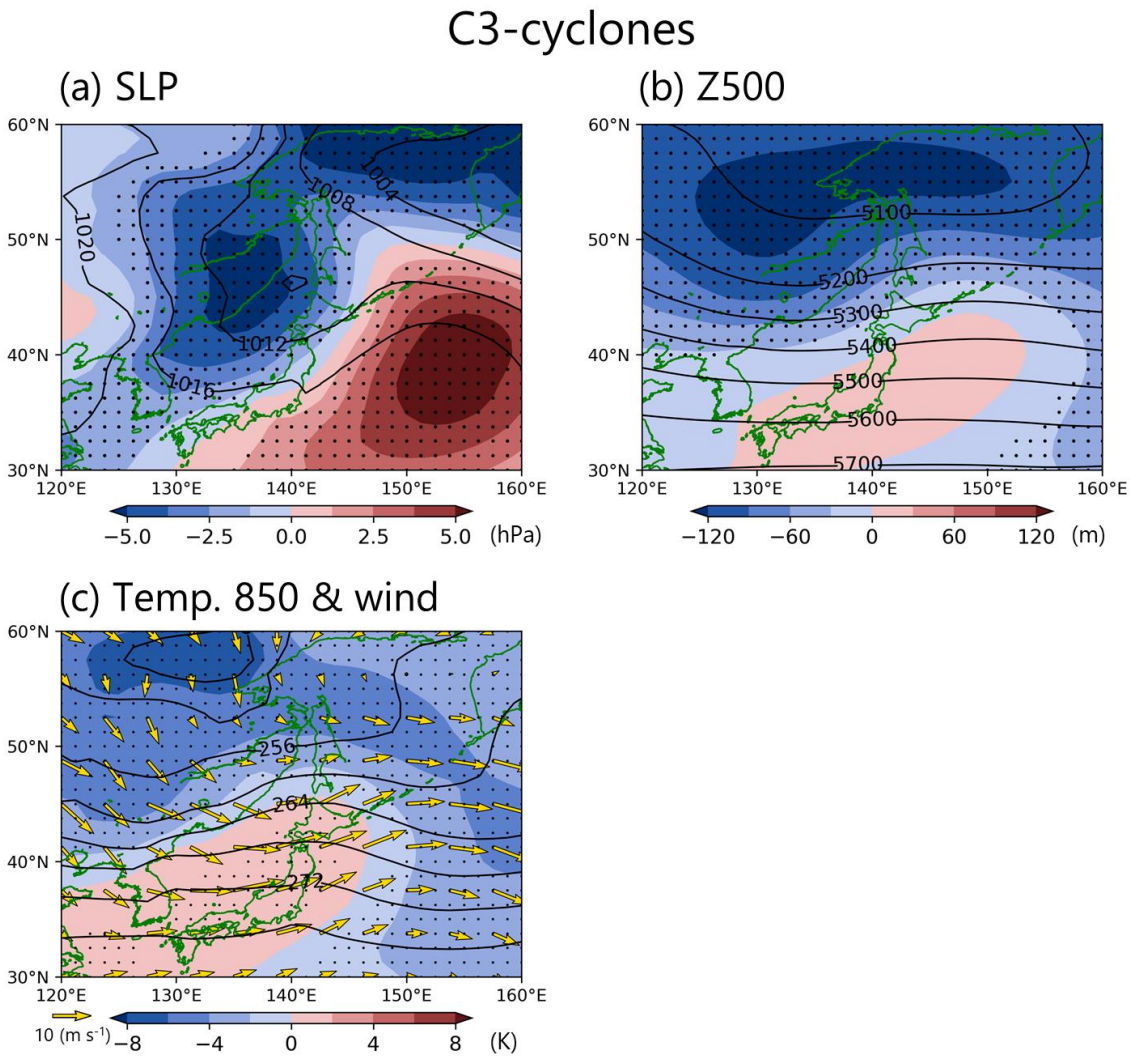


Figure 4.6. As in Figure 4.4 but for the C3-cyclones.

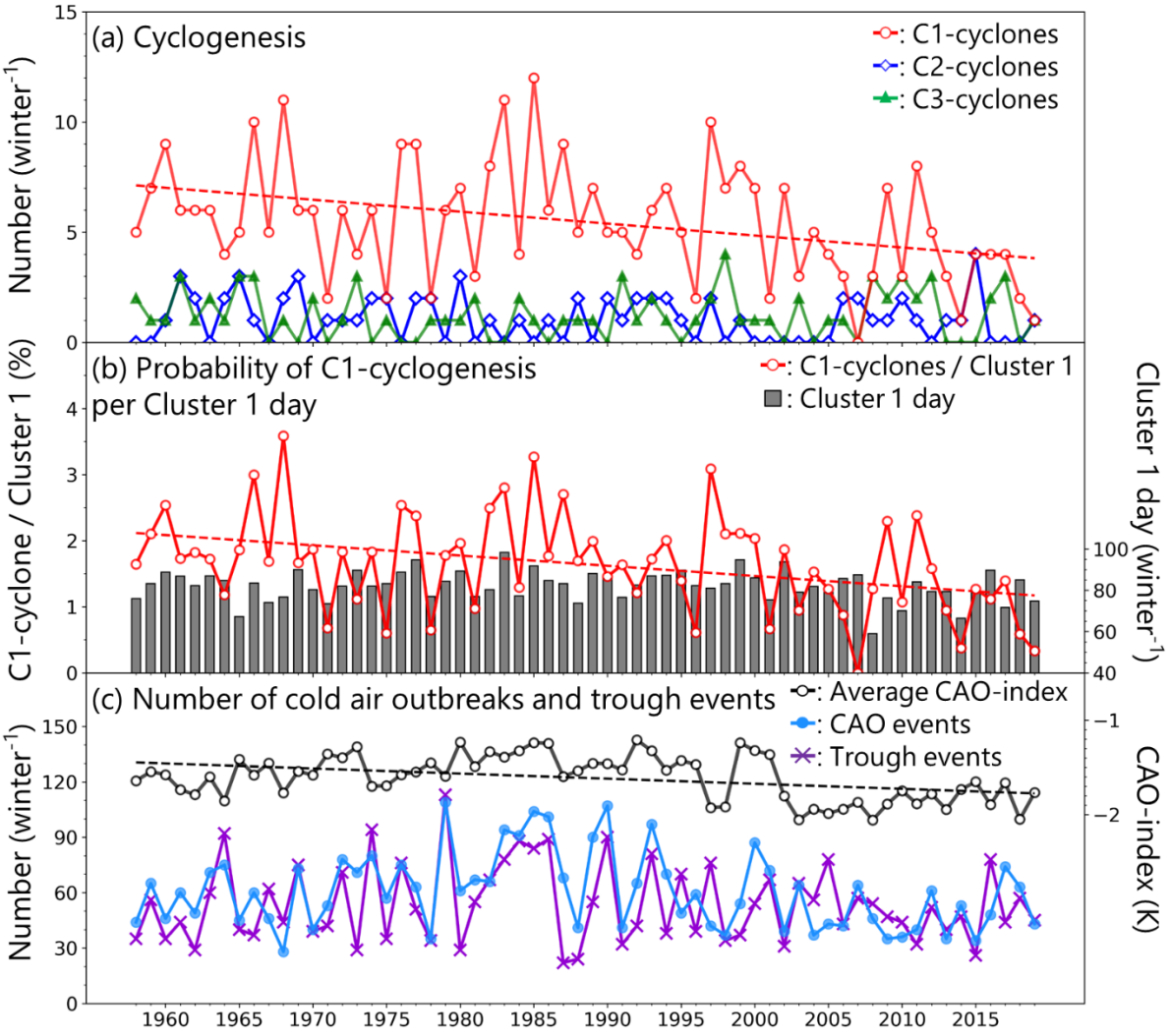


Figure 4.7. (a) Number of occurrences of cyclogenesis for C1-cyclones (red), C2-cyclones (blue), and C3-cyclones (green). (b) Number of Cluster 1 days (bars) and the probability (%) of C1-cyclone genesis per Cluster 1 days (lines). (c) Number of cold air outbreaks and upper-level trough events over the offshore region west of Hokkaido (Figure 3.2; red), and average CAO-index at the occurrence of cold air outbreak. Black broken line indicates significant trends for the average CAO-index exceeding the 95% confidence level in the t-test for ordinary least squares regression.

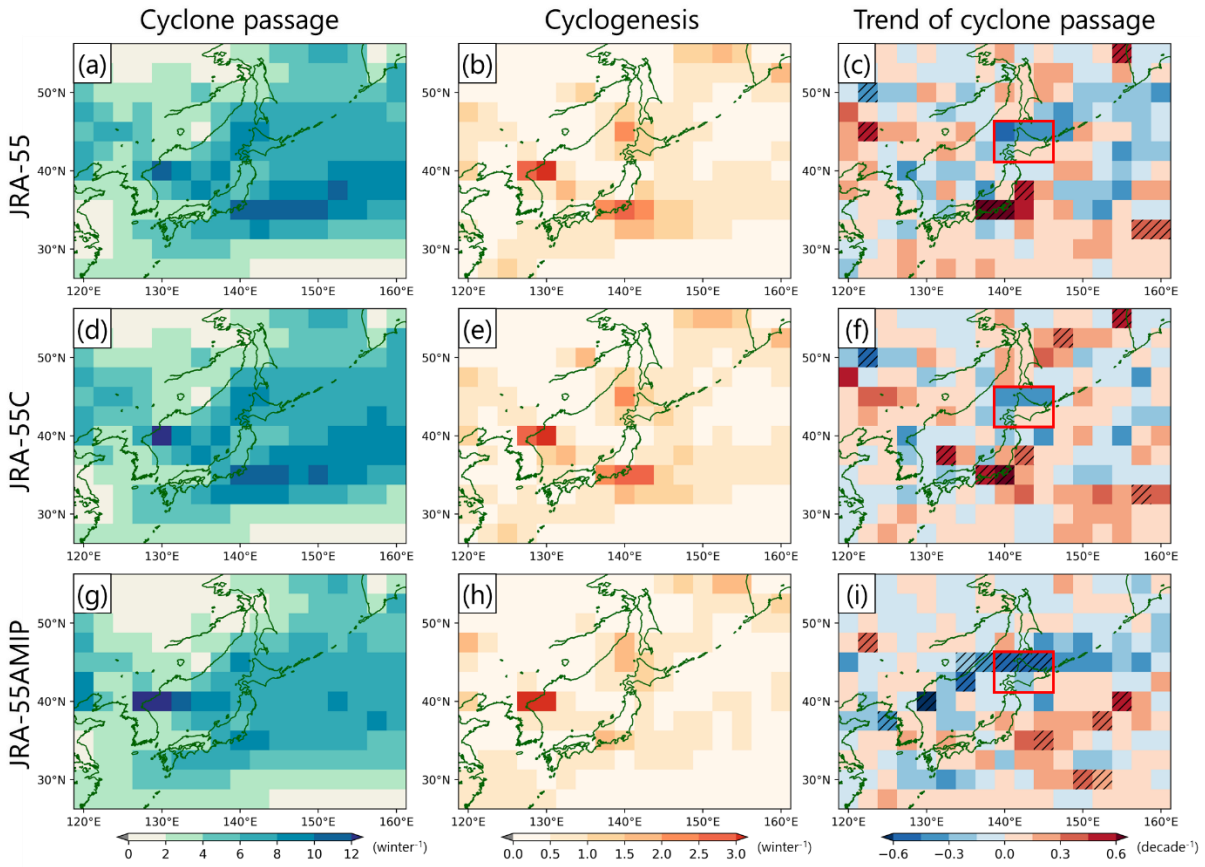


Figure 4.8. As in Figure 3.1 but during 1958–2011. (a), (d), and (g) number of cyclone passages, (b), (e), and (h) occurrence of cyclogenesis, (c), (f), and (i) linear trend of the number of cyclone passages. (a), (b), and (c) JRA-55, (d), (e), and (f) JRA-55C, (g), (h), and (i) JRA-55AMIP.

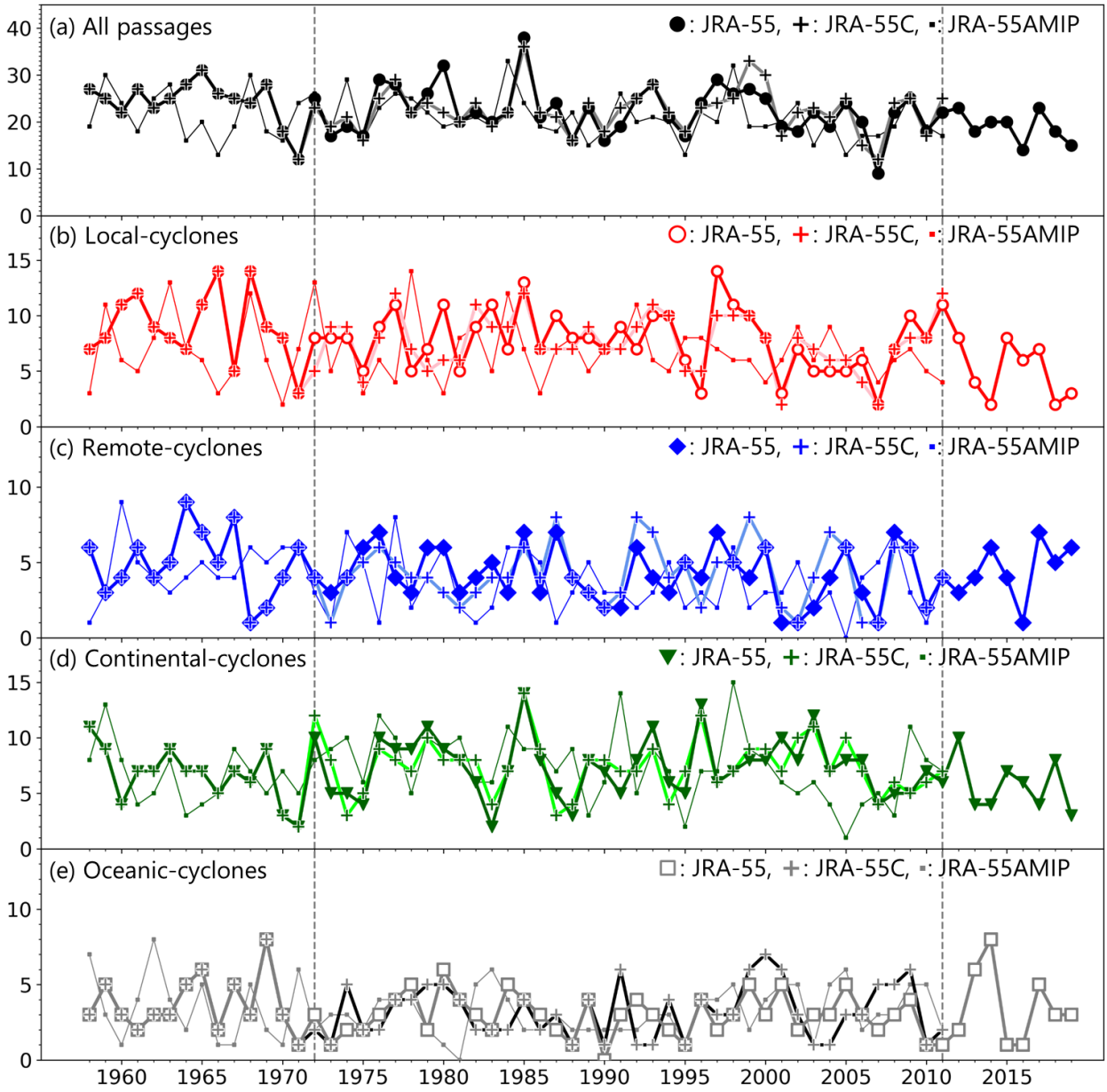


Figure 4.9. As in Figure 3.3a but for each dataset (JRA-55, JRA-55C, and JRA-55AMIP). Gray dashed lines indicate the period when the assimilated data in JRA-55 and JRA-55C are different (1972–2011).

Table 4.1. Linear trends shown in Figure 4.9 for each dataset. All passages refer to all cyclones that passed over the target area (red rectangle in Figure 3.1c). Local-cyclones, Remote-cyclones, Continental-cyclones, and Oceanic-cyclones are the cyclone generated in each area defined in Figure 3.2. Correlation coefficients are calculated against the interannual variation of cyclone passages in JRA-55. Trends and the correlation coefficients exceeding the 95%, 99%, and 99.9% confidence levels are marked by superscripts *, **, and ***, respectively.

| | Trend (1958-2011) (decade$^{-1}$) | | | Correlation coefficient with JRA-55 (JRA-55C: 1972-2011, JRA-55AMIP: 1958-2011) | |
|---|---|---|---|---|---|
| | JRA-55 | JRA-55C | JRA-55AMIP | JRA-55C | JRA-55AMIP |
| All passages | -0.84 | -0.55 | -0.65 | 0.82*** | 0.12 |
| Local-cyclones | -0.41 | -0.41 | -0.18 | 0.78*** | -0.18 |
| Remote-cyclones | -0.29 | -0.15 | -0.29 | 0.70*** | -0.02 |
| Continental-cyclones | 0.05 | 0.06 | -0.19 | 0.84*** | 0.14 |
| Oceanic-cyclones | -0.19 | -0.04 | 0.007 | 0.46** | -0.03 |

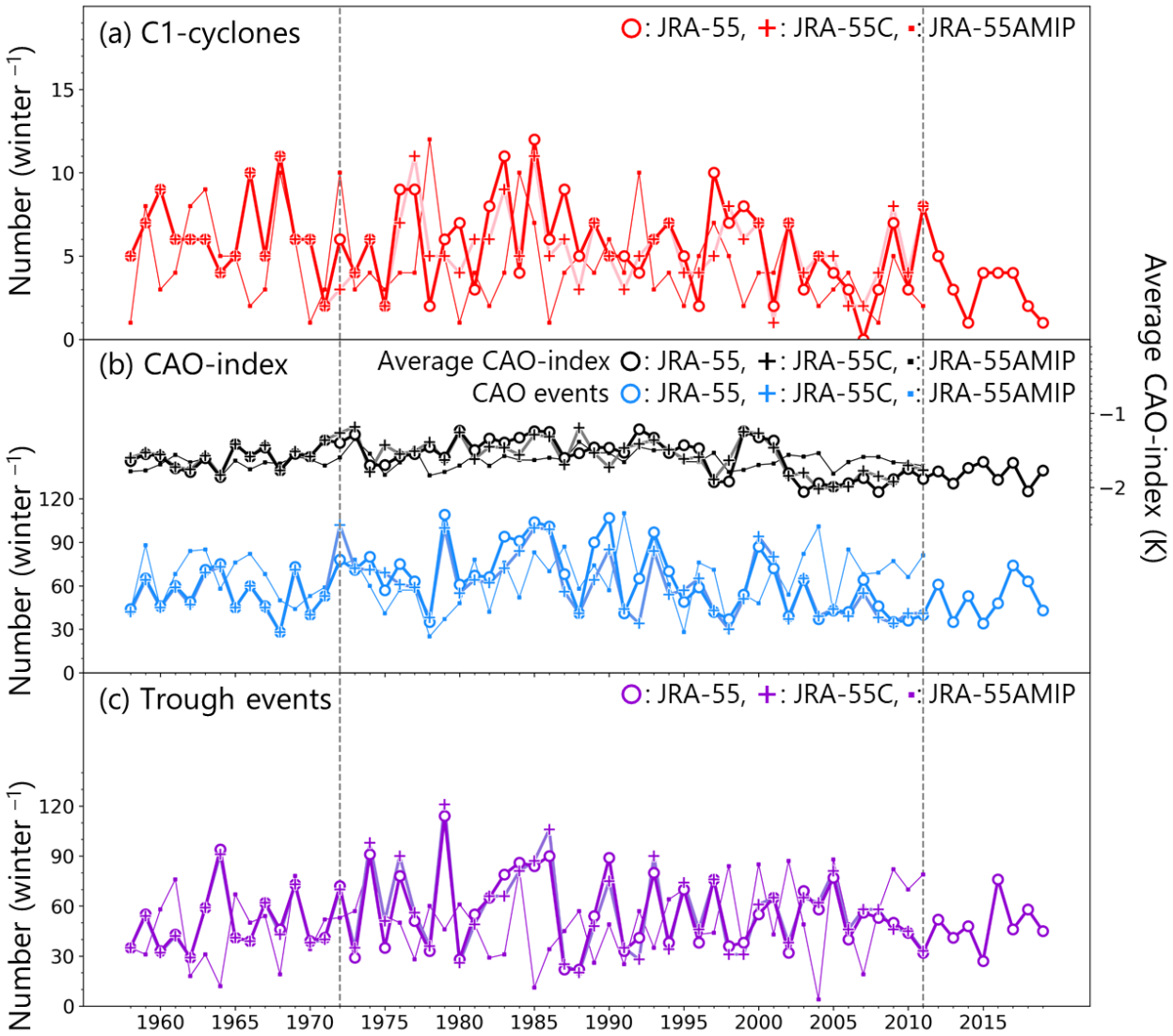


Figure 4.10. As in Figure 4.7 (a) C1-cyclone genesis (b) CAO-index (c) trough events, but for each dataset (JRA-55, JRA-55C, and JRA-55AMIP). Gray dashed lines indicate the period when the assimilated data in JRA-55 and JRA-55C are different (1972–2011).

# 5. Mesoscale cyclone activity around Hokkaido

## 5.1 Introduction

In Chapter 3, the interannual variation of the number of winter cyclone passages around Japan, including mesocyclones, was investigated. Chapter 4 showed that the relationship between the synoptic-scale surface pressure patterns around Hokkaido and the number of occurrences of cyclogeneses around the offshore region west of Hokkaido. In those studies, the number of occurrences of cyclogenesis on the west-east high and low surface pressure pattern was found to be decreasing over the offshore region west of Hokkaido. However, as shown in Section 2.3, the reanalysis dataset and the cyclone tracking algorithm used in Chapters 3 and 4 are unable to detect cyclones without a distinct low pressure minimum. In addition, relatively weak mesoscale cyclones with diameters of less than 200 km occur over the offshore region west of Hokkaido, but the horizontal resolution of JRA-55 (1.25° grid) might not be finer enough to capture them, especially in the initial developmental stage of the mesocyclones. Therefore, an additional analysis using a higher-resolution dataset is needed to investigate the factors behind the occurrence of the mesoscale cyclogenesis, which are thought to be decreasing in number over the offshore west of Hokkaido.

In this chapter, numerical experiments using a regional climate model were conducted to generate the long-term, high-resolution dataset to reproduce and extract mesoscale cyclones generated in the offshore region west of Hokkaido. Sensitivity experiments using modified topography were also conducted to investigate the effect of the mountains over the eastern end of the Eurasian Continent on the mesoscale cyclogenesis in this region. In addition, the SOM used in Chapter 4 was used to summarize the relationship between the synoptic-scale atmospheric conditions and the mountains over the eastern edge of the Eurasian Continent on the mesoscale

cyclogenesis. Numerical experiments and cyclone tracking algorithms in Chapter 5 are based on Tamura and Sato (2020) as detailed in Section 5.2.

## 5.2 Model and experimental designs

Numerical experiments using the Weather Research and Forecasting (WRF) Model version 3.2.1 with the Advanced Research version of the WRF core (Skamarock et al. 2008). Model domain is shown in Figure 5.1a. The domain had 140 × 100 horizontal grid points with a 20 km grid size and 32 vertical levels from the surface to the 50 hPa level. This horizontal grid size can resolve mesoscale cyclones that diameter exceeds at least 100 km. This would reproduce most of the mesoscale cyclones generated in the domain because their diameter is typically larger than 100 km (Tsuboki and Wakahama 1992; Yanase et al. 2016). Physics schemes are summarized in Table 5.1. These physics schemes well simulate the mean and interannual variation of the precipitation around the Sea of Japan in the winter season (Sato and Sugimoto 2013). Initial and boundary conditions were obtained from the JRA-55 (Kobayashi et al. 2015), OISST and the sea ice concentration (Reynolds et al. 2007).

In this study, two types of experiments were conducted to investigate the effect of the mountains on mesoscale cyclogenesis. The first experiment used realistic topography (hereafter, REAL, see Figure 5.1a). In the second experiment, the Sikhote-Alin mountain range, which is thought to contribute to the occurrence of cumulus convection and PMC genesis over the offshore area west of Hokkaido (Ohtake et al. 2009; Watanabe et al. 2017), was modified (hereafter, NoMt; see Figure 5.1b). In this experiment, the terrain height of the Sikhote-Alin mountain range was flattened to 100 m, where the elevation is higher than 100 m. Each experiment covered 36 winter

seasons (1 November 1981–31 March 2017). The experiments are started on 1 November and terminated on 31 March for each winter season. The first month (November) was regarded as a spin-up period and thus is not used for analysis.

## 5.3 Algorithm for tracking mesocyclones

Mesocyclones that include local disturbances were detected by using a new tracking algorithm developed in this study. Figure 5.2 shows the workflow of the algorithm. First, a local minimum grid point of the 850 hPa geopotential height is detected as the center of low pressure (Figure 5.2b). Next, the detected center of low pressure, with relative vorticity at 850 hPa greater than $1.0 \times 10^{-5}$ $s^{-1}$, is designated as a cyclone center and its movement is tracked (Figure 5.2c). In the next time step, if the cyclone center is detected within 50 km of a previous cyclone center, the cyclone is regarded as the same cyclone (Figure 5.2c). This tracking process is repeated for all low pressures. The above procedure could also detect synoptic-scale cyclones (i.e., extratropical cyclones) whose horizontal size is much greater than a mesocyclone. To remove synoptic-scale cyclones, the following procedure was incorporated. The 850 hPa geopotential height field derived from the original 20 km mesh WRF output (Figure 5.2a) is smoothed to a 100 km mesh grid (Figure 5.2d), and centers of low pressure are detected using the smoothed field (Figure 5.2e). Eventually, the absolute location of the center within a 100 km mesh grid is determined by using the original 20 km mesh data (850 hPa geopotential height minima) so that the locations of the low pressure center are consistent before and after smoothing (Figure 5.2e). In this attempt, only large-scale cyclone (diameter is over ~ 300 km) are detected (Figure 5.2f), which is in contrast to the cyclones detected without smoothing (i.e., 20 km mesh grid) that include all cyclone features (Figure 5.2c). If the

detected cyclone tracks in both attempts are exactly the same, that cyclone is regarded as a synoptic-scale cyclone (Figure 5.2g). The diameter of the mesocyclone may exceed 300 km during the tracking. In such a case, the cyclone is regarded as a mesocyclone because the cyclone track is different before and after smoothing. In other words, only the cyclones with a diameter greater than 300 km from the beginning are considered as synoptic-scale cyclones and excluded from the analysis. Of the remaining cyclones, the cyclones that track last for at least 12 hours are regarded as mesocyclones (hereafter polar mesocyclones: PMCs).

## 5.4 Results

### 5.4.1 Number of PMCs

The distribution of PMC genesis is shown in Figure 5.3. In the REAL experiment, PMCs frequently occur over the area offshore west of Hokkaido and over the Strait of Tartary (Figure 5.3a). This distribution pattern is similar to that of polar lows detected using reanalysis data (Yanase et al. 2016). However, the number of PMC genesis over the offshore region west of Hokkaido is relatively higher in the present study because the smaller-scale PMCs are detected by using finer mesh data and weaker thresholds. The number of generated PMCs is lower in the NoMt experiment than that in the REAL experiment, especially over the western coastal sea of Hokkaido (Figure 5.3b), and the difference is clearly shown in Figure 5.3c which indicates the difference in the distribution of PMCs genesis between the NoMt and REAL experiments (NoMt − REAL). This result indicates that the Sikhote-Alin mountain range strongly enhances PMC genesis over the offshore region west of Hokkaido. The following analysis will focus on this region.

The seasonal variation in the number of PMCs generated in the area offshore region west of

Hokkaido (42–49°N, 136–142°E; area indicated by red lines in Figure 5.3c) is shown in Figure 5.4. In the REAL experiment, the number of generated PMCs is lowest in December, reaches a peak in January, and then falls through February and March, which is consistent with satellite data analysis (Fujiyoshi et al. 1988). In the NoMt experiment, the number of PMCs generated in January dramatically decreases to 56% of the REAL experiment followed by December (59%) and February (60%), whereas there is a slight decrease in March (65%). Therefore, the contribution of the Sikhote-Alin mountain range to PMC genesis has a strong monthly variation. This suggests that PMCs could be classified into two groups: those sensitive to topographic effects and those less sensitive.

The direction of movement of PMCs generated in the area offshore region west of Hokkaido varies depending on the synoptic-scale environments prevailing at the time of their occurrence. A PMC moves southward when an extratropical cyclone is located to its east, whereas it moves eastward in association with an eastward-migrating upper-level trough (Yanase et al. 2016). The number of PMCs moving in each of the four main cardinal directions is shown in Figure 5.5. Here the direction of movement is defined as the orientation of the line connecting the points of PMC occurrence and disappearance. The dominant directions of movement in the REAL experiment are southward and eastward. Southward-moving PMCs occur more frequently in January than in the other months. In comparison with the REAL experiment, the number of southward-moving PMCs in the NoMt experiment is reduced, whereas that of eastward-moving PMCs is only slightly reduced.

### 5.4.2 Classification based on the SOM maps

To understand the relationship between the direction of the movement of PMC and the synoptic-scale conditions, the classification method SOM, which is used in Chapter 4, is applied here. This analysis expands the SOM-based classification of the SLP pattern in JRA-55 (Section 4, Figure 4.1) to hourly data of the WRF outputs. First, standardized SLP fields in JRA-55 are compared with each node of the SOM map in Section 4 (Figure 4.1) and chose the node with the closest Euclidean distance. By this procedure, the correspondence between the date and time every 6 hours and the node number of the SOM map is obtained. Next, utilizing the settings that JRA-55 is used for the boundary condition in the WRF experiments, the node numbers as determined above are assigned to the date and time for WRF outputs (e.g., the same node number on 1 December 00 UTC classified in JRA-55 is assigned from 1$^{st}$ December 00 UTC to 1$^{st}$ December 05 UTC in WRF experiments). Hereafter, the number of occurrences of PMC geneses in the WRF outputs at each node are investigated using this correspondence. Figure 5.6 shows the number of PMC occurrences at each node of the SOM map illustrated in Figure 4.1. Figure 5.7 shows the composite SLP fields when a PMC occurs. In Figure 5.7, both SLP fields are similar to the SOM map in Figure 4.1. Therefore, it is appropriate to assume that this analysis based on the classification by SOM in Chapter 4 is applicable to the WRF outputs.

Here, relation between the main direction of the movement of the PMCs, namely southward and eastward, and the synoptic-scale atmospheric conditions when the PMCs occur is examined. Number of southward moving PMC (Figure 5.6a) is large at the upper left nodes and less at the lower right node. Based on the classification in Figure 4.1, interannual variation of the number of PMC genesis in Cluster 1 show a decreasing but not significant (southward-moving: −0.3 decade$^{-1}$).

Decadal trends in the number of PMCs generated in Cluster 2 (southward-moving: 0.33 decade$^{-1}$, eastward-moving: −0.001 decade$^{-1}$) and Cluster 3 (southward-moving: 0.04 decade$^{-1}$, eastward-moving: −0.22 decade$^{-1}$) are not significant. Although the comparison is affected by the difference in the analysis period and method, the results in this section and Chapter 4 suggest that the number of cyclogeneses over the offshore region west of Hokkaido from 1981 to 2016 does not vary, but the number of the developed cyclone, which can be captured in JRA-55, is decreased.

Focusing on the differences in each node of SOM map, the node in (2,b) and (2,c) show a clear west-east high and low surface pressure pattern consisting of a synoptic-scale low pressure over the Sea of Okhotsk and a high pressure over the continent (Figure 5.7a). This is a typical surface pressure pattern of the southward-moving PMCs (Yanase et al. 2016). The surface pressure patterns at nodes (3,a) and (4,a) are also similar to those of mesoscale cyclogenesis, which consists of a temperature gradient in the lower troposphere induced by the synoptic-scale cyclone located in the southeast of Hokkaido (Ninomiya et al. 1993). Unlike the southward-moving PMC, the eastward-moving PMC occurs in all nodes. Contrary to the nodes (2,b) and (2,c), nodes (4,b), (5,b), (4,c), and (5,c) have the west-east low and high surface pressure anomaly around Hokkaido (Figure 5.7b). This surface pressure pattern is similar to the characteristics of the eastward-moving PMC (Yanase et al. 2016). However, a large number of eastward-moving PMCs also occur at the left node, which consists of a west-east high and low surface pressure pattern. Moreover, the number of southward-moving PMCs generated in (2,b) and (2,c) showed a significant decreasing trend of −0.64 decade$^{-1}$ ($p = 0.03$), but the tendency of the number of eastward-moving PMC is not significant. (−0.18 decade$^{-1}$, $p = 0.43$). These results suggest that SOM-based classification in this

study may provide a more detailed classification of PMCs.

Differences in the number of PMCs genesis (i.e., NoMt – REAL) for each direction of movement are shown in Figure 5.8. Number of southward-moving PMC shows a large decrease around the node (2,b) (Figure 5.8a). At the bottom right node in Figure 5.8a, where the number of PMCs is originally small (Figure 5.6a), the numbers remain almost the same. The number of eastward-moving PMC is reduced to less than half at the node (2,b) (Figure 5.8b). In the nodes on the right, there is a large decrease at (5,b), but not much change in the other nodes. The nodes (2,b) and (2,c) where PMCs occurred in the west-east high and low surface pressure pattern (Figure 5.7) are defined as Type 1. Additionally, the nodes (4,b), (5,b), (4,c) and (5,c) where PMCs occurred in the west-east low and high surface pressure pattern are defined as Type 2.

### 5.4.3 Atmospheric conditions

Figure 5.9 shows the composite fields of geopotential height at 500 hPa for the 12 h before PMC genesis in the REAL experiment and track of PMCs. In the case of Type 1, the conditions in prior to PMC genesis are similar for both southward- and eastward-moving PMC, and the upper-level trough is located over the offshore region west of Hokkaido (Figures 5.9a and 5.9b). This upper-level condition and the west-east high and low surface pressure pattern in Type 1 (Figure 5.7) are consistent with the synoptic-scale conditions at the southward-moving PMC genesis indicated in Yanase et al. (2016). In both cases, locations of the PMCs genesis are concentrated near the western coast of Hokkaido. In contrast to Type 1, the conditions for the occurrence of PMCs in Type 2 differ according to the direction of movement (Figures 5.9c and 5.9d). Before the occurrence of southward-moving PMCs, low pressure is located over the north of Hokkaido, and although the

number of occurrences is small, their genesis locations are concentrated in the Strait of Tartary (Figure 5.9c). In the case of eastward-moving PMCs, a deep trough is located over the continent, and a ridge is located over the east of the Sea of Okhotsk (Figure 5.9d). These features are consistent with the synoptic-scale atmospheric conditions at the occurrence of eastward-moving PMCs (Yanase et al., 2016).

The composite fields of potential temperature and wind at 900 hPa 12 h before PMC genesis in the REAL experiment for the PMCs are shown in Figures 5.10 (Type 1) and 5.11 (Type 2). In the case of Type 1, the temperature gradient from northwest to southeast across the domain suggests the occurrence of cold air outbreaks (Figures 5.10a and 5.10b). A part of the cold air outbreaks passes across the southern part of the Sikhote-Alin mountain range, where the elevation is relatively low and then causes northwesterly wind over the Sea of Japan (Figure 5.1a). Additionally, northerly wind blowing from the Strait of Tartary is found (Figures 5.10a and 5.10b). These wind systems can form horizontal wind shear over the offshore region west of Hokkaido. In the case of Type 2, the winds and temperature field over the offshore region west of Hokkaido is westerly and weak cold air advection in southward-moving PMC (Figure 5.11a), but in eastward-moving PMC is southwesterly and warm air advection (Figure 5.11b). The difference in 900-hPa winds between the NoMt and REAL experiments (NoMt − REAL) is presented (Figures 5.10c, 5.10d, 5.11c, and 5.11d) to investigate how the Sikhote-Alin mountain range might modulate the lower-tropospheric wind. Here, the reference time for the composite analysis is common for both experiments, i.e., 12 h before PMC genesis in the REAL experiment. In the NoMt experiment, compared with the REAL experiment, the westerly wind component is stronger, and the potential temperature is lower over

the offshore region west of Hokkaido (Figures 5.10c, 5.10d, and 5.11c). Additionally, the northerly wind over the Strait of Tartary is slightly weak, and the potential temperature is a little higher in the NoMt experiment, which is the common circulation change for many PMC types as found in Figures 5.10c, 5.10d, and 5.11c. These differences are not clear in the case of eastward-moving PMCs in Type 2 (Figure 5.11d).

Most of the PMCs in Type 1 occurred near the west coast of Hokkaido, and the number of occurrences of the PMC was reduced by strong westerly winds in the NoMt experiment. Therefore, the vortex of the PMCs in Type 1 may have been caused by low-level wind shear in the offshore region west of Hokkaido induced by the north-south topographic contrast of the Sikhote-Alin mountain range. To investigate the effect of the mountain on the wind fields, the gradient of the zonal wind in the lower troposphere is shown in Figure 5.12. In the case of Type 1, over the offshore region west of Hokkaido, westerly component is added to the northerly wind from the Strait of Tartary. This results in a weakening of the zonal wind gradient from the southern end of the Sikhote-Alin mountain range to near the western coast of Hokkaido, and the zonal wind gradient is slightly strengthened over the Strait of Tartary (Figures 5.12a and 5.12b). In the case of Type 2, the zonal wind gradient is weakened over the offshore west of Hokkaido in the southward-moving PMCs, while no significant change is observed in the eastward-moving PMCs (Figures 5.12c and 5.12d). Therefore, the PMC in Type 1 is considered to have been suppressed by the removal of the mountain range, which weakens the horizontal shear of the lower-level winds over the offshore west of Hokkaido. In the case of the southward-moving PMCs in Type 2, the number of occurrences does not change despite the change in the wind field over the offshore west of Hokkaido due to the

removal of the mountain range. This is because most of the PMCs occur over the Strait of Tartary, and the effect of the change in the wind field is small. This result suggests that the influence of the Sikhote-Alin mountain range on the occurrence of PMCs varies with slight differences in the location of the PMCs genesis.

## 5.5 Discussion and conclusion

In this section, long-term numerical experiments were conducted to investigate the effects of topography (i.e., the Sikhote-Alin mountain range) on PMCs generated over the northern Sea of Japan. The cyclone tracking and weather pattern classification clarified that the effects of the Sikhote-Alin mountain range on PMCs vary depending on differences in synoptic-scale atmospheric conditions. Among the many PMCs investigated, those generated over the offshore region west of Hokkaido with the west-east high and low surface pressure pattern (Type 1) are most sensitive to topographic effects, whereas those generated with the west-east low and high surface pressure pattern (Type 2) are less sensitive.

The difference in sensitivity is due to the difference in the development mechanism of PMC. During PMC genesis on the Type 1 condition, the horizontal wind shear over the offshore region west of Hokkaido is formed because of two wind systems: a northwesterly wind from the continent and a northerly wind from the Strait of Tartary (Figures 5.10a, 5.10b). This horizontal wind shear is likely induced by the high pressure over the continent (Siberian high) and the synoptic-scale low pressure over the Sea of Okhotsk (Aleutian low) (Figures 5.7a and 5.7b). The northwesterly wind over the Sea of Japan originates from the air mass passing across the Sikhote-Alin mountain range. Therefore, the wind shear is very sensitive to the local topography.

The westerly wind over the mountain can cause vertical shrinkage of the air column and enhances anticyclonic vorticity over the mountain in terms of the conservation of potential vorticity (Ohtake et al. 2009). Therefore, the removal of the mountain region can suppress the anticyclonic rotation resulting in the cyclonic wind anomalies over the Sikhote-Alin mountain range (Figures 5.10c, 5.10d, 5.11c, and 5.11d). Moreover, the Sikhote-Alin mountain range modulates the westerly winds over the Sea of Japan due to the difference in elevation between the northern and southern parts of the mountains (Ohtake et al. 2009). Specifically, the relatively higher region over the northern part of the mountain (around the north of 45°N) blocks low-level westerly wind. In contrast, over the southern part of the mountain, westerly wind passes over the mountain. Therefore, by removing the Sikhote-Alin mountain range, the westerly wind from the continent can blow directly over the Sea of Japan. Consequently, the westerly wind over the offshore region west of Hokkaido becomes horizontally uniform and wind shear becomes negligibly weak, which discourages PMCs genesis. However, in eastward-moving PMCs generated on the Type 2 condition, the wind and temperature fields do not vary by removing the Sikhote-Alin mountain range (Figures 5.11d and 5.12d). The baroclinic instability is likely to be a primary development mechanism for this type of PMCs (Yanase et al. 2016). Therefore, the occurrence of this type of PMCs may not require lower-level wind shear. As the southward-moving PMCs generated on the Type 2 condition occur further north than where wind fields changed, it is likely that the effect of the removal of the mountains was small. Moreover, sea ice extends to the northern part of the Strait of Tartary in mid-winter (Figure 5.1). Near the ice edge, low-level baroclinicity stimulates the development of PMCs (Mailhot et al. 1996). Hence, southward-moving PMC genesis on the Type 2 conditions is

likely affected more strongly by sea ice than by the Sikhote-Alin mountain range.

Through the long-term numerical experiments, analysis of this study showed that, in a climatology sense, PMC generated with the west-east high and low surface pressure pattern is sensitive to the topography. Since the present study considers many PMCs, the sensitivity here means the tendency of behavior for the PMC population. Considering that the expected response of PMC to mountains varies for each case, probably depending on the background synoptic patterns, the statistical approach like the present study is useful to comprehensively understand the characteristics of PMC in the studied area.

Besides the orographic effects, SST has been known to affect the development of PMCs. PMC is likely to be modulated by the variability of local sea surface conditions (Kolstad and Bracegirdle 2017). Furthermore, variations in SST and sea ice distribution can modulate the pattern and frequency of PMC genesis at various timescales, e.g., interannual to decadal. To elucidate the trend of PMCs within such timescales, it will be important to analyze many PMC cases using long-term and high-resolution numerical simulations that have recently become possible. Consideration of the effect of air–sea interaction is also necessary. The numerical experiment in the present study was conducted by an atmospheric model that does not predict oceanic response to modified atmospheric circulation. This offline ocean setting might underestimate the reduction of PMC genesis due to the removal of mountains. The accelerated low-level westerly and intensified cold air outbreaks in the NoMt experiment enhance heat fluxes from the ocean and, consequently, could decrease SST (Kawamura and Wu 1998). The formation of PMC could be further reduced over the colder SST (Watanabe et al. 2017) in comparison with our NoMt experiment. To investigate the role of air–sea

interaction, future studies need a coupled model experiment with sufficiently high spatial resolution and with better ability in simulating planetary boundary layer processes and mesoscale convection.

Table 5.1. Physics schemes used in the numerical experiments using the WRF Model.

| | Physics | Reference |
|---|---|---|
| Cloud Microphysics | WRF Single-Moment 6-class microphysical scheme | (Hong et al. 2004) |
| Cumulus Convection | Grell 3d ensemble cumulus scheme | (Grell and Dévényi 2002) |
| Longwave Radiation | Rapid Radiative Transfer Model (RRTM) | (Mlawer et al. 1997) |
| Shortwave Radiation | Dudhia scheme | (Dudhia 1989) |
| Surface Layer | Nakanishi–Niino PBL surface layer scheme | (Nakanishi and Niino 2004) |
| Planetary Boundary Layer | Mellor–Yamada Nakanishi–Niino Level 2.5 boundary layer scheme | (Nakanishi and Niino 2004) |
| Land Surface | Noah Land Surface Model (Noah LSM) | (Chen and Dudhia 2001) |

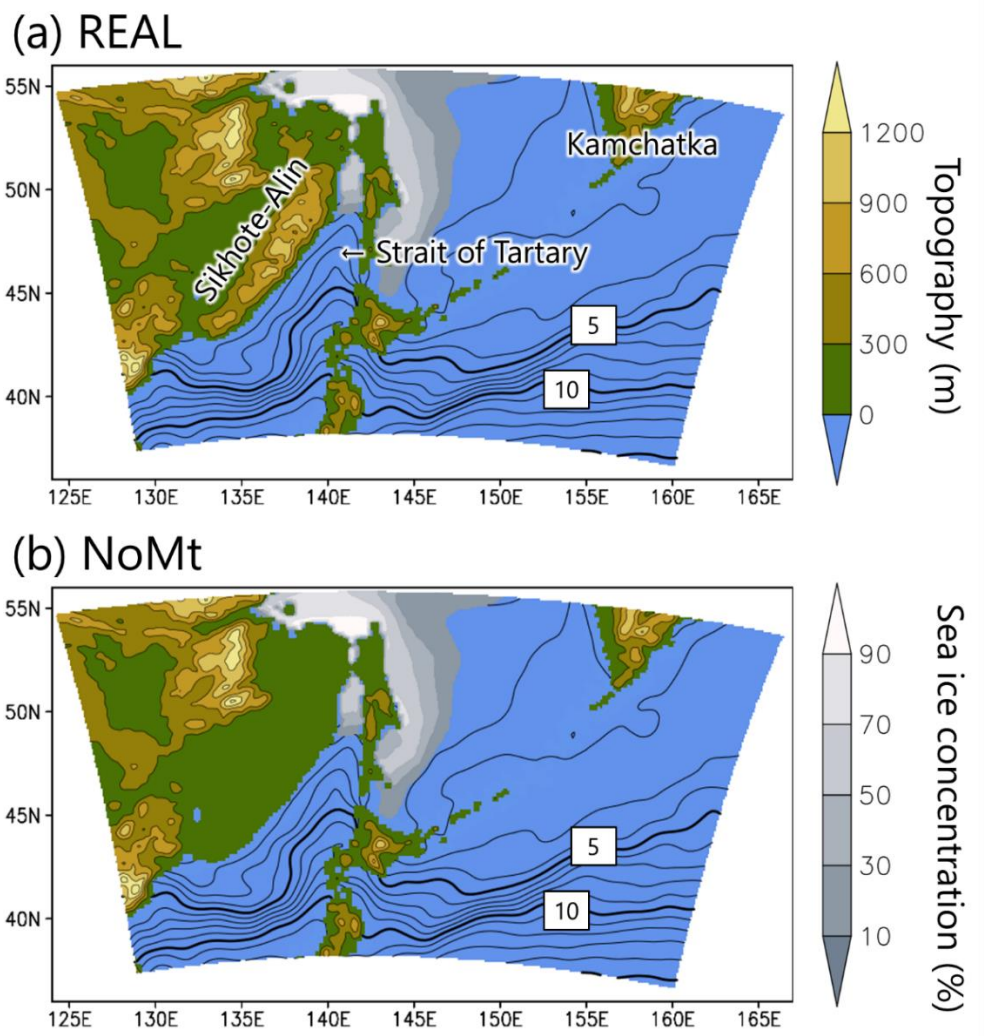


Figure 5.1. Topography (color; m), January mean sea surface temperature (contours; interval 1°C), and distribution of sea ice concentration (gray shading; %) around Hokkaido in the numerical simulations. Topography shown in (a) was used for the REAL experiment, whereas that shown in (b) was used for the NoMt experiment.

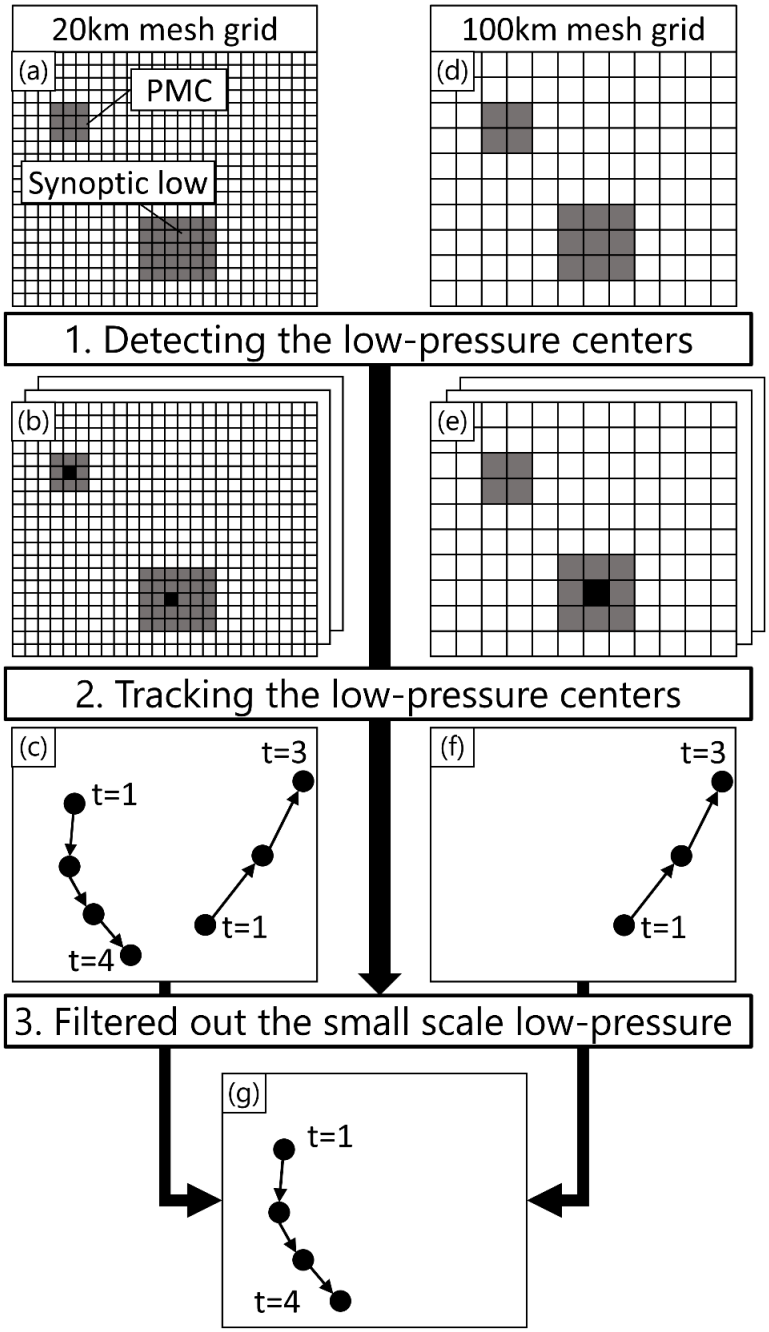


Figure 5.2. Schematic of the workflow of the PMC detection algorithm. (a) Original grid (20-km mesh grid) and (d) smoothed grid (100 km mesh grid). (b) and (e) Gray-filled grids indicate the search area validating whether there is a local minimum 850-hPa geopotential height within 3 × 3 grids. Black-filled grids indicate detected centers of low pressure. (c) and (f) Detected centers of low pressure and their tracks. (g) Track of a detected PMC. Full details are provided in the text.

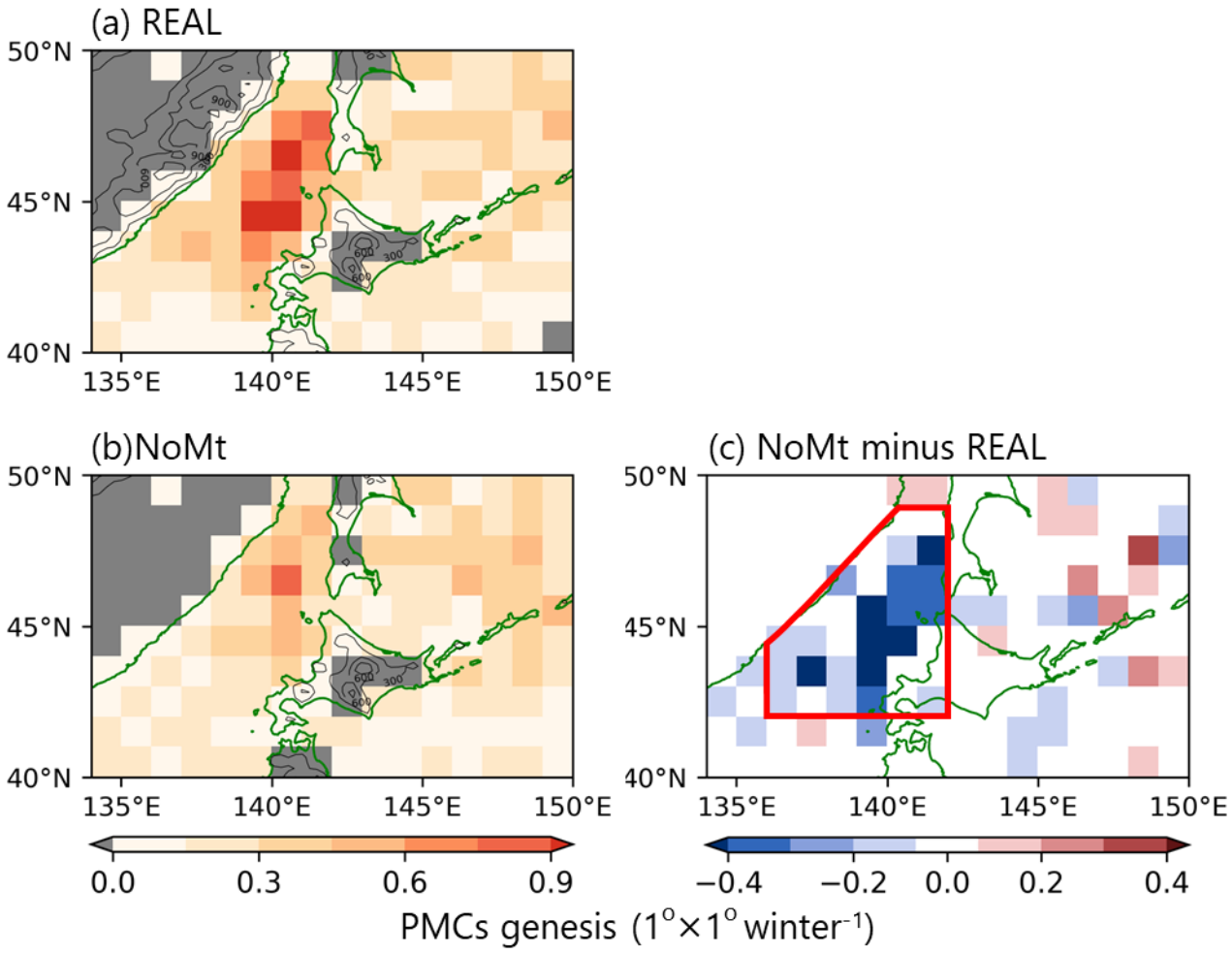


Figure 5.3. Distribution of PMC genesis over the 36 winter seasons between December 1981 and March 2017: (a) the REAL experiment, (b) the NoMt experiment, and (c) difference (i.e., NoMt − REAL). Colors indicate the number of PMCs per winter generated within each 1° × 1° box. Contours indicate the altitude at 100 m intervals. The area in which the number of PMC genesis decreased substantially (42°–49°N, 136°–142°E; red rectangle in Figure 5.3c) is defined as the target of the following analysis.

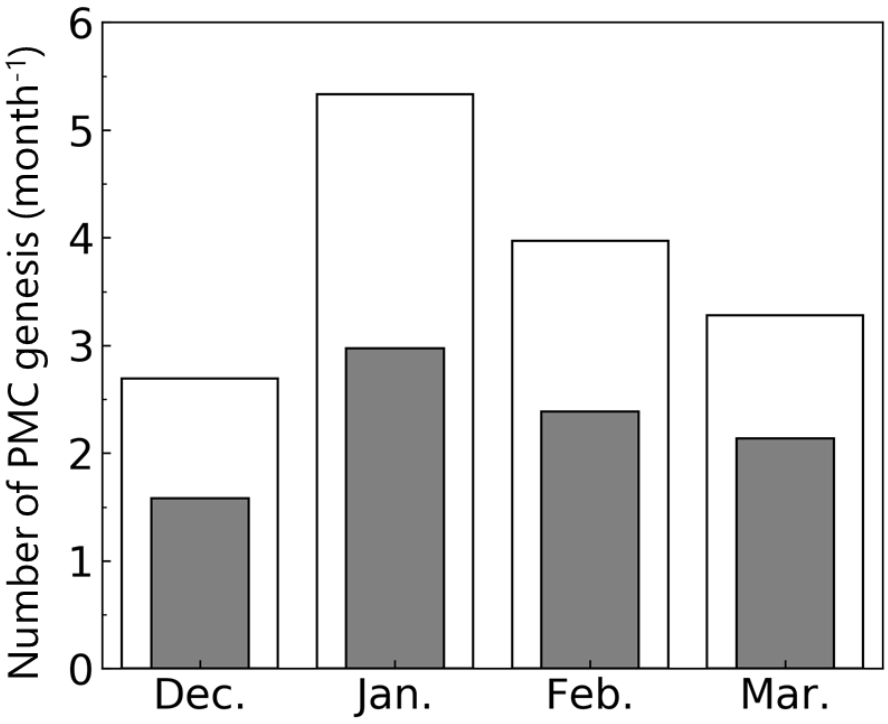


Figure 5.4. Number of PMCs generated within the analysis domain (42–49°N, 136–142°E; red rectangle in Figure 5.3c) in each month. White (gray) bar indicates the REAL (NoMt) experiment.

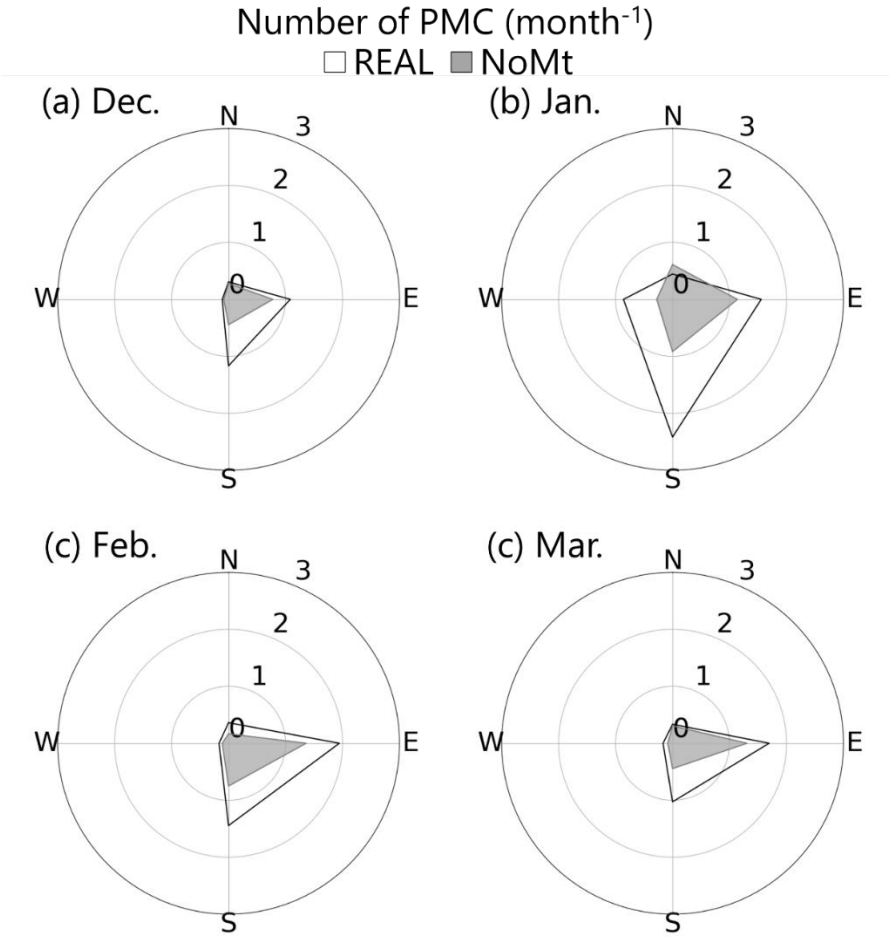


Figure 5.5. Number of PMCs moving in each of the four main cardinal directions. Black line (gray shading) indicates PMCs in the REAL (NoMt) experiment

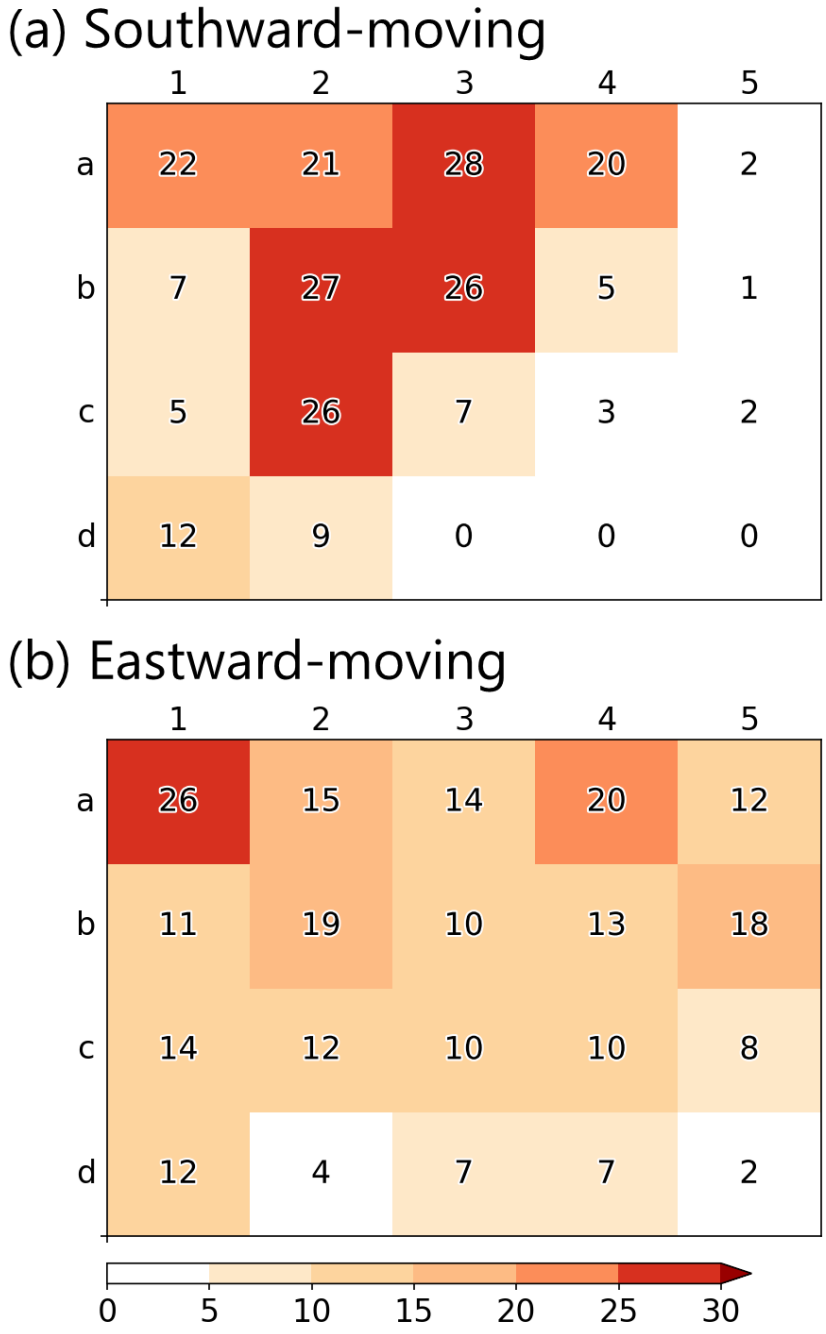


Figure 5.6. Total number of PMC genesis in the REAL experiment in the SOM illustrated in Figure 4.1. Upper (bottom) panels show southward (eastward)-moving PMCs.

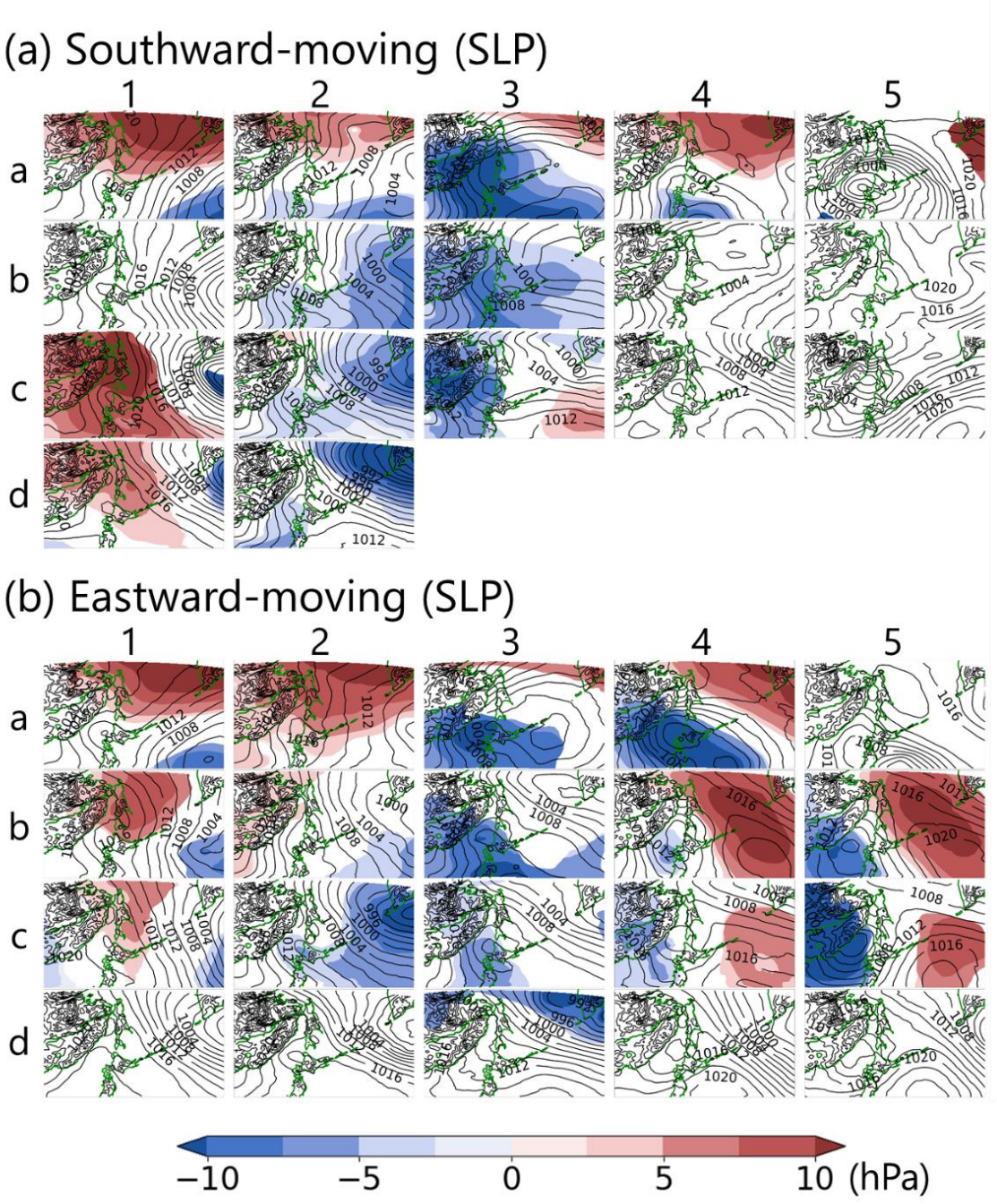


Figure 5.7. Composite map of SLP (hPa) fields averaged for cases having (a) southward-moving and (b) eastward-moving PMCs genesis. Shading indicates the mean differences between the raw data (contours) in each case and the daily climatology of 1981–2016 winters, and the difference is significant at the 0.05 confidence level (Welch's t-test). Blank nodes in (a) mean that there is no PMCs genesis.

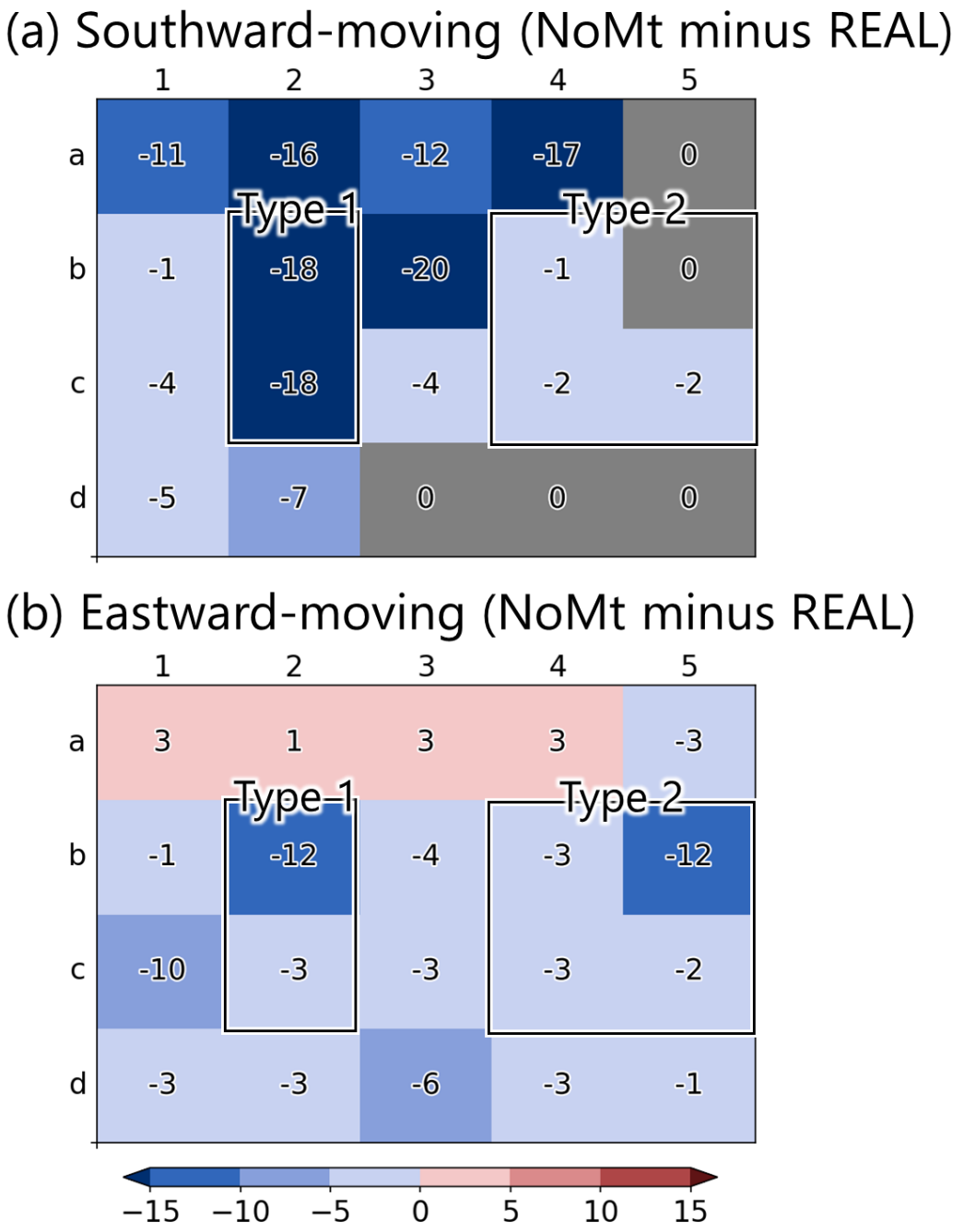


Figure 5.8. As in Figure 5.6, but for the difference (i.e., NoMt – REAL).

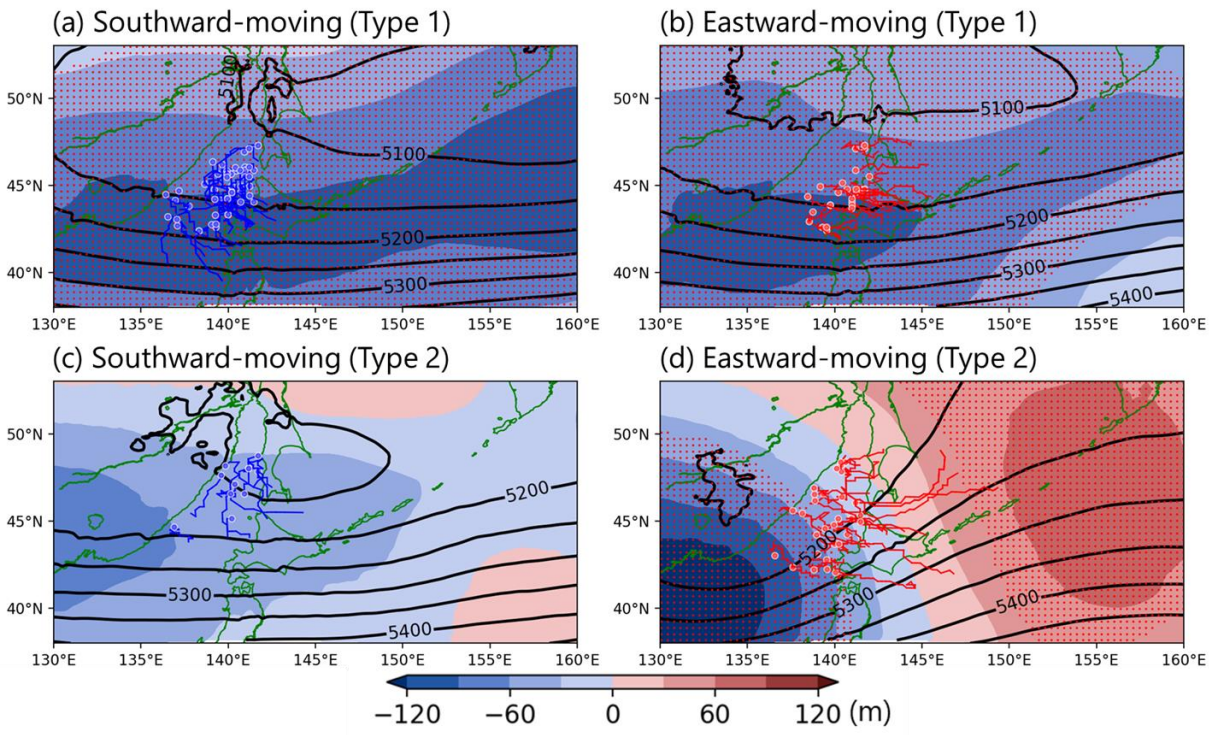


Figure 5.9. Composite fields of geopotential height at 500 hPa (m) for the 12 h before PMC genesis in REAL experiment. (a) and (b) PMCs generated in Type 1, (c) and (d) those generated in Type 2. (a) and (c) southward-moving, (b) and (d) eastward-moving PMCs. Shading indicates the mean differences between the raw data (contours) in each case and the daily climatology of 1981–2016 winters. Red dots indicate statistical significance at the 5% level for the difference (Welch's t-test). Colored dots and tracks indicate genesis location and track of PMCs (blue: southward-moving PMCs, red: eastward-moving PMCs), respectively

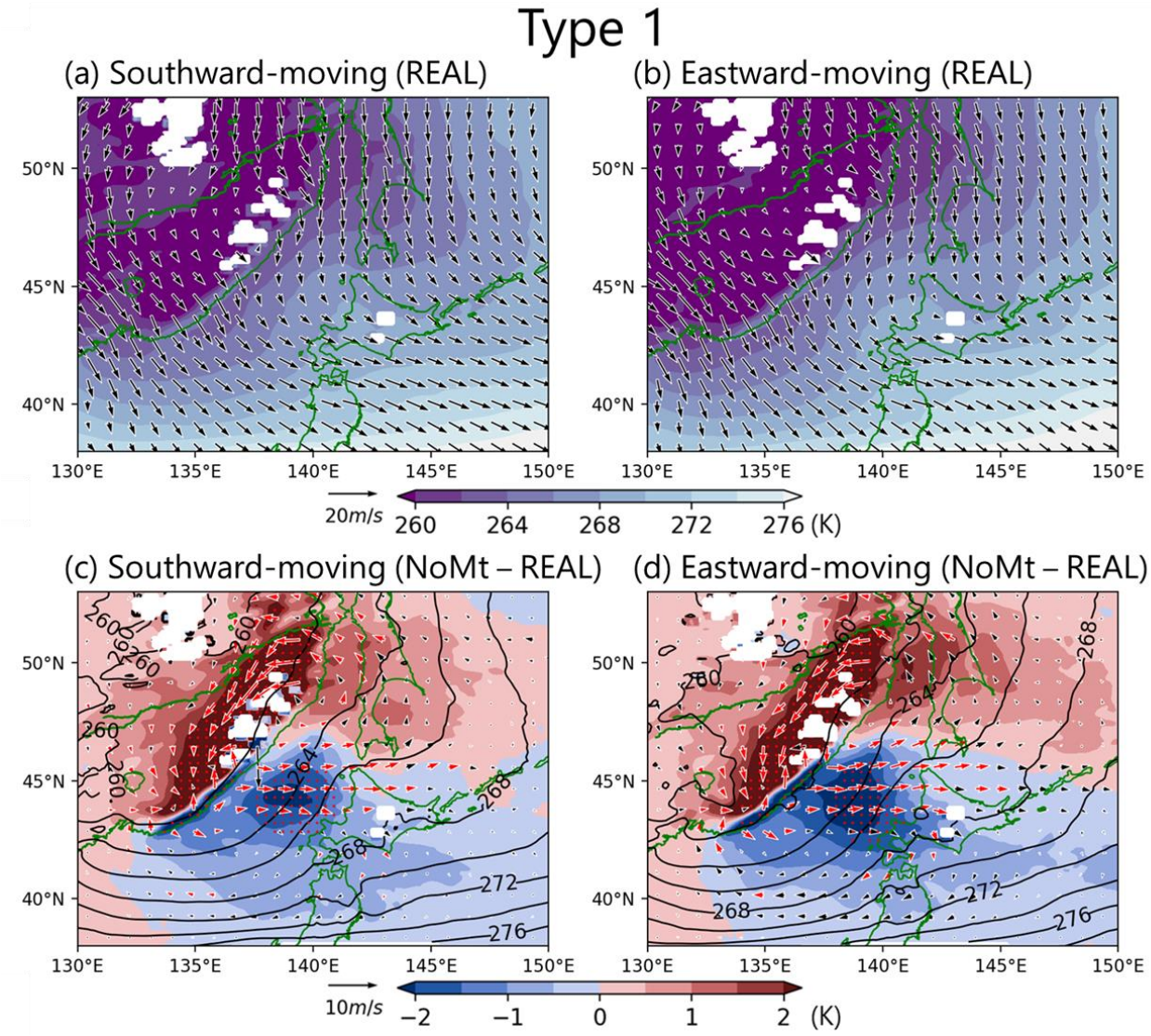


Figure 5.10. Composite and anomaly (i.e., NoMt – REAL) fields of potential temperature (shading; K) and horizontal winds (vectors) at 900 hPa for the 12 h before PMC genesis in Type 1: (a) and (c) represent southward-moving PMCs, and (b) and (d) represent eastward-moving PMCs. Red dots and arrows indicate statistical significance at the 5% level for the difference between the experiments (Welch's t-test).

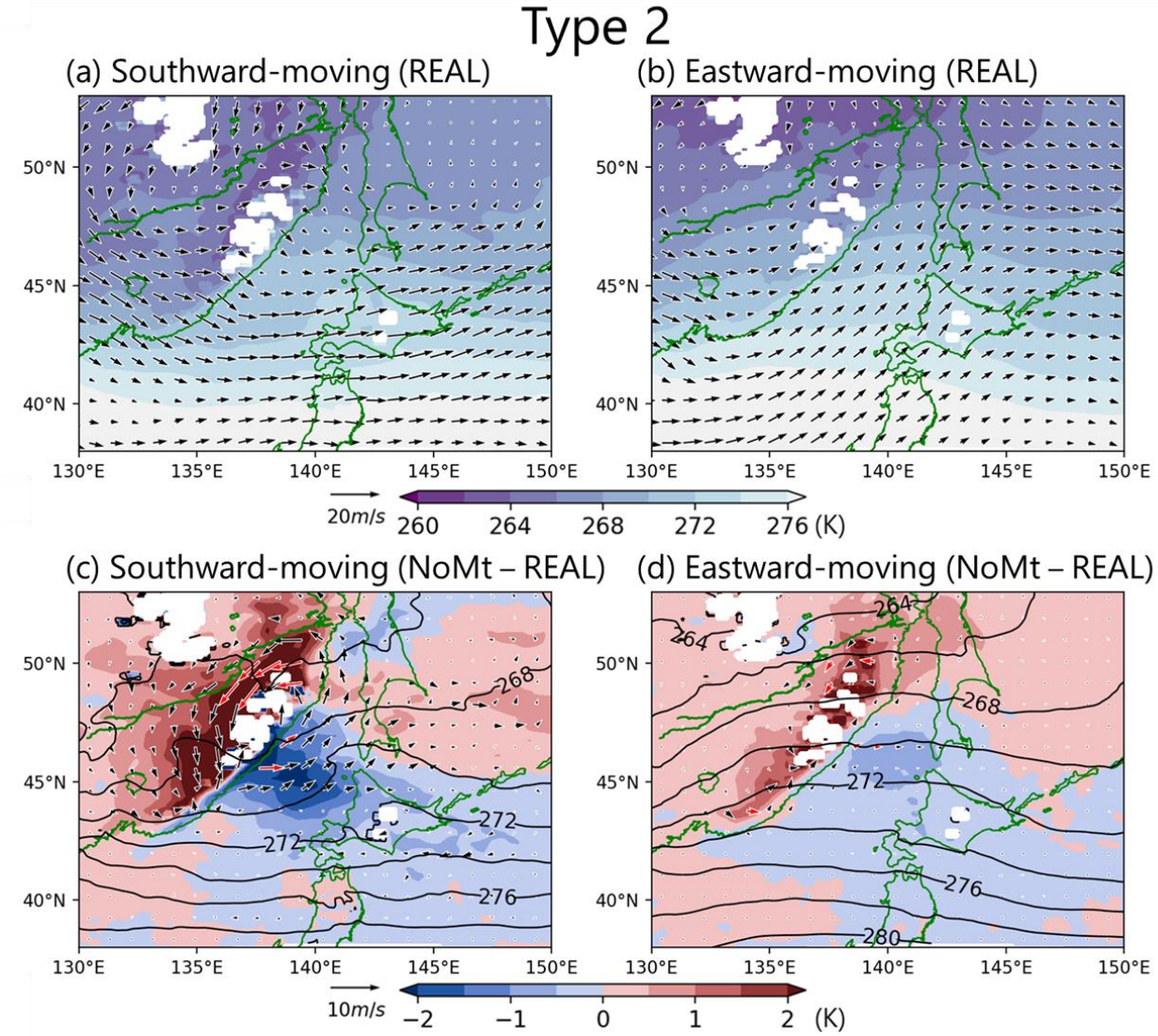


Figure 5.11. As in Figure 5.10, but for the Type 2 cyclone.

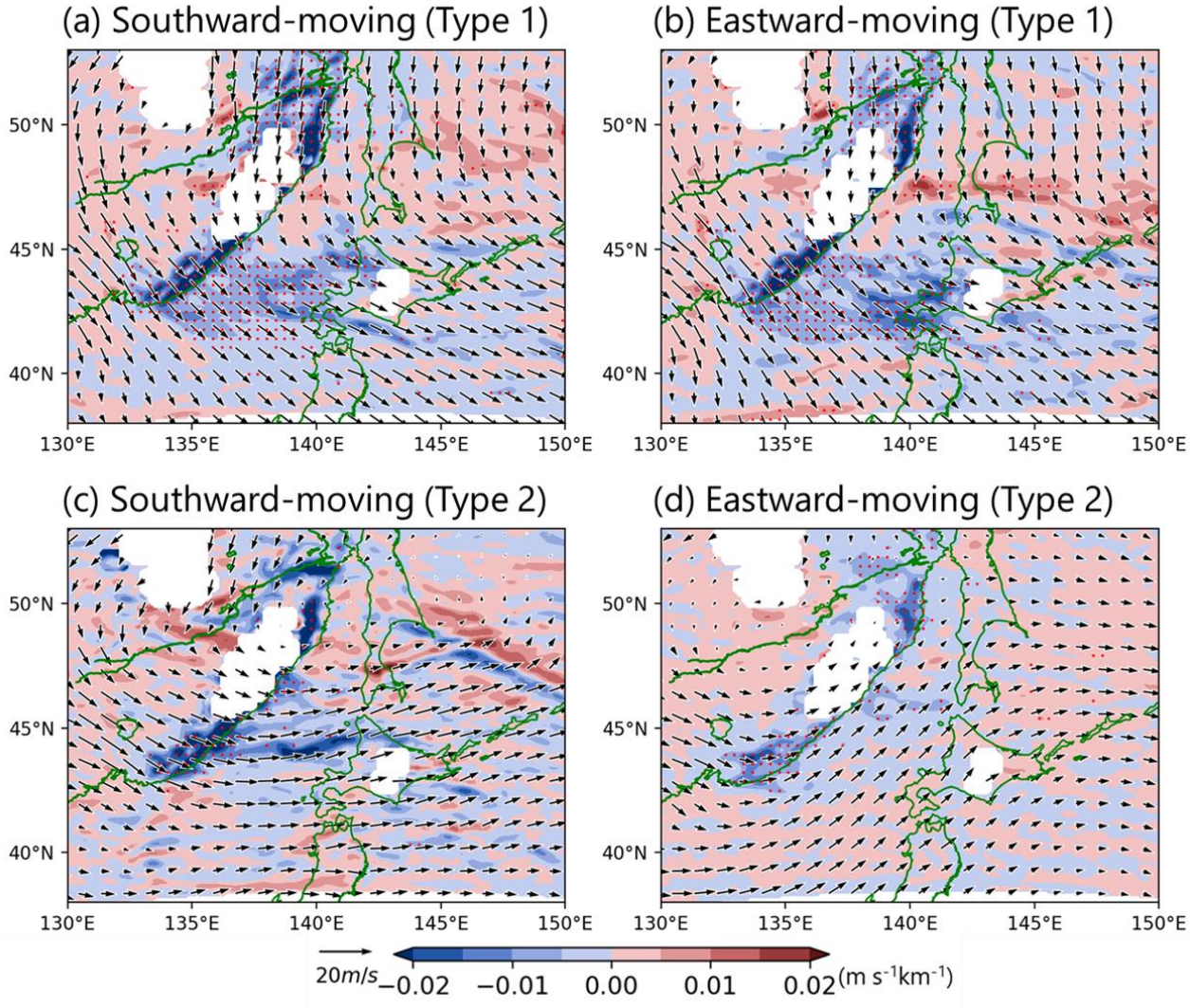


Figure 5.12. Anomaly fields of the magnitude of zonal wind gradient (i.e., NoMt – REAL) and wind field in the NoMt experiment (vector) at 900 hPa for the 12 h before PMC genesis. (a) and (b) PMCs generated in the Type 1, (c) and (d) Type 2. (a) and (c) for southward-moving PMCs and (b) and (d) for eastward-moving PMCs. Red dots indicate statistical significance at the 5% level for the difference between the experiments (Welch's t-test).

# 6. Summary and discussion

Strong winds and precipitation brought by winter cyclones have caused disasters in many parts of Japan. Therefore, it is important to study the interannual variations of winter cyclone activity from the viewpoint of adaptation to climate change. In East Asia, the number of winter cyclones is expected to become less with climate change (Mizuta et al. 2011). This tendency is also observed in long-term trends over recent years (Lee et al. 2020). In addition to extratropical cyclones, mesoscale cyclones also occur around Japan in winter. Therefore, the inclusion of mesoscale cyclones in the analysis may reveal regional characteristics in the long-term trend of winter cyclone activity. In this study, analysis of the long-term changes in winter cyclone activity and its factors for the cyclones around Japan were conducted.

In this study, three statistical analyses for winter cyclone activity around Japan are presented. The first analysis is implemented by the objective tracking of cyclones, in which a cyclone tracking algorithm is applied to the long-term reanalysis data in order to reveal the interannual variations of the number of cyclone passages. The results show that the frequency of cyclone passages around Hokkaido, located in northern Japan, tends to decrease. The main source regions of those cyclones are the offshore region west of Hokkaido and the western part of the Sea of Japan. Only the number of cyclogeneses over and around the offshore region west of Hokkaido is significantly decreased. It is also found that this cyclone has a short lifetime and a relatively small horizontal scale and that it occurs with the upper-level trough located over the offshore region west of Hokkaido. These results suggest that most of the cyclones decreasing are mesoscale cyclones.

The second is the classification of surface pressure patterns using self-organizing maps, which

is a kind of machine learning technique. In this study, the self-organizing maps was adapted to classify winter surface pressure patterns around Hokkaido to clarify the characteristics of the synoptic-scale atmospheric conditions at the occurrence of the cyclone generated around the offshore region west of Hokkaido. As a result, it is found that most of the cyclones are generated when cold air is advected over the offshore region west of Hokkaido by a west-east high and low surface pressure pattern consisting of high pressure over the continent (Siberian High) and low pressure over the Sea of Okhotsk (Aleutian Low). The characteristics of these atmospheric fields are similar to the atmospheric conditions at the mesoscale cyclogenesis over the offshore region west of Hokkaido. Furthermore, the number of occurrences of this cyclone showed a significant decreasing trend, suggesting that the decrease in the number of mesocyclones over the offshore region west of Hokkaido is the main reason for the decrease in the number of cyclone passages around Hokkaido.

The third is a numerical experiment using a regional climate model. In this study, a long-term, high-resolution experiment was conducted to statistically analyze the relationship between the factors that cause mesocyclones over the offshore west of Hokkaido and the synoptic-scale atmospheric conditions at the time of cyclone occurrence. In addition, a sensitivity experiment was conducted by removing a mountain range on the eastern edge of the Eurasian Continent, which is considered to be a factor in the occurrence of the mesocyclone. Statistical analysis shows that the number of mesocyclones generated over the offshore west of Hokkaido decreases with the removal of the Sikhote-Alin mountain range. Analysis using the self-organizing map-based classification revealed that most of the mesocyclones occurring in the west-east high and low surface pressure

pattern are generated by the presence of the mountains. The Sikhote-Alin mountain range blocks some of the cold air advection from the continent to the Sea of Japan, and the relatively low elevation on the south of the mountain region causes horizontal wind shear in the lower troposphere over the offshore region west of Hokkaido. This horizontal wind shear is considered to be the initial disturbance causing the formation of the mesocyclone over this region. This study was able to clarify the regional characteristics of winter cyclones around Hokkaido through the analysis of reanalysis data and high-resolution data from the regional climate model. The results are summarized as follows.

1) The number of cyclone passages around Hokkaido has been decreasing since the 1960s, and 60% of the decrease can be explained by a decrease in the number of cyclones generated in the area around the offshore region west of Hokkaido.

2) Among the cyclones occurring around the offshore region west of Hokkaido, the number of mesocyclones, which occur in a west-east high and low surface pressure pattern, has markedly decreased.

3) The weakening of lower-level cold air advection into the area over the offshore region west of Hokkaido is likely to be suppressed the number of occurrences of cyclogenesis in this area.

4) The mesoscale cyclones that develop over the offshore area west of Hokkaido under a west-east high and low surface pressure pattern are generated by lower-level wind shear caused by the presence of the mountains at the eastern edge of the continent.

Winter cyclones bring disasters caused by strong winds and snowfall, which have a huge impact on human activities. For example, the winter of 2021/2022 brought record snowfalls

associated with cyclone activities (Japan Meteorological Agency 2022), causing many problems, especially in Hokkaido, including cancellations of trains and airplanes and traffic disruptions. Therefore, the characteristics of winter cyclone activity around Hokkaido shown in this study may be an important finding from the viewpoint of adaptation to climate change. Furthermore, comparison of cyclone activity among the JRA-55 products in this study suggested that data assimilation of conventional observations determines the atmospheric conditions over Eurasia, and hence the cyclone activity around Hokkaido is determined. This means that the expansion of the observations over Eurasia may contribute to improved winter weather forecasts in Japan, especially in Hokkaido. I hope that this new insight will contribute to the development of many kinds of research related to the winter climate around Japan. Since cyclone activity also affects the activities of wildlife such as seabirds (Clairbaux et al. 2021), the results of the present study may also contribute to the assessment of the effects of regional climate on animal activity in and around Hokkaido. Therefore, the study of regional climate can create new interdisciplinary research through a combination of data from other fields.

# Reference


Adachi, S., and F. Kimura, 2007: A 36-year Climatology of Surface Cyclogenesis in East Asia Using High-resolution Reanalysis Data. *SOLA*, **3**, 113–116, https://doi.org/10.2151/sola.2007-029.

Asai, T., 1988: Mesoscale Features of Heavy Snowfalls in Japan Sea Coastal Regions of Japan. *Tenki*, **35**, 156–161, (in Japanese).

Blackmon, M. L., J. M. Wallace, N.-C. Lau, and S. L. Mullen, 1977: An Observational Study of the Northern Hemisphere Wintertime Circulation. *J. Atmos. Sci.*, **34**, 1040–1053, https://doi.org/10.1175/1520-0469(1977)034<1040:AOSOTN>2.0.CO;2.

Boyle, J. S., and T.-J. Chen, 1987: Synoptic Aspects of the Wintertime East Asian Monsoon. *Monsoon Meteorology*, 125–160.

Carleton, A. M., and D. A. Carpenter, 1990: Satellite Climatology of 'Polar Lows' and Broadscale Climatic Associations for the Southern Hemisphere. *Int. J. Climatol.*, **10**, 219–246, https://doi.org/10.1002/joc.3370100302.

Chang, C.-P., J. E. Erickson, and K. M. Lau, 1979: Northeasterly Cold Surges and Near-Equatorial Disturbances over the Winter MONEX Area during December 1974. Part I: Synoptic Aspects. *Mon. Weather Rev.*, **107**, 812–829, https://doi.org/10.1175/1520-0493(1979)107<0812:NCSANE>2.0.CO;2.

Chang, E. K. M., 1993: Downstream Development of Baroclinic Waves As Inferred from Regression Analysis. *J. Atmos. Sci.*, **50**, 2038–2053, https://doi.org/10.1175/1520-0469(1993)050<2038:DDOBWA>2.0.CO;2.

Chen, F., and J. Dudhia, 2001: Coupling an Advanced Land Surface–Hydrology Model with the Penn State–NCAR MM5 Modeling System. Part I: Model Implementation and Sensitivity. *Mon. Weather Rev.*, **129**, 569–585, https://doi.org/10.1175/1520-0493(2001)129<0569:CAALSH>2.0.CO;2.

Chen, S.-J., Y.-H. Kuo, P.-Z. Zhang, and Q.-F. Bai, 1991: Synoptic Climatology of Cyclogenesis over East Asia, 1958-1987. *Mon. Weather Rev.*, **119**, 1407–1418, https://doi.org/10.1175/1520-0493(1991)119<1407:SCOCOE>2.0.CO;2.

——, ——, P.-Z. Zhang, and Q.-F. Bai, 1992: Climatology of Explosive Cyclones off the East Asian Coast. *Mon. Weather Rev.*, **120**, 3029–3035, https://doi.org/10.1175/1520-0493(1992)120<3029:COECOT>2.0.CO;2.

Chung, Y.-S., K. D. Hage, and E. R. Reinelt, 1976: On Lee Cyclogenesis and Airflow in the Canadian Rocky Mountains and the East Asian Mountains. *Mon. Weather Rev.*, **104**, 879–891, https://doi.org/10.1175/1520-0493(1976)104<0879:OLCAAI>2.0.CO;2.

Clairbaux, M., and Coauthors, 2021: North Atlantic Winter Cyclones Starve Seabirds. *Curr. Biol.*, **31**, 3964-3971.e3, https://doi.org/10.1016/j.cub.2021.06.059.

Ding, Y., and T. N. Krishnamurti, 1987: Heat Budget of the Siberian High and the Winter Monsoon. *Mon. Weather Rev.*, **115**, 2428–2449, https://doi.org/10.1175/1520-0493(1987)115<2428:HBOTSH>2.0.CO;2.

Dudhia, J., 1989: Numerical Study of Convection Observed during the Winter Monsoon Experiment Using a Mesoscale Two-Dimensional Model. *J. Atmos. Sci.*, **46**, 3077–3107, https://doi.org/10.1175/1520-0469(1989)046<3077:NSOCOD>2.0.CO;2.

Emanuel, K. A., and R. Rotunno, 1989: Polar Lows as Arctic Hurricanes. *Tellus Ser. A Dyn. Meteorol. Oceanogr.*, **41 A**, 1–17, https://doi.org/10.1111/j.1600-0870.1989.tb00362.x.

Esteban, P., P. D. Jones, J. Martín-Vide, and M. Mases, 2005: Atmospheric Circulation Patterns Related to Heavy Snowfall Days in Andorra, Pyrenees. *Int. J. Climatol.*, **25**, 319–329, https://doi.org/10.1002/joc.1103.

Farukh, M. A., and T. J. Yamada, 2018: Synoptic Climatology of Winter Daily Temperature Extremes in Sapporo, Northern Japan. *Int. J. Climatol.*, **38**, 2230–2238, https://doi.org/10.1002/joc.5329.

Fujiyoshi, Y., K. Tsuboki, H. Konishi, and G. Wakahama, 1988: Doppler Radar Observation of Convergence Band Cloud Formed on the West Coast of Hokkaido Island (I): Warm Frontal Type. *Tenki*, **35**, 427–439, (in Japanese).

Gan, B., and L. Wu, 2013: Seasonal and Long-Term Coupling between Wintertime Storm Tracks and Sea Surface Temperature in the North Pacific. *J. Clim.*, **26**, 6123–6136, https://doi.org/10.1175/JCLI-D-12-00724.1.

Gong, D.-Y., S.-W. Wang, and J.-H. Zhu, 2001: East Asian Winter Monsoon and Arctic Oscillation. *Geophys. Res. Lett.*, **28**, 2073–2076, https://doi.org/10.1029/2000gl012311.

Grell, G. A., and D. Dévényi, 2002: A Generalized Approach to Parameterizing Convection Combining Ensemble and Data Assimilation Techniques. *Geophys. Res. Lett.*, **29**, 38-1-38–4, https://doi.org/10.1029/2002gl015311.

Gyakum, J. R., J. R. Anderson, R. H. Grumm, and E. L. Gruner, 1989: North Pacific Cold-Season Surface Cyclone Activity: 1975–1983. *Mon. Weather Rev.*, **117**, 1141–1155, https://doi.org/10.1175/1520-0493(1989)117<1141:NPCSSC>2.0.CO;2.

Hanson, H. P., and B. Long, 1985: Climatology of Cyclogenesis over the East China Sea. *Mon. Weather Rev.*, **113**, 697–707, https://doi.org/10.1175/1520-0493(1985)113<0697:COCOTE>2.0.CO;2.

Harold, J. M., G. R. Bigg, and J. Turner, 1999: Mesocyclone Activity over the North-East Atlantic.

Part 1: Vortex Distribution and Variability. *Int. J. Climatol.*, **19**, 1187–1204, https://doi.org/10.1002/(sici)1097-0088(199909)19:11<1187::aid-joc419>3.0.co;2-q.

Hayasaki, M., and R. Kawamura, 2012: Cyclone Activities in Heavy Rainfall Episodes in Japan during Spring Season. *SOLA*, **8**, 45–48, https://doi.org/10.2151/sola.2012-012.

Hirata, H., 2021: Climatological Features of Strong Winds Caused by Extratropical Cyclones around Japan. *J. Clim.*, **34**, 4481–4494, https://doi.org/10.1175/JCLI-D-20-0577.1.

Hong, S.-Y., J. Dudhia, and S.-H. Chen, 2004: A Revised Approach to Ice Microphysical Processes for the Bulk Parameterization of Clouds and Precipitation. *Mon. Weather Rev.*, **132**, 103–120, https://doi.org/10.1175/1520-0493(2004)132<0103:ARATIM>2.0.CO;2.

Iizuka, S., M. Shiota, R. Kawamura, and H. Hatsushika, 2013: Influence of the Monsoon Variability and Sea Surface Temperature Front on the Explosive Cyclone Activity in the Vicinity of Japan during Northern Winter. *SOLA*, **9**, 1–4, https://doi.org/10.2151/sola.2013-001.

Inatsu, M., S. Kawazoe, and M. Mori, 2021: Trends and Projection of Heavy Snowfall in Hokkaido, Japan, as an Application of Self-organizing Map. *J. Appl. Meteorol. Climatol.*, **60**, 1483–1494, https://doi.org/10.1175/JAMC-D-21-0085.1.

Iwasaki, T., T. Shoji, Y. Kanno, M. Sawada, M. Ujiie, and K. Takaya, 2014: Isentropic Analysis of Polar Cold Airmass Streams in the Northern Hemispheric Winter. *J. Atmos. Sci.*, **71**, 2230–2243, https://doi.org/10.1175/JAS-D-13-058.1.

Japan Meteorological Agency, 2022: Press Release (Characteristics of 2022 Winter). https://www.jma.go.jp/jma/press/2203/01b/tenko221202.html, (in Japanese).

Jhun, J.-G., and E.-J. Lee, 2004: A New East Asian Winter Monsoon Index and Associated Characteristics of the Winter Monsoon. *J. Clim.*, **17**, 711–726, https://doi.org/10.1175/1520-0442(2004)017<0711:ANEAWM>2.0.CO;2.

Kanno, Y., M. R. Abdillah, and T. Iwasaki, 2016: Long-term Trend of Cold Air Mass Amount Below a Designated Potential Temperature in Northern and Southern Hemispheric Winters using Reanalysis Data Sets. *J. Geophys. Res.*, **121**, 10,138-10,152, https://doi.org/10.1002/2015jd024635.

Kashiwabara, T., 1988: On the Recent Winter Cooling in the North Pacific. *Tenki*, **34**, 771–781, (in Japanese).

Kawamura, H., and P. Wu, 1998: Formation Mechanism of Japan Sea Proper Water in the Flux Center off Vladivostok. *J. Geophys. Res.*, **103**, 21611–21622, https://doi.org/10.1029/98jc01948.

Kawase, H., and Coauthors, 2018: Characteristics of Synoptic Conditions for Heavy Snowfall in Western to Northeastern Japan Analyzed by the 5-km Regional Climate Ensemble Experiments.

*J. Meteor. Soc. Japan*, **96**, 161–178, https://doi.org/10.2151/jmsj.2018-022.

——, and Coauthors, 2021: Regional Characteristics of Future Changes in Snowfall in Japan under RCP2.6 and RCP8.5 Scenarios. *SOLA*, **17**, 1–7, https://doi.org/10.2151/sola.2021-001.

Kawazoe, S., M. Inatsu, T. J. Yamada, and T. Hoshino, 2020: Climate Change Impacts on Heavy Snowfall in Sapporo Using 5-km Mesh Large Ensemble Simulations. *SOLA*, **16**, 233–239, https://doi.org/10.2151/sola.2020-039.

Kobayashi, C., H. Endo, Y. Ota, S. Kobayashi, H. Onoda, Y. Harada, K. Onogi, and H. Kamahori, 2014: Preliminary Results of the JRA-55C, an Atmospheric Reanalysis Assimilating Conventional Observations Only. *SOLA*, **10**, 78–82, https://doi.org/10.2151/sola.2014-016.

Kobayashi, S., and Coauthors, 2015: The JRA-55 Reanalysis: General Specifications and Basic Characteristics. *J. Meteor. Soc. Japan*, **93**, 5–48, https://doi.org/10.2151/jmsj.2015-001.

Kohonen, T., 1982: Self-organized Formation of Topologically Correct Feature Maps. *Biol. Cybern.*, **43**, 59–69, https://doi.org/10.1007/BF00337288.

——, 2001: *Self-organizing Maps*. Springer Science & Business Media, 501 pp.

Kolstad, E. W., 2011: A Global Climatology of Favourable Conditions for Polar Lows. *Q.J.R. Meteorol. Soc.*, **137**, 1749–1761, https://doi.org/10.1002/qj.888.

——, 2017: Higher Ocean Wind Speeds during Marine Cold Air Outbreaks. *Q.J.R. Meteorol. Soc.*, **143**, 2084–2092, https://doi.org/10.1002/qj.3068.

——, and T. J. Bracegirdle, 2017: Sensitivity of an Apparently Hurricane-like Polar Low to Sea-surface Temperature. *Q.J.R. Meteorol. Soc.*, **143**, 966–973, https://doi.org/10.1002/qj.2980.

——, ——, and I. A. Seierstad, 2009: Marine Cold-air Outbreaks in the North Atlantic: Temporal Distribution and Associations with Large-scale Atmospheric Circulation. *Clim. Dyn.*, **33**, 187–197, https://doi.org/10.1007/s00382-008-0431-5.

Kristjánsson, J. E., S. Thorsteinsson, E. W. Kolstad, and A. M. Blechschmidt, 2011: Orographic Influence of East Greenland on a Polar Low over the Denmark Strait. *Q.J.R. Meteorol. Soc.*, **137**, 1773–1789, https://doi.org/10.1002/qj.831.

Lau, N.-C., and K.-M. Lau, 1984: The Structure and Energetics of Midlatitude Disturbances Accompanying Cold-Air Outbreaks over East Asia. *Mon. Weather Rev.*, **112**, 1309–1327, https://doi.org/10.1175/1520-0493(1984)112<1309:TSAEOM>2.0.CO;2.

Lee, J., S.-W. Son, H.-O. Cho, J. Kim, D.-H. Cha, J. R. Gyakum, and D. Chen, 2020: Extratropical Cyclones over East Asia: Climatology, Seasonal Cycle, and Long-Term Trend. *Clim. Dyn.*, **54**, 1131–1144, https://doi.org/10.1007/s00382-019-05048-w.

Lennard, C., and G. Hegerl, 2015: Relating Changes in Synoptic Circulation to the Surface Rainfall Response Using Self-organising Maps. *Clim. Dyn.*, **44**, 861–879, https://doi.org/10.1007/s00382-014-2169-6.

Lund, I. A., 1963: Map-Pattern Classification by Statistical Methods. *J. Appl. Meteorol. Climatol.*, **2**, 56–65, https://doi.org/10.1175/1520-0450(1963)002<0056:MPCBSM>2.0.CO;2.

Mailhot, J., D. Hanley, B. Bilodeau, and O. Hertzman, 1996: A Numerical Case Study of a Polar Low in the Labrador Sea. *Tellus Ser. A Dyn. Meteorol. Oceanogr.*, **48**, 383–402, https://doi.org/10.3402/tellusa.v48i3.12067.

Mizuta, R., M. Matsueda, H. Endo, and S. Yukimoto, 2011: Future Change in Extratropical Cyclones Associated with Change in the Upper Troposphere. *J. Clim.*, **24**, 6456–6470, https://doi.org/10.1175/2011JCLI3969.1.

Mlawer, E. J., S. J. Taubman, P. D. Brown, M. J. Iacono, and S. A. Clough, 1997: Radiative Transfer for Inhomogeneous Atmospheres: RRTM, a Validated Correlated-k Model for the Longwave. *J. Geophys. Res.*, **102**, 16663–16682, https://doi.org/10.1029/97jd00237.

Murakami, T., and A. Sumi, 1981: Large-scale Aspects of the 1978-79 Winter Circulation over the Greater WMONEX Region. *J. Meteor. Soc. Japan*, **59**, 646–671, https://doi.org/10.2151/jmsj1965.59.5_646.

Nakanishi, M., and H. Niino, 2004: An Improved Mellor–Yamada Level-3 Model with Condensation Physics: Its Design and Verification. *Bound.-Layer Meteorol.*, **112**, 1–31, https://doi.org/10.1023/B:BOUN.0000020164.04146.98.

Ninomiya, K., 1989: Polar/Comma-Cloud Lows over the Japan Sea and the Northwestern Pacific in Winter. *J. Meteor. Soc. Japan*, **67**, 83–97, https://doi.org/10.2151/jmsj1965.67.1_83.

——, 1991: Polar Low Development over the East Coast of the Asian Continent on 9-11 December 1985. *J. Meteor. Soc. Japan*, **69**, 669–685, https://doi.org/10.2151/jmsj1965.69.6_669.

——, K. Wakahara, and H. Ohkubo, 1993: Meso-α-scale Low Development over the Northeastern Japan Sea under the Influence of a Parent Large-scale Low and a Cold Vortex Aloft. *J. Meteor. Soc. Japan*, **71**, 73–91, https://doi.org/10.2151/jmsj1965.71.1_73.

——, J. Fujimori, and T. Akiyama, 1996: Multi-scale Features of the Cold Air Outbreak over the Japan Sea and the Northwestern Pacific. *J. Meteor. Soc. Japan*, **74**, 745–761, https://doi.org/10.2151/jmsj1965.74.6_745.

Ohba, M., S. Kadokura, Y. Yoshida, D. Nohara, and Y. Toyoda, 2015: Anomalous Weather Patterns in Relation to Heavy Precipitation Events in Japan during the Baiu Season. *J. Hydrometeorol.*, **16**, 688–701, https://doi.org/10.1175/JHM-D-14-0124.1.

Ohtake, H., M. Kawashima, and Y. Fujiyoshi, 2009: The Formation Mechanism of a Thick Cloud

Band over the Northern Part of the Sea of Japan during Cold Air Outbreaks. *J. Meteor. Soc. Japan*, **87**, 289–306, https://doi.org/10.2151/jmsj.87.289.

Orlanski, I., 1975: A Rational Subdivision of Scales for Atmospheric Processes. *Bull. Amer. Meteor. Soc.*, **56**, 527–534, https://doi.org/10.1175/1520-0477-56.5.527.

Parkinson, C. L., 1990: The Impact of the Siberian High and Aleutian Low on the Sea-Ice Cover of the Sea of Okhotsk. *Ann. Glaciol.*, **14**, 226–229, https://doi.org/10.3189/S0260305500008636.

Rasmussen, E., 1979: The Polar Low as an Extratropical CISK Disturbance. *Q.J.R. Meteorol. Soc.*, **105**, 531–549, https://doi.org/10.1002/qj.49710544504.

Rasmussen, E., 1985: A Case Study of a Polar Low Development over the Barents Sea. *Tellus Ser. A Dyn. Meteorol. Oceanogr.*, **37**, 407–418, https://doi.org/10.3402/tellusa.v37i5.11685.

Rasmussen, E. A., and J. Turner, 2003: *Polar Lows*. Cambridge University Press, 612 pp.

Reed, R. J., and C. N. Duncan, 1987: Baroclinic Instability as a Mechanism for the Serial Development of Polar Lows: a Case Study. *Tellus Ser. A Dyn. Meteorol. Oceanogr.*, **39**, 376–384, https://doi.org/10.3402/tellusa.v39i4.11766.

Reynolds, R. W., T. M. Smith, C. Liu, D. B. Chelton, K. S. Casey, and M. G. Schlax, 2007: Daily High-Resolution-Blended Analyses for Sea Surface Temperature. *J. Clim.*, **20**, 5473–5496, https://doi.org/10.1175/2007JCLI1824.1.

Sakai, K., R. Kawamura, and Y. Iseri, 2010: ENSO-induced Tropical Convection Variability over the Indian and Western Pacific Oceans during the Northern Winter as Revealed by a Self-organizing map. *J. Geophys. Res.*, **115**, https://doi.org/10.1029/2010jd014415.

Sanders, F., and J. R. Gyakum, 1980: Synoptic-Dynamic Climatology of the “Bomb.” *Mon. Weather Rev.*, **108**, 1589–1606, https://doi.org/10.1175/1520-0493(1980)108<1589:SDCOT>2.0.CO;2.

Sato, T., and S. Sugimoto, 2013: A Numerical Experiment on the Influence of the Interannual Variation of Sea Surface Temperature on Terrestrial Precipitation in Northern Japan during the Cold Season. *Water Resour. Res.*, **49**, 7763–7777, https://doi.org/10.1002/2012WR013206.

Sergeev, D., I. A. Renfrew, and T. Spengler, 2018: Modification of Polar Low Development by Orography and Sea Ice. *Mon. Weather Rev.*, **146**, 3325–3341, https://doi.org/10.1175/MWR-D-18-0086.1.

Shimizu, H., R. Kawamura, T. Kawano, and S. Iizuka, 2017: Dynamical Modulation of Wintertime Synoptic-Scale Cyclone Activity over the Japan Sea due to Changbai Mountain in the Korean Peninsula. *Advances in Meteorology*, **2017**, https://doi.org/10.1155/2017/6216032.

Shinoda, Y., R. Kawamura, T. Kawano, and H. Shimizu, 2021: Dynamical Role of the Changbai

Mountains and the Korean Peninsula in the Wintertime Quasi-Stationary Convergence Zone over the Sea of Japan. *Int. J. Climatol.*, **41**, https://doi.org/10.1002/joc.6713.

Skamarock, W., J. Klemp, J. Dudhia, D. Gill, D. Barker, W. Wang, X.-Y. Huang, and M. Duda, 2008: *A Description of the Advanced Research WRF Version 3*. UCAR/NCAR,.

Stoll, P. J., R. G. Graversen, G. Noer, and K. Hodges, 2018: An Objective Global Climatology of Polar Lows based on Reanalysis Data. *Q.J.R. Meteorol. Soc.*, **144**, 2099–2117, https://doi.org/10.1002/qj.3309.

Takano, I., 2002: Analysis of an Intense Winter Extratropical Cyclone that Advanced along the South Coast of Japan. *J. Meteor. Soc. Japan*, **80**, 669–695, https://doi.org/10.2151/jmsj.80.669.

Takaya, K., and H. Nakamura, 2005: Mechanisms of Intraseasonal Amplification of the Cold Siberian High. *J. Atmos. Sci.*, **62**, 4423–4440, https://doi.org/10.1175/JAS3629.1.

Tamura, K., and T. Sato, 2020: Responses of Polar Mesocyclone Genesis to Topographic Forcing along the Eastern Coast of Eurasian Continent. *J. Meteor. Soc. Japan*, **98**, 1261–1277, https://doi.org/10.2151/jmsj.2020-065.

Terpstra, A., I. A. Renfrew, and D. E. Sergeev, 2021: Characteristics of Cold-Air Outbreak Events and Associated Polar Mesoscale Cyclogenesis over the North Atlantic Region. *J. Clim.*, **34**, 4567–4584, https://doi.org/10.1175/JCLI-D-20-0595.1.

Tsuboki, K., and G. Wakahama, 1992: Mesoscale Cyclogenesis in Winter Monsoon Air Streams: Quasi-Geostrophic Baroclinic Instability as a Mechanism of the Cyclogenesis off the West Coast of Hokkaido Island, Japan. *J. Meteorol. Soc. Japan*, **70**, 77–93, https://doi.org/10.2151/jmsj1965.70.1_77.

——, and T. Asai, 2004: The Multi-scale Structure and Development Mechanism of Mesoscale Cyclones over the Sea of Japan in Winter. *J. Meteor. Soc. Japan*, **82**, 597–621, https://doi.org/10.2151/jmsj.2004.597.

Tsukijihara, T., R. Kawamura, and T. Kawano, 2019: Influential Role of Inter-decadal Explosive Cyclone Activity on the Increased Frequency of Winter Storm Events in Hokkaido, the Northernmost Island of Japan. *Int. J. Climatol.*, **39**, 1700–1715, https://doi.org/10.1002/joc.5910.

Watanabe, S.-I. I., and H. Niino, 2014: Genesis and Development Mechanisms of a Polar Mesocyclone over the Japan Sea. *Mon. Weather Rev.*, **142**, 2248–2270, https://doi.org/10.1175/MWR-D-13-00226.1.

——, ——, and W. Yanase, 2016: Climatology of Polar Mesocyclones over the Sea of Japan Using a New Objective Tracking Method. *Mon. Weather Rev.*, **144**, 2503–2515, https://doi.org/10.1175/MWR-D-15-0349.1.

——, ——, and ——, 2017: Structure and Environment of Polar Mesocyclones over the Northeastern Part of the Sea of Japan. *Mon. Weather Rev.*, **145**, 2217–2233, https://doi.org/10.1175/MWR-D-16-0342.1.

——, ——, and ——, 2018: Composite Analysis of Polar Mesocyclones over the Western Part of the Sea of Japan. *Mon. Weather Rev.*, **146**, 985–1004, https://doi.org/10.1175/MWR-D-17-0107.1.

Yamashita, Y., R. Kawamura, S. Iizuka, and H. Hatsushika, 2012: Explosively Developing Cyclone Activity in Relation to Heavy Snowfall on the Japan Sea Side of Central Japan. *J. Meteor. Soc. Japan*, **90**, 275–295, https://doi.org/10.2151/jmsj.2012-208.

Yamazaki, A., M. Honda, and A. Kuwano-Yoshida, 2015: Heavy Snowfall in Kanto and on the Pacific Ocean Side of Northern Japan Associated with Western Pacific Blocking. *SOLA*, **11**, 59–64, https://doi.org/10.2151/sola.2015-013.

Yanase, W., and H. Niino, 2007: Dependence of Polar Low Development on Baroclinicity and Physical Processes: An Idealized High-Resolution Numerical Experiment. *J. Atmos. Sci.*, **64**, 3044–3067, https://doi.org/10.1175/JAS4001.1.

——, ——, S.-I. I. Watanabe, K. Hodges, M. Zahn, T. Spengler, and I. A. Gurvich, 2016: Climatology of Polar Lows over the Sea of Japan Using the JRA-55 Reanalysis. *J. Clim.*, **29**, 419–437, https://doi.org/10.1175/JCLI-D-15-0291.1.

Yoshida, A., and Y. Asuma, 2004: Structures and Environment of Explosively Developing Extratropical Cyclones in the Northwestern Pacific Region. *Mon. Weather Rev.*, **132**, 1121–1142, https://doi.org/10.1175/1520-0493(2004)132<1121:SAEOED>2.0.CO;2.

Acknowledgments

I would like to sincerely thank Prof. Tomonori Sato, who always advises and encourages me with great patience. The members of this dissertation committee provided many insightful comments: Prof. Yasuhiro Yamanaka, Prof. Takeshi Horinouchi, Prof. Masaru Inatsu, Prof. Masayuki Kawashima, and Prof. Masayuki Senzaki. I also thank Prof. Hiroyuki Tomita, who gave me insightful comments in the pre-dissertation defense. I appreciate all the members and old-members of the Regional Climate System Research Group: Dr. Tetsu Nakamura, Ms. Keiko Ono, Mr. Anowarul Mohammad Islam, Mr. Shixue Li, Ms. Xiling Zhou, Mr. Kousuke Nagahiro, Mr. Takehiro Morioka, Mr. Akinobu Ogasawara, Ms. GuanYu Song, Mr. Tasuro Kotsuji, Ms. Ferreira Ramim Bruna, Dr. Daisuke Hatsuzuka, Ms. Keiko Ishizaki, Prof. Koji Yamazaki, Dr. Enkhbat Erdenebat, Dr. Chinh Huu Ta, Mr. Ahsan SM Habib, Ms. Yumi Matsushita, Mr. Koki Kasai, Mr. Hiroki Teramura, Mr. Hironobu Ochiai, Mr. Yoshihito Higuchi, Mr. Kevin Ray E. Lucas, Mr. Motoharu Sawayanagi, Dr. Muhammad Mubashar Ahmad Dogar, Ms. Yu Gao, Ms. Yuki Sato, Ms. Nozomi Matsudera, Mr. Deokyoung Han, Mr. Hiromu Yahata, Mr. Yoshiaki Shirai, Mr. Kousuke Kimura, Mr. Boniface Wainaina Kariuki, Mr. Keita Yamakoshi, Mr. Takuya Ichigi, Mr. Seigo Nakamura, Mr. Toshiyuki Amazawa, Mr. Toshinari Tomosada, Dr. Keisuke Mori, Mr. Takuya Akitake, Mr, Makoto Tamamoto, Mr. Radyan Putra Pradana, Mr. Zhang Xing. I am also thankful for the great experience I had with the members at the Division of Environmental Science Development, Course in Human and Ecological Systems, and the Division of Earth System Science, Course in Atmosphere-Ocean and Climate Dynamics. I would thank Prof. Masafumi Hirose, who introduced me to the world of meteorological research when I was a student at the Department of

Environmental Science and Technology, Meijo University. Finally, I would like to thank my family for their warm encouragement.

JRA-55, JRA-55C, and JRA-55AMIP were collected from the Data Integration and Analysis System data server (http://www.diasjp/net). OISST v2.0 were provided by NOAA (http://www.esrl.noaa.gov/psd/data/gridded/data.noaa.oisst.v2.html).